Preclinical Development of Novel Bifunctional Compounds for Parkinson's Disease

A Thesis Submitted to the
College of Graduate and Postdoctoral Studies
In partial Fulfillment of the Requirements
For the Degree of Master of Science
In the College of Pharmacy and Nutrition
University of Saskatchewan
Saskatoon

By

Chukwunonso Kingsley Nwabufo

PERMISSION TO USE

In presenting this thesis in partial fulfillment of the requirements for a Postgraduate degree from the University of Saskatchewan, I agree that the Libraries of this University may make it freely available for inspection. I further agree that permission for copying of this thesis in any manner, in whole or in part, for scholarly purposes may be granted by Dr. Ed Krol or, in his absence, by the Head of the Department or the Dean of the College of Pharmacy and Nutrition. It is understood that any copying or publication or use of this thesis or parts thereof for financial gain shall not be allowed without my written permission. It is also understood that due recognition shall be given to me and to the University of Saskatchewan in any scholarly use which may be made of any material in my thesis.

Requests for permission to copy or to make other uses of materials in this thesis in whole or part should be addressed to:

Dean
College of Pharmacy and Nutrition
104 Clinic Place
University of Saskatchewan
Saskatoon, SK S7N 2Z4 Canada

OR

Dean
College of Graduate and Postdoctoral Studies
University of Saskatchewan
116 Thorvaldson Building, 110 Science Place
Saskatoon, SK S7N 5C9 Canada

Abstract

The development of disease-modifying drugs and differential diagnostic agents is a current focus of research in Parkinson's disease (PD) and one putative target is alpha-synuclein (AS). Recently, we reported that two bifunctional compounds composed of a caffeine scaffold attached to nicotine (C_8-6-N) and 1-aminoindan (C_8-6-I) could prevent AS mediated toxicity in a yeast model of PD. Although caffeine linked to caffeine (C_8-6-C_8) did not show any therapeutic potentials, it demonstrated the strongest binding to AS. To better understand the biodistribution of C_8-6-I, C_8-6-N, and C_8-6-C_8 *in vivo* we are developing methods to label the bifunctional compounds with Fluorine-18 (^{18}F) to use in positron emission tomography (PET) imaging studies. Given the therapeutic and diagnostic potentials of these bifunctional compounds, it is necessary to conduct further preclinical studies to understand their safety and efficacy. The overall goal of this study is to establish the tandem mass spectrometric fingerprints of the target compounds which can help in metabolite identification and for the development of qualitative and quantitative methods. Also, the metabolic profile for C_8-6-I, C_8-6-N, and C_8-6-C_8 in human, mouse, and rat liver microsomes (HLM, MLM, and RLM) were evaluated. Tandem mass spectrometric studies were performed using hybrid quadrupole-time of flight and triple quadrupole-linear ion trap mass spectrometers. Metabolite profiling was accomplished using accurate mass measurement and tandem mass spectrometry. A significant observation in the fragmentation of C_8-6-C_8 suggests that a previously reported loss of acetaldehyde during caffeine fragmentation is instead a loss of CO_2. While the caffeine scaffold in C_8-6-N, C_8-6-I, and C_8-6-C_8 was metabolically stable, the nicotine and 1-aminoindan moieties were either cleaved off (dealkylation) or hydroxylated in HLM, MLM and RLM indicating that the caffeine moiety may be the preferable spot for the inclusion of ^{18}F

radioisotope in these bifunctional compounds. Given the similarity in the metabolic pathways, mouse and rat may be useful surrogates for future animal studies of C_8-6-I, C_8-6-N, and C_8-6-C_8.

Acknowledgements

I appreciate God Almighty for his loving-kindness throughout my graduate studies.

I am very grateful to my supervisor Dr. Ed Krol for his mentorship and support during my graduate studies. Dr. Ed's mentorship has made me a better researcher.

Additionally, I appreciate my committee members, Drs Anas El-Aneed and Kate Dadachova for making out time to evaluate my research progress and for providing mechanistic suggestions that made my graduate program a success.

I acknowledge all my laboratory members especially Dr. Kevin Allen and Paul Omozojie for synthesizing the bifunctional compounds that I used for my research. Also, I appreciate Dr. Kevin Allen for training me on the use of Agilent 1200 HPLC.

Furthermore, I acknowledge Ms. Deborah Michel and Mr. Ken Thoms for training me on the mass spectrometers that I used for my research. I am also thankful to Ms. Deborah Michel for training me on the preventive maintenance of Agilent 1200 and 1100 HPLC and for providing all the technical support required for the operation of the analytical instruments.

More so, I appreciate the following organizations for providing awards to me: College of Pharmacy and Nutrition, University of Saskatchewan, International Society for the Study of Xenobiotics, Drug Metabolism Discussion Group, and University of Saskatchewan American Association of Pharmaceutical Scientists. I appreciate NSERC and SHRF for funding my graduate research.

Finally, my sincere appreciation goes to my parents and siblings for all their support and care during my graduate studies.

Dedication

This thesis is dedicated to …

… My Lovely Parents

Mr. and Mrs. Michael Nwabufo

Your love and care made this possible

…And my Siblings

Obinna, Ifeanyi, Obianuju, and Chidiogo

Your support made this study possible

TABLE OF CONTENTS

LIST OF TABLES

LIST OF FIGURES

LIST OF ABBREVIATIONS

3-OH-AI	3-hydroxy-1-aminoindan
[^{11}C]-CFT	^{11}C-2β-carbomethoxy-3β-(4-fluorophenyl) tropane
[^{11}C]-PK11195	^{11}C-1-(2-chrorophynyl)-*N*-methylpropyl)-3 isoquinoline carboxamide
[^{11}C]-PIB	N-methyl-[^{11}C]2-(4'-methylaminophenyl)-6-hydroxybenzothiazole (Pittsburgh Compound-B)
[18F]-DOPA	^{18}F-Dihydroxyphenylalanine
[18F]-FDG	^{18}F-2-Fluoro-2-deoxy-D-glucose
[^{18}F]-FDDNP	1-(6-[(2-[^{18}F]fluoroethyl)(methyl)amino]-2-naphthyl) ethylidene)malononitrile
AD	Alzheimer's disease
AFMU	5-acetylamino-6-formylamino-3-methyluracil
AS	Alpha-synuclein
BBB	Blood-brain barrier
BCRP	Breast cancer resistance protein
BP	Binding potential
CE	Collision energy
CID-MS/MS	Collision-induced dissociation-tandem mass spectrometry
CNS	Central nervous system
CSF	Cerebrospinal fluid
CT	X-ray computed tomography
CV	Coefficient of variation
DAT	Dopamine active transporter
DLB	Dementia with Lewy bodies

ELISA	Enzyme-linked immunosorbent assay
ESI	Electrospray ionization
GIT	Gastrointestinal tract
FLZ	N-2-(4-hydroxy-phenyl)-ethyl]-2-(2,5-dimethoxy-phenyl)-3-(3-methoxy-4-hydroxy-phenyl)-acrylamide
FMO3	Flavin-containing monooxygenase 3
HLM	Human liver microsomes
HPLC	High-performance liquid chromatography
HQC	High quality control
ITC	Isothermal calorimetry
KH_2P0_4	Monopotassium phosphate
K_2HPO_4	Dipotassium phosphate
LC-MS	Liquid chromatography-mass spectrometry
LC-MS/MS	Liquid chromatography-tandem mass spectrometry
LLOQ	Lower limit of quantification
LOD	Limit of detection
LQC	Low quality control
LRRK	Leucine rich repeat kinase
LSVT	Lee Silverman Voice Treatment
$MgCl_2$	Magnesium chloride
MLM	Mouse liver microsomes
MMPPD	2,2-di-(3-methoxymethylphenyl) 1,3-propanediol
MPP^+	1-methyl-4-phenylpyridinium
MPPP	1-methyl-4-phenyl-propionoxypiperidine
MPTP	1-methyl-4-phenyl-1,2,3,6-tetrahydropyridine

MRI	Magnetic resonance imaging
MRM	Multiple reaction monitoring
MQC	Middle quality control
MSA	Multiple system atrophy
NADPH	Reduced nicotinamide adenine dinucleotide
NAT2	N-acetyl transferase 2
NCEs	New chemical entities
NL	Neutral loss
NNK	Nicotine-derived nitrosamine ketone
P450	Cytochrome P450
PBR	Peripheral benzodiazepine receptor
PD	Parkinson’s disease
PDD	Parkinson’s disease with dementia
PET	Positron emission tomography
P-gp	P-glycoprotein
QCs	Quality controls
RatCAP	Rat conscious animal PET
RBC	Red blood cells
RDA	Retro-Diels-Alder
RLM	Rat liver microsomes
SNpc	Substantia nigra pars compacta
SPECT	Single photon emission computed tomography
SPP	Sodium pyrophosphate
$t_{1/2}$	Half-life
UGT	Uridine diphosphate glucuronosyltransferase

1.0 Chapter One: Introduction

Parkinson's disease (PD) is ranked the second most common neurodegenerative disorder after Alzheimer's disease (AD), and more than ten million people worldwide are diagnosed with PD (1). The development of disease-modifying treatments and differential diagnostic agents are important aspects of research in PD. Alpha-synuclein (AS) has been identified as one of the putative biological targets for the development of disease-modifying drugs and differential diagnostic agents for PD. AS is an intrinsically disordered protein that is thought to be involved in the mobilization of synaptic vesicles for neurotransmission (2, 3); however, the misfolding of AS is a critical event in the pathogenesis of PD (3). Our laboratory has focused on developing novel compounds that can interact with AS and ultimately prevent the pathological pathway that leads to PD. Recently, we reported that two bifunctional compounds composed of a caffeine scaffold attached to nicotine (C_8-6-N), and 1-aminoindan (C_8-6-I) (Figure 1.1) were the most promising candidates in preventing the pathological pathway that leads to PD (3). Although caffeine linked to caffeine (C_8-6-C_8) (Figure 1.1) did not show any therapeutic potential, it demonstrated the strongest binding to AS making it a suitable candidate for the development of imaging probes for the diagnosis of PD. In view of this new evidence, new research is proposed to develop Fluorine-18 (^{18}F) analogues of C_8-6-C_8, C_8-6-N, and C_8-6-I as positron emission tomography (PET) imaging probes to assess the biodistribution of the bifunctional compounds and for the diagnosis of PD.

Given the therapeutic and diagnostic potentials of these novel bifunctional compounds, it is of great importance to determine their metabolic stability at this early stage of drug

discovery and development. The evaluation of the metabolic stability of these novel bifunctional compounds can provide useful information about their safety and efficacy which will contribute to the improvement of the intellectual property of these new chemical entities (NCEs).

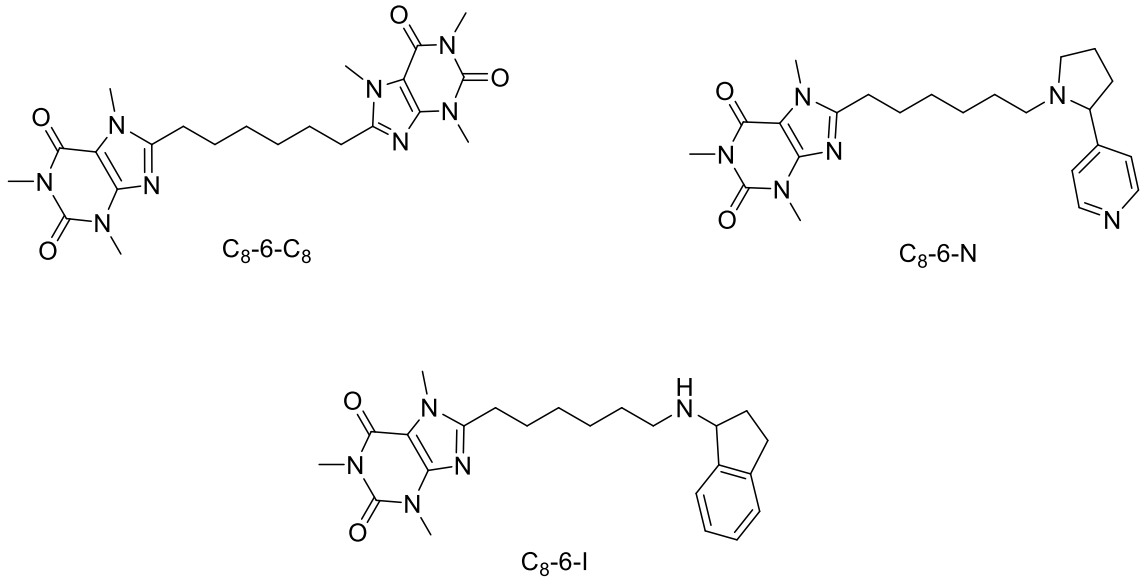

Figure 1.1 Structure of C_8-6-C_8, C_8-6-N, and C_8-6-I

The overall goal of my research is to determine the metabolic stability of C_8-6-I, C_8-6-N, and C_8-6-C_8 in human, mouse, and rat liver microsomes (HLM, MLM, and RLM). The outcome will be useful in determining the location of ^{18}F incorporation in the imaging probes. These studies will provide a reference for future metabolic studies of the stable fluorine-19 (^{19}F) analogues of C_8-6-I, C_8-6-N, and C_8-6-C_8. Tested compounds and future analogues have the potential to be used as therapeutics or diagnostics for PD and the work in this thesis will contribute to the development of predictive structural models to maximize biodistribution (high brain penetrance and AS selectivity) and minimize metabolic degradation (optimize lifetime). Additionally, comparison of the metabolic profile of RLM

and MLM with those of HLM will help to identify the most relevant model for future animal studies.

2.0 Chapter Two: Literature Review

2.1 Parkinson's disease

PD is a chronic neurodegenerative disorder that is associated with the progressive loss of dopaminergic neurons in the substantia nigra pars compacta (SNpc) (1). Approximately 1% and 4% of the general population over the ages of 60 and 80 years, respectively, are diagnosed with PD (2). Parkinsonism or Parkinsonian syndrome is a condition with a similar clinical appearance as in PD but different etiology; for instance, some patients have parkinsonism secondary to antidopaminergic drugs without the pathology of the SNpc (3). PD is the most common form of Parkinsonism and is sometimes called "idiopathic Parkinsonism", meaning Parkinsonism with no identifiable cause (4, 5).

2.2 Etiology of Parkinson's disease

Previous studies have identified several predisposing factors associated with PD.

2.2.1 Genetic factors

It has been reported that about 15% of patients with PD have a first-degree relative who has the disease (4). Research has shown that about 5% of patients diagnosed with PD have forms of the disease that occurs as a result of a mutation of one of the several specific genes (6) and correlations between the incidence of PD and the mutation of specific genes have been identified (3). Mutations in genes that code for AS (*SCNA*) and leucine rich repeat kinase 2 (*LRRK2;* LRRK2) are implicated in PD (7, 8). Genomic multiplication and point mutations of *SCNA* are associated with familial PD (9-12). Additionally, several *in vitro* studies suggest that authentic phosphorylation of *SCNA* at serine-129 (13-17) but not phosphorylation-mimicking mutations (18, 19) results in an increase in fibril formation. This suggests that authentic phosphorylation of *SCNA* at serine-129 may be associated with

the aggregation phenomenon that leads to PD. G2019S is the most common disease associated mutation in *LRRK2,* and it displays higher kinase activity than the wild-type (3), suggesting that overactivation of LRRK2 may be associated with the pathogenesis of PD (20). Given that AS deposited in Lewy bodies is highly phosphorylated at serine-129, LRRK2 and AS may play a synergistic role in the pathogenesis of PD. A simple way to explain this is that LRRK2 is the kinase that mediates phosphorylation of AS(7). Interestingly, only one study showed that recombinant AS is phosphorylated by cell lysates overexpressing LRRK2 from HEK293 cells (21), however, there is no evidence that LRRK2 increases phosphorylation of AS in cell or animal systems (7).

2.2.2 Biochemical factors

The loss of dopaminergic neurons in the SNpc of the brain is the primary pathological feature of PD. Dopaminergic neurons use dopamine as a neurotransmitter. Dopamine is a catecholaminergic neurotransmitter responsible for transmitting signals between the SNpc and the corpus striatum to produce smooth purposeful movement (22-25). Loss of dopaminergic neurons results in abnormal nerve firing patterns within the brain that cause impaired movement (22-25). Previous research has shown that patients diagnosed with PD have lost about 60 to 80% of dopaminergic neurons in the SNpc prior to the onset of symptoms (22-25).

The biochemical consequence of the progressive loss of dopaminergic neurons in the SNpc is the gradual denervation of the striatum, the main target projection for the SNpc neurons (24, 25). Other target regions of these neurons include the intralaminar and parafascicular nuclei of the thalamus, the globus pallidus, and the subthalamic nucleus (24, 25). Dopamine denervation of the putamen, the motor portion of the striatum, leads to many of the motor

symptoms of PD and symptoms develop when striatal dopamine depletion reaches 50–70% (24, 25).

2.2.3 Environmental factors

Previous studies have implicated exposure to certain toxins such as 1-methyl-4-phenyl-1,2,3,6-tetrahydropyridine (MPTP) in the etiology of PD (3). MPTP, a common contaminant of the opioid 1-methyl-4-phenyl-propionoxypiperidine (MPPP), is a lipophilic drug that crosses the blood-brain barrier (BBB) and is metabolized by monoamine oxidase-B to the neurotoxic form, 1-methyl-4-phenylpyridinium (MPP^+) (26). MPP^+ selectively destroys dopaminergic neurons in the SNpc. MPP^+ is also an uncoupler of the electron transport chain coupled oxidative phosphorylation pathway thereby leading to the release of free radicals which contribute to cell destruction. The neurotoxic effect of MPP^+ is mediated through a high-affinity uptake process in the dopaminergic nerve terminal that would otherwise mediate the reuptake of excess dopamine in the synaptic cleft (26).

Furthermore, exposure to compounds such as amphetamine (27, 28) and the insecticide paraquat (29-31) has been reported to increase the incidence of the disease. Amphetamine and paraquat mediate their neurotoxic effect by binding to AS at the N-terminus and causing it to adopt a more compact conformation (32) which is more prone to the aggregation phenomenon that leads to PD.

Given the implication of AS misfolding in the etiology of PD, it is essential to understand how the structure of AS affects its function. Such information will be useful in developing novel compounds that can maintain the structural integrity of AS, thereby preventing the misfolding pathway that leads to PD.

2.3 Structure-function relationship of alpha-synuclein

Synucleins are a group of secondary structural proteins which include alpha-, beta-, and gamma-synuclein (33). AS is encoded by the *SCNA* gene and there are at least four known isoforms of AS encoded by the same *SCNA* gene in humans and produced through alternative splicing (51). These variants are characterized by their unique number of amino acids and aggregation potentials (51). Furthermore, the high molecular weight isoforms (containing about 140 amino acids) retain all the sites responsible for post-translational modifications (52) while the low molecular weight isoforms (containing 112,126 or 98 amino acids) do not retain these sites and may be predisposed to abnormal aggregation (33, 52). This indicates that post-translational modification may be a predisposing factor to amyloidosis. AS is mainly expressed in the brain at the presynaptic terminals where it is thought to play a significant role in the mobilization of synaptic vesicles for the exocytotic release of neurotransmitters into the synaptic cleft (53, 54). Furthermore, AS has been reported to account for up to 1% of total protein in soluble cytosolic brain fractions. This suggests that it may play a significant role in neuronal function (53). Although AS is mostly an intracellular protein, it has also been found in extracellular fluids such as cerebrospinal fluid (CSF), blood, and plasma (55-59).

The structure of the major variant (AS-140) can be divided into two functionally distinct regions namely, the N and C terminal (33). The N- terminal region ranges from 1 to 103 amino acid residues and contains amphipathic apolipoprotein binding helical motifs, which are responsible for binding lipids such as phospholipids (33, 60). This binding to phospholipids induces AS to adopt a helical conformation (60), which is critical for its role in neurotransmission (61). The N-terminal also includes a hydrophobic region, the non-

amyloid-β-component which is responsible for protein-protein interactions (60). This protein-protein interaction induces AS to adopt a beta sheet conformation which is a critical event in the prion-like aggregation phenomena associated with PD (60, 61). A unique feature of this prion-like aggregation phenomena is permissive templating, in which the misfolded AS interacts with a normal AS and converts it to an amyloidogenic form (62-64). The aggregation of the misfolded AS results in the formation of insoluble fibrils and their subsequent inclusion in Lewy bodies (61). The C-terminal region has been suggested to be involved in mediating interactions of AS with other cytosolic or membrane-bound proteins (60, 62).

2.4 Diagnosis of Parkinson's disease

Clinical diagnosis of PD is mostly based on the triad motor symptoms: resting tremors, rigidity and bradykinesia, non-motor symptoms such as constipation, anosmia, cognitive dysfunction, depression, and dysautonomia (33-36), as well as postmortem pathological examination. The clinical diagnosis of PD can be less challenging when obvious signs and symptoms are present, as well as good response to levodopa treatment; however, diagnosis becomes more challenging at the onset of the disease due to similar signs and symptoms associated with PD and other neurodegenerative disorders such as PD with dementia (PDD), dementia with Lewy bodies (DLB) and multiple system atrophy (MSA) (36). This implies that the only definitive confirmation of PD remains postmortem pathological examination where progressive degeneration of dopaminergic neurons at the SNpc along with AS-rich Lewy bodies are observed (35, 37, 38). Consequently, about 15% of patients diagnosed with PD do not strictly meet the clinical criteria for the disease (39) and postmortem pathological examination of the diseased brain show a different diagnosis in

about 35% of PD patients (40-43). The misdiagnosis of PD can be explained by the overlapping neuropathological, cognitive and clinical profile of PD with several other neurodegenerative disorders (33). For example, depending on the stage of the disease, dementia is present in 10% to 80% of PD patients (44, 45) and so the cognitive profile of PDD overlaps with DLB and MSA (33).

Clearly, accurate diagnosis presents a serious problem in PD and recent research has focused on developing accurate diagnostic tools that would be useful for early detection, as well as tracking of the disease progression. Early detection of the disease will allow administration of disease-modifying treatments and most likely circumvent the onset of motor symptoms. To develop a putative biomarker, an understanding of the molecular and biochemical mechanism of the disease will be an inevitable step. There is also a good chance that such a putative biomarker will provide a novel target for drug discovery and development in PD.

Given the implication of AS in the pathophysiology of PD, AS might be a good candidate for diagnosis of PD. Furthermore, the fact that the misfolding of AS is a critical event in the pathogenesis of PD implies that aberrant AS may be present in the early stages of the disease. In addition, a point mutation in the *SCNA* gene has been implicated in familial PD (11, 46). Also, genetic risk factors involving relatively rare duplications or triplications of the *SCNA* gene locus result in elevated AS in both brain and blood (33, 47). Hence, AS in plasma, serum or CSF may serve as a useful diagnostic marker for PD (33). Several studies have identified pathological AS in CSF, blood, and saliva (48-50).

2.5 Assay of alpha-synuclein in peripheral tissues and body fluids

As previously discussed, the non-motor symptoms of PD are usually present at the onset of the disease before the classical clinical symptoms appear (51). Estimation of pathological AS in these affected tissues might be useful in early diagnosis of PD. Pathological AS in solid tissues, such as within Lewy bodies and Lewy neurites, has been visualized in multiple peripheral tissues using immunohistochemistry (33). Furthermore, several analytical techniques such as western blot, enzyme-linked immunosorbent assay (ELISA), luminex assay and mass spectrometry have been used to assay for total AS, as well as oligomeric and phosphorylated AS in body fluids such as CSF, plasma, and serum. The variation in the specificity, sensitivity, and precision of these analytical techniques account for variations in the assay. However, not one method appears to be entirely better than the other as each has its advantages and disadvantages (33).

2.5.1 Alpha-synuclein in peripheral tissues

Ante-mortem and post-mortem tissue samples have been studied for the presence of pathological AS. These tissues include cardiac plexus (52), sympathetic ganglia (52, 53), gastric myenteric plexus (54), colonic tissue (55-59), gastrointestinal tract (GIT) (53),cardiac sympathetic nervous system (60), heart (61, 62), salivary gland (63-65), and vagus nerve (65, 66). However, the outcome of assays using these tissues is quite variable. These variabilities can be caused by different methods of AS analysis, the severity of PD between studies, site of biopsy collection, specificity and sensitivity of the applied analytical method and cohort size (33, 67). To overcome these challenges associated with the measurement of pathological AS in peripheral tissues, standardized protocols for sample collection as well as validated analytical techniques are needed (33).

2.5.2 Alpha-synuclein in body fluids

2.5.2.1 Cerebrospinal fluid

There is evidence indicating that CSF AS may be the most consistent, sensitive, and specific marker for the diagnosis of PD (33). Assays of total CSF AS have been reported to be 61 to 94% sensitive and 25 to 64% specific for distinguishing PD from controls (67-71).

It has been observed that while monomeric AS is not affected in PD (72, 73), both oligomeric (70, 74, 75) and phosphorylated (71, 76) AS increased in PD patients compared with the control group. Several studies have shown that CSF AS may be useful in the differential diagnosis of PD and several other neurodegenerative disorders (69, 77, 78). Although CSF seems to be the best specimen for diagnosis of PD, the relatively invasive nature by which it is obtained makes the procedure almost impracticable (67).

2.5.2.2 Plasma and serum

Given the less invasive nature by which plasma and serum are collected as well as its availability, plasma and serum may be the most appropriate clinical specimen for assay of pathological AS (33). Assays of the levels of serum AS showed conflicting results finding either that they are unaffected in PD patients (79) or are decreased compared with control groups in a larger cohort (80). Similarly, several conflicting results have been reported for the measurement of total plasma AS using ELISA (74, 81-83), western blot (84), mass spectrometry (82) and luminex assay (67, 85). The reason for the differing results can be explained by the variation in the analytical techniques used for the study.

Furthermore, a recent study has shown that total plasma AS measured with ELISA decreased in both familial and sporadic PD patients compared with the control groups (86).

The authors suggested that the lack of significance could be attributed to the small cohorts in the familial group (86). The conflicting results in studies assessing plasma AS could be caused by factors such as hemolysis, contamination of platelets in plasma, inadequate age-matched controls, and variation in the specificity and sensitivity of the analytical techniques used (67).

A way to overcome some of these confounders may be to assay exosomal AS (33). Measurement of exosomal AS has shown diagnostic sensitivity and specificity comparable to those determined by CSF AS (87), making it potentially valuable in the diagnosis of PD and determination of disease severity (33). Another possible way to minimize the confounding factors associated with measurement of plasma AS is to assay for pathological variants of AS (33). For example, oligomeric AS has been reported to either increase (81, 88) or be unaffected (74, 82, 89) in PD patients compared with controls while phosphorylated AS is increased in PD patients compared with controls (82). However, the interpretation of this report should be handled with caution as the study involved only a small cohort.

2.5.2.3 Blood

As red blood cells (RBC) are a significant source of AS, accounting for about 99% of its blood levels, RBC may serve as a potential specimen for diagnosis of PD (33). Several studies involving the assay of total RBC AS have shown controversial results (47, 90). The variation could be accounted for by differences in the analytical technique used and cohort size. To validate the potential of blood as a specimen for accurate diagnosis of PD, further studies should be conducted to determine the effect of PD on blood AS and RBC count which could cause alterations in AS levels (33).

2.5.2.4 Saliva

As saliva is a readily available specimen compared to other body fluids already discussed, salivary AS may be a good candidate for diagnosis of PD; however, assays of unstimulated salivary AS using western blot, luminex or mass spectrometry showed no significant difference in either the cellular component, supernatant (91) or cellular pellet lysate (76). Previous studies have shown conflicting results of either an increase in salivary AS in PD patients compared with the control group (92) or no alterations in salivary AS (76, 91). Further studies are required to provide a standardized protocol for the collection of saliva, as well as the most appropriate method of analysis (33).

Given the current challenge in the diagnosis of PD by estimation of pathological AS from body fluids or tissues, recent research has focused on developing molecular imaging probes for diagnosis of PD. The next section will focus on molecular imaging and the application of PET imaging probes in the diagnosis of PD.

2.6 Molecular imaging probes for diagnosis of Parkinson's disease

Molecular imaging is one of the most widely used technologies in clinical and preclinical studies that help researchers to understand the pathophysiology, and drug treatment monitoring of various diseases including neurodegenerative disorders such as PD, by providing a real-time visualization for *in vivo* characterization and qualification of biological processes at the molecular and cellular level (93). Molecular imaging consists of the imaging probe and imaging modalities. A molecular imaging probe is an agent used to visualize, characterize and quantify biological processes in living systems (94, 95).

The molecular imaging probe exists in a number of forms such as radiotracers, contrast agents or molecular beacons (96). A molecular imaging probe consists of a linker, a signal

moiety, and a target moiety. The signal agent usually produces a signal that can be detected *in vivo* to image different tissues. The type of imaging probe used for a given imaging modality can be determined by the physical property of the signal moiety; for example, a PET imaging probe requires a positron-emitting radionuclide as the signal agent whereas a single photon emission computed tomography (SPECT) imaging probe employs a gamma-emitting radionuclide (96).

The targeting moiety interacts with a biomarker in a specific biological process, and such targeting ligands include but are not limited to small molecules, peptides, proteins, antibodies and its fragments, and nanoparticles (96). The linker used in a molecular imaging probe can couple the targeting moiety with the signal agent, minimize the interaction between the targeting moiety and the signal agent and, most importantly, modify the pharmacokinetics of the imaging probe (96). It is important to mention that because many aspects need to be optimized to obtain the best imaging outcome, in some cases not all three components - the signal agent, the linker, and the targeting moiety are simultaneously present in a molecular imaging probe (96).

A molecular imaging probe with clinical translation is expected to have high binding affinity to the target, high specificity to target, high sensitivity, high contrast ratio, high *in vivo* stability, low immunogenicity and toxicity (96). Several emerging molecular neuroimaging modalities have made it possible to non-invasively identify the fundamental biological processes involved in several degenerative disorders (93). These molecular imaging modalities include magnetic resonance imaging (MRI), x-ray computed tomography (CT), PET and SPECT.

The advantages of molecular imaging reside in the real-time elucidation of the complex biological and metabolic pathways of various diseases at the molecular and cellular levels (95) compared to the quantitative estimation of the biological target which can be challenged by both variations in analytical techniques and specimen. Additionally, molecular imaging provides useful information that makes it possible to diagnose the diseases at an early stage as well as conduct therapeutic trials of various disease conditions (97). Of all the molecular imaging modalities, PET and SPECT have been used extensively in clinical neuroscience for the diagnosis of neurodegenerative disorders such as PD and AD; however, we will focus on the application of PET in the diagnosis of PD.

2.6.1 PET molecular imaging

PET is a high-performance molecular imaging technique that has found relevant applications in medical sciences due to its excellent sensitivity of 10^{-11}-10^{-12} mol/L and limitless depth of penetration (93). The modus operandi of PET involves recording pairs of high-energy γ-rays emitted indirectly from the decay of radioisotopes which are introduced into the subject (93). Most commonly used PET radioisotopes include ^{11}C, ^{13}N, ^{15}O, ^{18}F, ^{64}Cu, ^{68}Ga, ^{82}Rb and ^{166}Ho. The positrons emitted from the radioactive decay of these imaging probes travel a few millimeters through the surrounding tissue, then they lose their kinetic energy rapidly (93). The positrons move slowly and annihilate with electrons to generate two 511 KeV γ-rays, which travel in opposite directions (98). Given that these radioisotopes have short half-lives ($t_{1/2}$) such as ^{18}F:$t_{1/2}$=109.8 minutes, ^{11}C: $t_{1/2}$=20.3 minutes, and ^{15}O: $t_{1/2}$=2.04 minutes, they need to be made at the site and introduced into the subject quickly (99). Of all the radioisotopes, ^{11}C, ^{15}O, and ^{18}F are the most frequently used radioisotopes for brain imaging (93).

PET scanning with the metabolic tracer ^{18}F-2-Fluoro-2-deoxy-D-glucose ([^{18}F]FDG) is widely used for detecting tumors, staging cancers, and drug treatment monitoring because cancer cells are actively metabolizing glucose (93). [^{18}F] FDG is a structural analog of glucose and when injected into the subject, it is transported into the cell by glucose transporters where it is phosphorylated by hexokinase; however, the phosphorylated [^{18}F] FDG does not have a transporter; hence it is trapped in the cell. The idea is that trapping the intact radiolabeled imaging probe provides information about the target cell.

Although PET has played a critical role in clinical research, a recent report has suggested that PET can be used in preclinical research involving small animal models; for instance, the Rat Conscious Animal PET (RatCAP) is a microPET instrument with a spatial resolution of 1-2mm and sensitivity of 10^{-11}-10^{-12} mol/L that has been constructed to allow small animal free of anesthesia to be scanned (93). Despite the benefits associated with PET, there are two major limitations of the technique and these are the use of high-cost cyclotron (100) for the development of radioisotopes and the short $t_{1/2}$ of the radioisotopes (93).

Several PET imaging probes have been reported to be used for diagnosing several central nervous system (CNS) diseases such as 1-(6-[(2-[^{18}F]fluoroethyl)(methyl)amino]-2-naphthyl)ethylidene) malononitrile ([^{18}F]-FDDNP) for AD (101), ^{18}F-dihydroxyphenylalanine ([^{18}F]-DOPA) for PD (102), N-methyl-[^{11}C]2-(4'-methylaminophenyl)-6-hydroxybenzothiazole termed Pittsburgh Compound-B (PIB) ([^{11}C]-PIB) for AD (103, 104), [^{11}C]-raclopride for PD, schizophrenia, and depression (105, 106), [^{11}C]-1-(2-chrorophynyl)-*N*-methylpropyl)-3 isoquinoline carboxamide ([^{11}C]-

PK11195) for AD, multiple sclerosis, and Huntington's disease (107, 108), [^{11}C]-flumazenil for epilepsy(109), and [^{11}C]-nicotine for AD (110) (Figure 2.1).

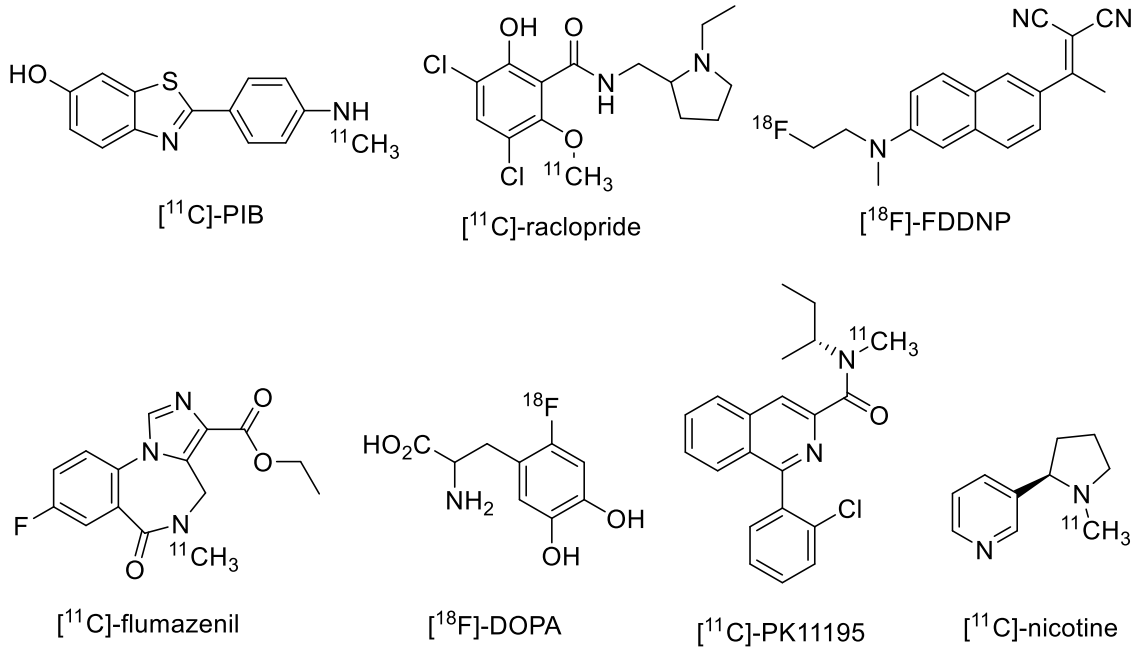

Figure 2.1 PET imaging probes for CNS diseases.

2.6.1.1 PET molecular imaging in Parkinson's disease

It is important to emphasize that PET imaging probes are chosen based on their ability to interact with a given molecular target involved in the etiology of a disease condition. Of all molecular agents, small molecules have been the most useful in diagnosing CNS disorders because of their ability to cross the BBB and be cleared from the tissue at a very fast rate (93). Some of these small molecules have a high affinity for specific transporters, ion channels or specific receptors such as peripheral benzodiazepine receptor (PBR) while others can reflect the enzymatic or metabolic activity of a given biochemical pathway involved in various disease conditions (93) such as the glycolytic pathway.

As previously mentioned, PD is characterized by the progressive loss of dopaminergic neurons in the SNpc (111, 112). By imaging the dopaminergic system, several functional and neurochemical changes can be used for early diagnosis, as well as differential diagnosis of PD.

Previous PET studies with ^{11}C-PK11195 for PBR have been used to understand the progression of the neurodegenerative process and disease state in PD patients (93). Furthermore, several studies suggest that there may be a correlation between the activation of the microglia and the loss of dopaminergic neurons in the SNpc (113-117). Microglia are known to be involved in the modulation of immune responses in the intact brain and become activated in response to inflammation, trauma, ischemia, tumor, and neurodegeneration (118, 119). Two PET studies have measured microglial activation using ^{11}C-PK11195, as well as the availability of the presynaptic dopamine active transporter (DAT) using^{11}C-2β-carbomethoxy-3β-(4-fluorophenyl)tropane ([^{11}C]-CFT) (119) and [^{18}F]-DOPA (120). DAT is a membrane-bound protein that is responsible for the high-affinity uptake of dopamine from the synaptic cleft back into the presynaptic neuron. The decrease in DAT may be indicative of loss of dopaminergic nerve terminals (119). Ouchi *et al*., (119) suggested that these *in vivo* imaging methods play dual roles in monitoring the progressive degeneration of dopaminergic neurons and these roles are: alterations in neuroinflammatory reactions on the cell-body side and the resulting deletion of nerve terminals in the striatum.

Ouchi *et al*., (119) studied the binding potential (BP) of [^{11}C]-PK11195 and [^{11}C]-CFT in ten early-stage drug-naïve PD patients and ten age-matched healthy subjects and showed that [^{11}C]-PK11195 BP in the midbrain is inversely related with [^{11}C]-CFT BP in the

putamen, which regulates movement, and directly related to motor severity. This inverse relationship was also reported to be positively correlated with the severity of motor symptoms (119). This study suggests that the oxidative stress triggered by microglia-mediated immune response contributes to the loss of dopaminergic nerve terminals indicating the importance of early therapeutic intervention with neuroprotective drugs (119).

Another study examined [^{11}C](R)-PK11195 BP and [^{18}F]-DOPA BP using 18 PD patients and 11 healthy subjects(120). Their study showed a significant increase in mean levels of [^{11}C](R)-PK11195 binding in the pons, basal ganglia, as well as frontal and temporal cortical regions compared to the healthy subjects (120). Furthermore, the longitudinal study conducted on 8 PD patients showed that their [^{11}C](R)-PK11195 signal remained stable for two years (120). The authors suggested that the absence of changes during the longitudinal study indicates that microglia are activated early in the disease and their levels remain relatively static, possibly driving the disease through cytokine release (120). The conclusion of their study agrees with that of Ouchi *et al*., that the activation of microglia is associated with the pathogenesis of PD (119, 120). However, Gerhard *et al*., reported that there is no positive correlation between the levels of microglia activation and the clinical severity of PD or putamen [^{18}F]-DOPA uptake (120). [^{18}F]-DOPA PET was the first neuroimaging technique suited for measuring the integrity of dopaminergic nerve terminals (111, 121).

These previous studies indicate that PET imaging provides useful information about the biochemical and neurological changes associated with PD. Not only can this information be used for diagnosis, but also for the discovery of neurotherapeutic agents for PD. Given

the benefits associated with PET, further studies are underway to identify imaging probes for differential diagnosis, early diagnosis, and drug treatment monitoring of PD.

2.7 Management of Parkinson's disease

Although several drugs can help provide relief from the symptoms of PD, there is currently no cure for PD (3). Furthermore, the gold-standard treatment depends on the phase of the disease therefore, PD patients are usually on several treatment regimens. These treatment regimens can be grouped into pharmacological and non-pharmacological therapies.

Non-pharmacological therapies include psychosocial intervention methods that can augment clinical improvement in PD patients (3). These methods include multiple forms of physical exercise such as tai chi or Lee Silverman Voice Treatment (LSVT Global, Inc, Tucson, AZ, USA) and speech therapy with the LSVT (122). Furthermore, exercise, physical therapy, speech and/or occupational therapy have been reported to have a sustainable effect for PD patients by improving their quality of life (122). Despite the importance of these non-pharmacological therapies, its relevance becomes useless without an augmentation of medical treatments.

Pharmacological therapies include drugs that provide symptomatic relief of the motor and non-motor deficits in PD patients (3). Ayano has previously reported the three different categories of medications for PD (3). The first category includes drugs that increase the level of dopamine in the brain such as levodopa. The second category involves drugs that affect other neurotransmitters in the body with the overall aim of easing the symptoms of the disease; for example, anticholinergic drugs interfere with the production or uptake of acetylcholine and are effective in reducing tremors. The third category includes drugs that

help control the non-motor symptoms of PD; for example, PD patients with depression may be prescribed antidepressants.

Additionally, there are several emerging new therapeutic options such as continuous pump therapies; for example, with apomorphine or parenteral levodopa, or the implantation of electrodes for deep brain stimulation (122). Furthermore, recent research has revealed that novel bifunctional compounds can rescue dopaminergic cell death in a yeast model of PD and this will be discussed further in the next section.

2.8 Novel bifunctional compounds as therapeutic agents for Parkinson's disease

Although the misfolding of AS is a critical event in the pathogenesis of PD, the exact cause of dopaminergic cell death is not well understood (123). However, it has been suggested that increasing the activity of the clearance pathways for the misfolded protein might provide improved therapies (124-126). Additionally, since the misfolding and prion-like aggregation of AS is a crucial event in the pathophysiology of PD, an emerging therapeutic target might be the prevention of the misfolding pathway (32).

Previous studies suggest that caffeine, nicotine, 1-aminoindan, and metformin might be neuroprotective (127-137); however, it is not exactly clear how these compounds exert their neuroprotective effects. It was previously hypothesized that compounds which bind to AS at the N and C terminals and induce it to adopt a loop conformation could be neuroprotective whereas compounds which cause more compact structure could be neurotoxic (123). In view of this hypothesis, Kakish *et al*., used nanopore analysis and isothermal calorimetry (ITC) to show that nicotine, caffeine, and 1-aminoindan all bind to AS at the N-and C-terminal (32). Their research suggests that caffeine, nicotine, and 1-aminoindan induce AS to adopt a loop conformation and that the stoichiometry of drug to

AS in the complex is 1:1 (32). They also reported that since metformin does not interact with the N-terminus, it may exert its neuroprotective effect by inhibiting C-terminal cleavage of AS (123). It was previously reported that C-terminal cleavage of AS increases the rate of aggregation and aggravates the neurodegeneration and propagation of PD in mouse models (138, 139).

In light of this new evidence, Kakish *et al*., reasoned that modifications to these neuroprotective compounds might increase their efficacy without necessarily increasing their toxicity (123). To do this, they prepared bifunctional compounds which are a linked combination of any two neuroprotective compounds such as caffeine-nicotine (C_8-6-N), caffeine-caffeine (C_8-6-C_8), and caffeine-1-aminoindan (C_8-6-I) (123) (with structures shown in Figure 1.1). These neuroprotective dimers all had a caffeine scaffold and were linked through a six carbon alkyl chain to minimize solubility problems and yet retain enough flexibility to allow both moieties to bind simultaneously (123). The dimers were screened by nanopore analysis and ITC. Finally, a yeast model of PD which expresses an alpha-synuclein-green fluorescent protein (AS-GFP) construct under the control of a galactose promoter was used to test the ability of these dimers to interact with AS in a cell system (123). Fluorescent microscopy revealed that in 5mM galactose the yeast strain would not grow and large cytoplasmic foci were observed (123). This implies that aberrant AS might have prevented the growth of the yeast strain. All the dimers and monomers were tested however, it was observed that two of the dimers, C_8-6-I and C_8-6-N at a concentration of 0.1μM were the most effective at rescuing yeast from AS-mediated cell death (123). This shows that some of the dimers are more effective at rescuing yeast growth compared to the monomers, either alone or in combination (123). The study concluded that

C_8-6-I and C_8-6-N are the only dimers that did not cause AS to adopt a more compact structure at high concentrations making these dimers the most promising candidates for preventing the progression of PD by prion-like aggregation (123). Given that the binding constants were in the order of $10^5 M^{-1}$, the authors suggested that other factors might be responsible for the protective effects of these dimers and these factors include: increased clearance of the dimer/AS complexes, inhibition of vesicle clustering, decreased expression of AS and inhibition of multimer formation by binding to key intermediates (123).

Since these novel dimers can bind AS, they can be developed as PET imaging probes for the diagnosis of PD. To achieve this goal, preclinical studies such as metabolism should be conducted. Metabolic studies of these compounds will provide useful information about their *in vitro* lifetime as well as the most appropriate position to include a signal moiety on the bifunctional compounds. To conduct the metabolic studies of these novel bifunctional compounds, an understanding of the concept of xenobiotic metabolism is essential.

2.9 Metabolism of xenobiotics

Xenobiotics are compounds that are foreign to an organism's normal biochemistry, such as drugs and poisons (140). Xenobiotic metabolism is the biotransformation of xenobiotics by specific enzyme-mediated pathways. The overall goal of xenobiotic metabolism is to facilitate the elimination of toxic compounds that would otherwise accumulate in the body at toxic concentrations. This is achieved by a series of enzyme-catalyzed reactions which modify the physicochemical properties of the xenobiotic thereby promoting their elimination from the body.

The liver is the major organ that is responsible for the metabolism of both endogenous and exogenous compounds. The liver contains the cofactors and enzymes required for xenobiotic metabolism. Xenobiotic metabolism can be divided into phase I, phase II, and membrane transporter-mediated processes (141). Lipophilic xenobiotics are often first metabolized by phase I enzymes, which function to make xenobiotics more polar and provide sites for conjugation reactions while phase II enzymes catalyze conjugation reactions and can also directly interact with xenobiotics but more commonly interact with metabolites produced by phase I enzymes (141). Furthermore, membrane transporters mediate the entry (uptake) and exit (efflux) of xenobiotics across the biological membrane (141).

Phase I reaction can occur by oxidation, reduction, and hydrolysis, (140). Phase I reaction is primarily mediated by the cytochrome P450-dependent mixed-function oxidase system (P450) and requires reduced nicotinamide adenine dinucleotide (NADPH) as a cofactor. Some common enzymes involved in phase 1 metabolism include cytochrome P450 monooxygenase, flavin-containing monooxygenase, and epoxide hydrolase (141). Phase II reactions may occur by methylation, sulfonation, acetylation, glucuronidation, and glutathione conjugation. The associated enzymes include methyltransferases, sulfotransferases, N-acetyltransferases, uridine diphosphate-glucuronosyltransferase (UGT), and glutathione-S-transferase. Uptake transporters such as multispecific solute carrier, and efflux transporters such as multidrug-resistance protein mediate the entry and exit of xenobiotics respectively across the biological membrane.

In general, NCEs are one of the most studied xenobiotics because of their tendency to cause toxicity to humans and animals. Given that these novel bifunctional compounds that bind

AS are NCEs, it is important to determine their metabolic stability at this early stage of drug discovery and development.

Since previous studies have elucidated the metabolic pathway of the monomeric units (caffeine, nicotine, and 1-aminoindan) of these novel bifunctional compounds, a review of their metabolic pathways will be an excellent guide to understanding the metabolic fate of the novel bifunctional compounds.

2.10 Metabolic pathway of caffeine

Caffeine is also known as 1,3,7-trimethylxanthine, and it is almost completely metabolized with about 3% being excreted unchanged in urine (142). The major reaction involved in caffeine metabolism is demethylation. The metabolic pathway of caffeine is shown in Figure 2.2 (142, 143). The primary route of caffeine metabolism in humans is the CYP1A2 mediated N-3-demethylation to form paraxanthine which accounts for about 70-80% of metabolite formation (142). Previous *in vitro* metabolism studies using HLM suggest that N-1-demethylation to theobromine accounts for about 7-8% of caffeine metabolism and N-7- demethylation to form theophylline also accounts for about 7-8% of caffeine metabolism (142). The remaining 15% is contributed by the xanthine oxidase-mediated C8-hydroxylation to form the 1,3,7-trimethyluric acid (142).

CYP1A2 has been reported to be responsible for about 95% of caffeine metabolism, and therefore caffeine is used as a probe drug for monitoring CYP1A2 activity with the relative ratios of urinary metabolites used as an indicator of the flux through the metabolic pathway (142). It has been suggested that knowledge of the activity of such isozymes is of toxicological importance since it has been implicated in the biotransformation of certain chemicals to the reactive carcinogenic intermediates (143).

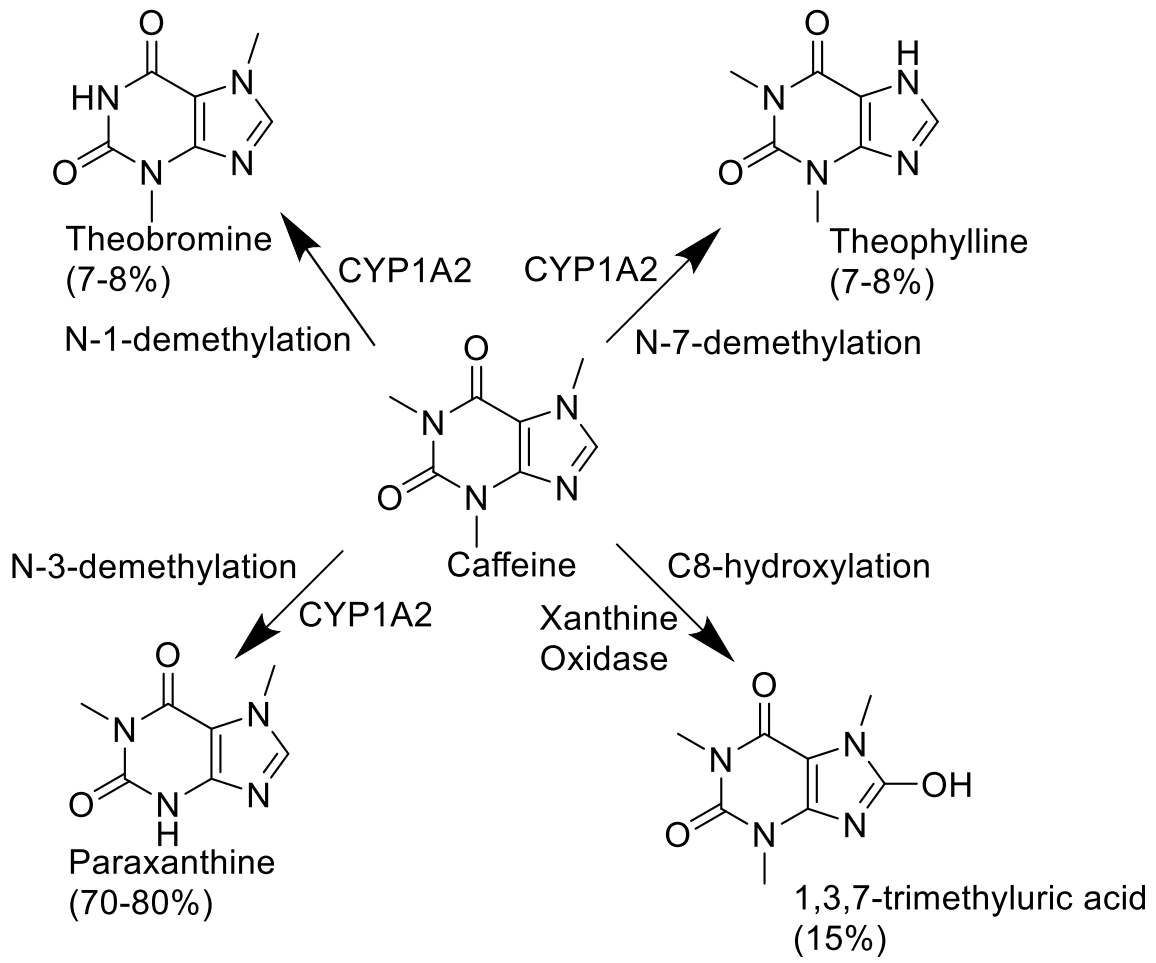

Figure 2.2 Primary metabolic pathway of caffeine.

Previous research reported that the major metabolites of caffeine in urine are paraxanthine, 1-methylxanthine, 1-methyluric acid, 5-acetylamino-6-formylamino-3-methyluracil, and 1,7-dimethyluric acid (144). These metabolites are formed by secondary metabolism of paraxanthine and are largely mediated by CYP1A2, CYP2A6, N-acetyl transferase 2, and xanthine oxidase (144). Previous *in vitro* studies have implicated CYP2E1 in the formation of theobromine and theophylline, whereas studies of recombinant proteins in microsomes do not support this but instead suggest that it contributes to the formation of 1,3,7-

trimethyluric acid (145, 146). Several microsomal metabolism studies have shown that CYP2C8, CYP2C9, and CYP3A4 are also involved in the primary metabolism of caffeine (145-147). Caffeine has a $t_{1/2}$ of 4 to 5 hours, and the $t_{1/2}$ may be prolonged by factors such as hepatic disease, age, and pregnancy (144).

2.11 Metabolic pathway of nicotine

Six primary metabolites of nicotine have been identified, and in most mammalian species, the most important metabolite of nicotine is the lactam derivative, cotinine (148). The metabolic pathway of nicotine is shown in Figure 2.3 (148, 149). In humans, about 70–80% of nicotine is converted to cotinine, and this biotransformation involves two steps. The first step involves the CYP2A6 mediated oxidation to produce nicotine-$\Delta^{1'(5')}$-iminium ion, which is in equilibrium with 5′-hydroxynicotine, while the second step involves a cytoplasmic aldehyde oxidase-mediated oxidation to form cotinine (148). It has been suggested that nicotine iminium ion could play a role in the pharmacology of nicotine since it is an alkylating agent (150). Nicotine N′-oxide is another primary metabolite of nicotine, accounting for about 4–7% of nicotine absorbed by smokers (151). The biotransformation of nicotine to nicotine N′-oxide involves a flavin-containing monooxygenase 3 (FMO3), which results in the formation of both possible diastereomers, the 1′-(R)-2′-(S)-cis and 1′-(S)-2′-(S)-trans-isomers in animals (149, 152). In humans, this pathway has been reported to be highly selective for the trans-isomer (149). Previous research has shown that only the trans-isomer of nicotine N′-oxide was detected in urine after administration of nicotine by intravenous infusion, transdermal patch or smoking (152). Nicotine-N-oxide does not appear to be further metabolized to any significant extent,

except by reduction back to nicotine in the intestines and this may lead to recycling nicotine in the body (151).

Oxidative N-demethylation of nicotine to nornicotine has been reported (148). A report from a study of the differences in nornicotine excretion in smokers during smoking and transdermal nicotine treatment shows that although nornicotine is a constituent of tobacco leaves, most urine nornicotine is derived from the metabolism of nicotine with less than 40% coming directly from tobacco (151). For most species, the N-demethylation pathway is a minor pathway in the metabolism of nicotine (148).

Additionally, 3′-hydroxycotinine has been reported to be the main nicotine metabolite detected in smokers' urine (148) which is also excreted as a glucuronide conjugate (151). 3′-hydroxycotinine and its glucuronide conjugate account for 40–60% of the nicotine dose in urine (151, 153). Previous studies have shown that the conversion of cotinine to 3′-hydroxycotinine in humans is highly stereoselective for the trans-isomer, as less than 5% is detected as *cis*-3′-hydroxycotinine in urine (154, 155). The only 3′-hydroxycotinine conjugate detected in urine is the O-glucuronide (153).

Hecht *et al*., reported a new pathway for the metabolism of nicotine (156). This pathway involves the cytochrome P450 mediated 2'-hydroxylation of nicotine to produce 4-(methylamino)-1-(3-pyridyl)-1-butanone with 2'-hydroxynicotine as an intermediate. 4-(methylamino)-1-(3-pyridyl)-1-butanone is also known as nicotine-derived nitrosamine ketone (NNK). 2′-hydroxynicotine is reduced to nicotine-Δ 1′ (2′) -iminium ion. 4-(methylamino)-1-(3-pyridyl)-1-butanone is further oxidized to 4-oxo-4-(3-pyridyl) butanoic acid and 4- hydroxy-4-(3-pyridyl) butanoic acid.

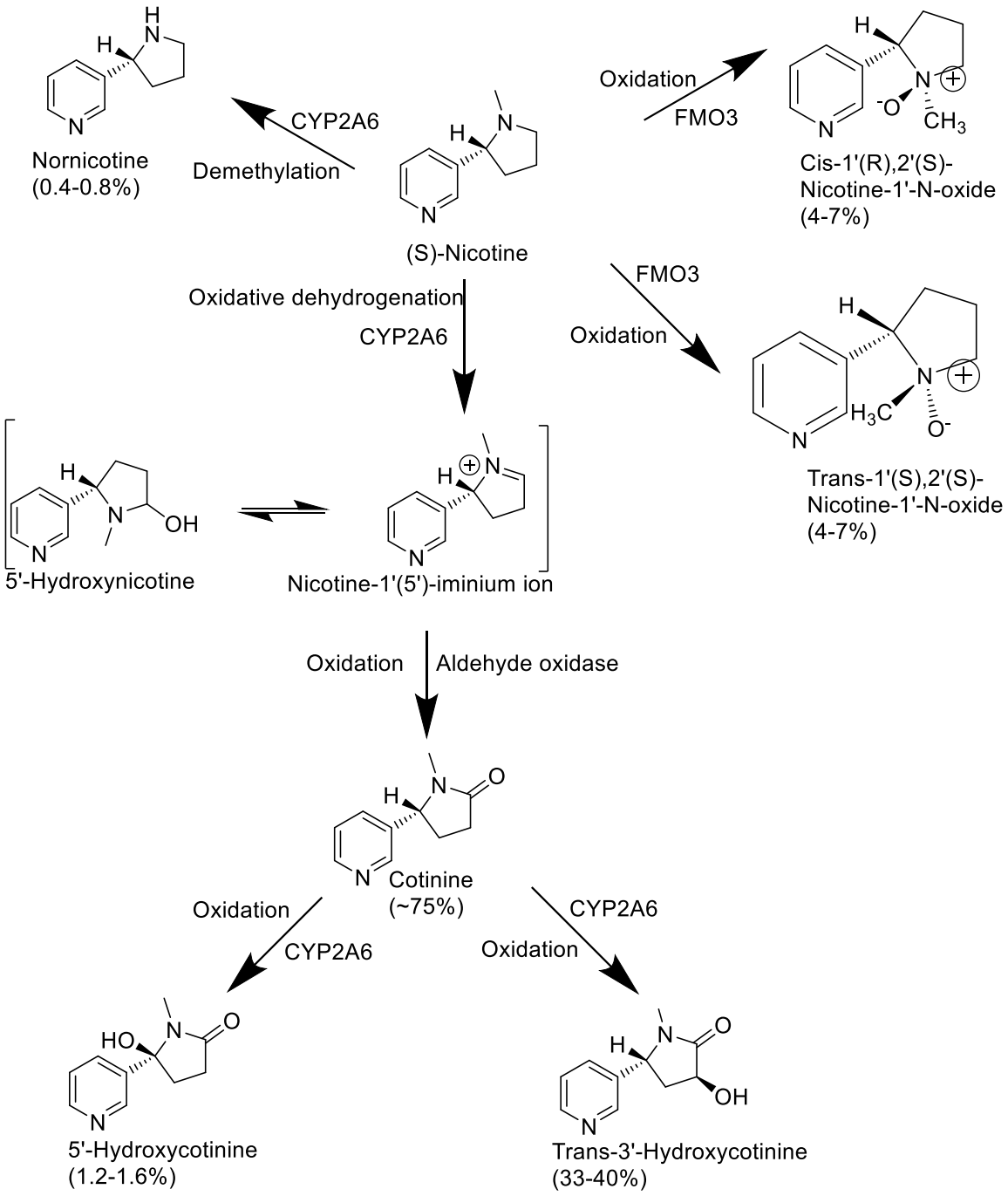

Figure 2.3 Primary metabolic pathway of nicotine.

This new pathway has been reported to be potentially significant since 4- (methylamino)-1-(3-pyridyl)-1-butanone can be converted to carcinogenic NNK(148). However,

endogenous production of NNK from nicotine has not been detected in humans or rats (157).

Additionally, nicotine also undergoes phase 2 metabolism, and these conjugation reactions are methylation and glucuronidation. The methylation of the pyridine nitrogen leads to the formation of nicotine isomethonium ion (also called N -methylnicotinium ion). About 3-5% of nicotine metabolism is accounted for by the glucuronidation pathway, and this reaction is mediated by UGT producing (S)-nicotine-N-β-glucuronide (148).

2.12 Metabolic pathway of 1-aminoindan

1-aminoindan has been identified as a metabolite of rasagiline (158). Rasagiline (N-propargyl-1(R)-aminoindan) is an irreversible inhibitor of monoamine oxidase-B which is usually used as a monotherapy in early PD and as a supplement in advanced PD to decrease off-time and improve the symptoms of PD in levodopa-treated patients with motor fluctuation (159, 160). The metabolism of rasagiline involves two main pathways which include N-dealkylation to yield 1-aminoindan and hydroxylation to yield 3-hydroxy-N-propargyl-1-aminoindan and 3-hydroxy-1-aminoindan (3-OH-AI) (161-163). The metabolic pathway of rasagiline is shown in figure 2.4 (164). CYP1A2 has been implicated as the major enzyme involved in the metabolism of rasagiline (161-163). Rasagiline also undergoes oxidative deamination to form indanone (164). Previous studies suggest that 1-aminoindan may contribute to the overall neuroprotective and antiapoptotic effects of rasagiline (128, 165-167). Furthermore, the hydroxylated metabolites of rasagiline may also have potential neuroprotective effects (168).

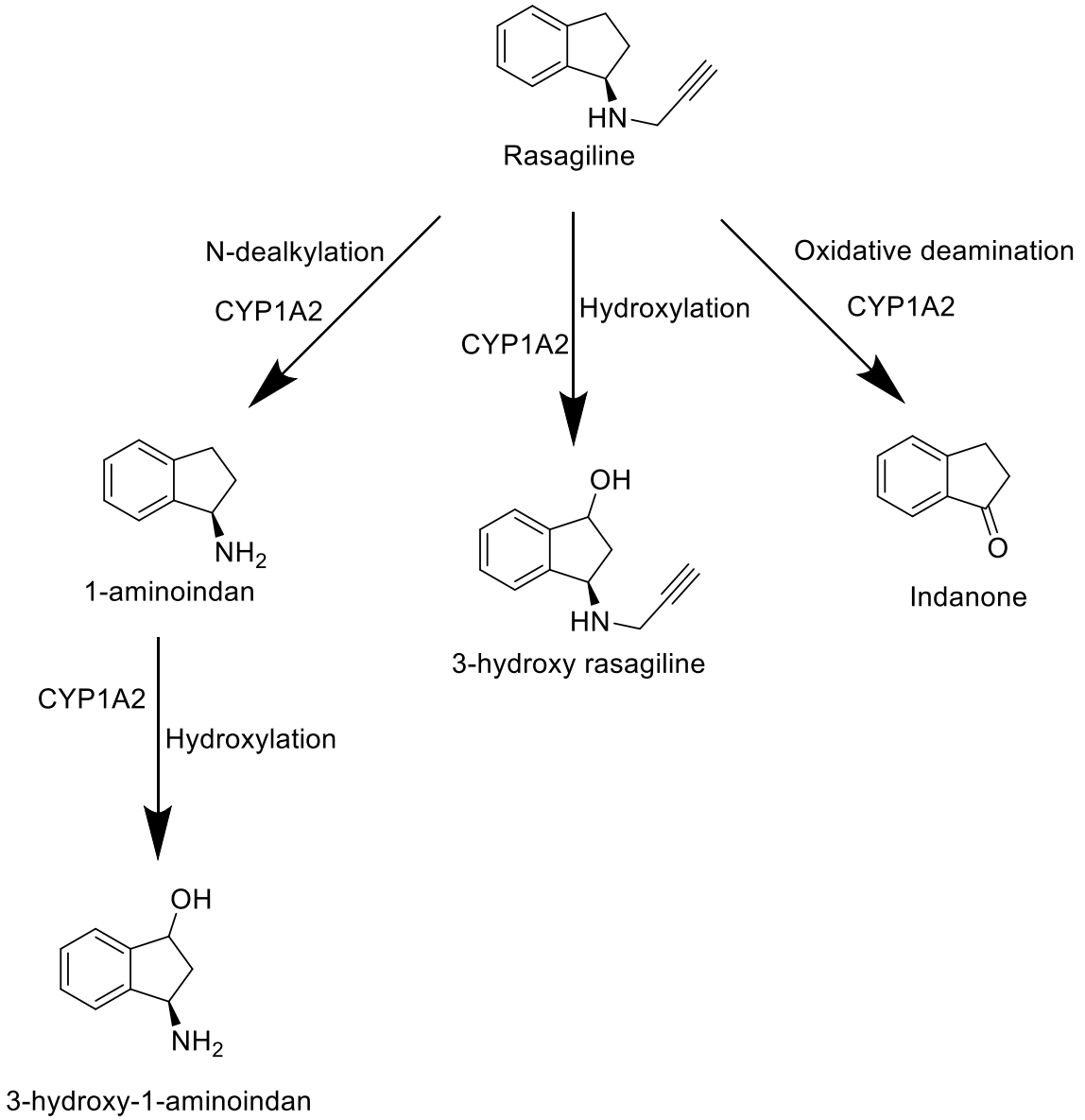

Figure 2.4 Metabolic pathway of rasagiline.

No information exists describing the metabolism of the three bifunctional compounds identified in previous studies for their ability to bind to AS or protect yeast cells from AS-induced toxicity. To establish the potential for using these compounds as therapeutic or diagnostic probes for PD, we are interested in determining their *in vitro* hepatic metabolism. An understanding of their metabolic profiles will guide us in the design of ^{18}F

labeled PET imaging probes and optimization of metabolic stability for treatment modalities.

2.13 Hypotheses

2.13.1 Hypothesis 1

Caffeine dissociation is the driving force in the tandem mass spectrometric fragmentation of C_8-6-C_8, C_8-6-N, and C_8-6-I.

2.13.1.1 Objective 1

1. To determine the tandem mass spectrometric fragmentation pathway of C_8-6-C_8, C_8-6-N, and C_8-6-I.

2.13.2 Hypothesis 2

C_8-6-C_8, C_8-6-N, and C_8-6-I undergo *in vitro* metabolism in HLM, MLM, and RLM.

2.13.2.1 Objective 2

To determine the metabolic profile of C_8-6-C_8, C_8-6-N, and C_8-6-I in HLM, MLM, and RLM.

3.0 Chapter Three: Tandem Mass Spectrometric Analysis of Novel Bifunctional Compounds for Parkinson's Disease

Chukwunonso K. Nwabufo, Anas El-Aneed, Ed S. Krol*

1. Drug Discovery and Development Research Group, College of Pharmacy and Nutrition, University of Saskatchewan, Saskatoon, SK

*Author to whom correspondence should be addressed
Dr. Ed S. Krol
Drug Discovery and Development Research Group
College of Pharmacy and Nutrition
University of Saskatchewan
Saskatoon, SK
Ph: 306-966-2011
ed.krol@usask.ca

Graphical Abstract

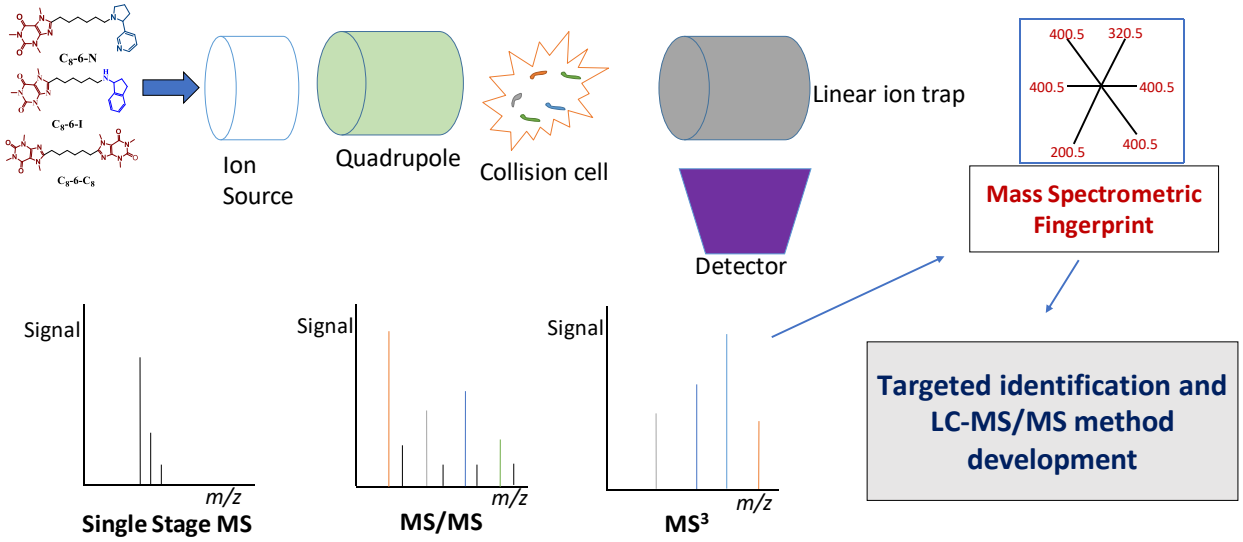

3.1 Abstract

Rationale

C_8-6-N, C_8-6-I, and C_8-6-C_8 are novel bifunctional compounds that are currently being investigated as therapeutics or diagnostics for Parkinson's disease (PD). In order to probe their biological activity, an appropriate analytical method is required. The goal of this study is to establish a tandem mass spectrometric (MS/MS) fingerprint for these bifunctional compounds.

Methods

Accurate mass measurement was performed using a hybrid quadrupole orthogonal time-of-flight mass spectrometer while multi-stage MS/MS and MS^3 analysis were conducted using a triple quadrupole-linear ion trap mass spectrometer. Both instruments are equipped with an electrospray ionization (ESI) source and were operated in the positive ion mode. The source and compound parameters were optimized for all tested bifunctional compounds.

Results

The MS/MS analysis indicates that the fragmentation of C_8-6-N and C_8-6-I is not driven by caffeine dissociation. A significant observation in our fragmentation of C_8-6-C_8 suggests that a previously reported loss of acetaldehyde during caffeine dissociation is instead a loss of CO_2.

Conclusion

The MS/MS analysis of these novel bifunctional compounds revealed diagnostic product ions and neutral losses (NLs) for all tested bifunctional compounds. The diagnostic product ions can be applied to the future development of liquid chromatography-multiple reaction monitoring (LC-MRM) methods for quantitative analysis while the diagnostic NLs can be used for targeted identification of these bifunctional compounds in biological matrices.

3.2 Introduction

Parkinson's disease (PD) is the second most common neurodegenerative disorder after Alzheimer's disease (2, 169-172). PD is associated with the progressive demise of dopamine-producing neurons in the substantia nigra (1, 173). Currently, there is no cure for PD, and accurate diagnosis can only be accomplished through post-mortem analysis; thus clinical misdiagnosis of PD is not uncommon (39, 174). Given these factors, the development of disease-modifying treatments, as well as early stage and differential diagnostic agents are important aspects of current PD research. One target under investigation for treatment and diagnosis of PD is alpha-synuclein (AS), a 140 amino acid intrinsically disordered protein that is known to aggregate and forms oligomeric species that are found in Lewy bodies of PD patients, suggesting they play a role in the pathophysiology of PD (32, 33). Our laboratory has focused on developing novel compounds that can interact with AS and ultimately prevent the pathological pathway that leads to PD. Recently, we reported that two bifunctional compounds composed of a caffeine scaffold attached to nicotine (C_8-6-N), and 1-aminoindan (C_8-6-I) (Figure 3.1) were the most promising candidates in preventing the pathological pathway that leads to PD (123). Although caffeine linked to caffeine (C_8-6-C_8) (Figure 3.1) did not show any therapeutic potential, it demonstrated the strongest binding to AS making it a suitable candidate for the development of imaging probes for PD diagnosis.

Given the therapeutic and diagnostic potentials of these novel bifunctional compounds, it is of great importance to conduct further preclinical studies at this early stage of drug discovery and development. The preclinical evaluation of the metabolic stability and

pharmacokinetics of these novel bifunctional compounds will provide useful information about their safety and efficacy.

Therefore, it is important to establish appropriate analytical methods for the qualitative and quantitative analysis of C_8-6-N, C_8-6-I, and C_8-6-C_8. Liquid chromatography coupled to tandem mass spectrometry (LC-MS/MS) has become an indispensable analytical tool for the identification, structural characterization, and quantitative analysis of pharmaceuticals (175-180). The characterization of new chemical entities (NCEs) using MS can be achieved through accurate mass measurement and collision-induced dissociation tandem mass spectrometric (CID-MS/MS) analysis.

The elucidation of CID-MS/MS fragmentation pathways for NCEs allows for the unambiguous confirmation of their structure, as well as identification of diagnostic product ions and neutral losses (NLs), which can subsequently be used for quantitative and qualitative analysis, respectively. NL can also be used in the identification of known and unknown metabolites in biological and non-biological matrices. For example, Bourcier *et al*., used diagnostic NLs identified from the fragmentation of 28 neurotransmitters and related compounds (181-185) to identify expected and unexpected metabolites in biological fluids (181). Additionally, Bourcier *et al*., used diagnostic NLs for the unambiguous differentiation of isomers, as well as the identification and localization of functional groups (186). In addition, CID-MS/MS analysis allows for the selection of diagnostic quantifier and qualifier ions for the development of multiple reaction monitoring (MRM) quantitative methods. For instance, a generalized MS/MS fingerprint was developed for a series of structurally similar novel drug delivery agents, namely gemini surfactants (187-189). Subsequently, the established CID-MS/MS fingerprint was used to

develop a targeted MS method for the quantification of these compounds within a cellular lysate (190-192).

In this present study, we evaluated the CID-MS/MS fragmentation behaviour of three novel bifunctional compounds, specifically designed for PD. Each bifunctional compound consists of a caffeine scaffold attached to nicotine (C_8-6-N), 1-aminoindan (C_8-6-I) or caffeine (C_8-6-C_8) through a six-carbon alkyl chain (Figure 3.1).

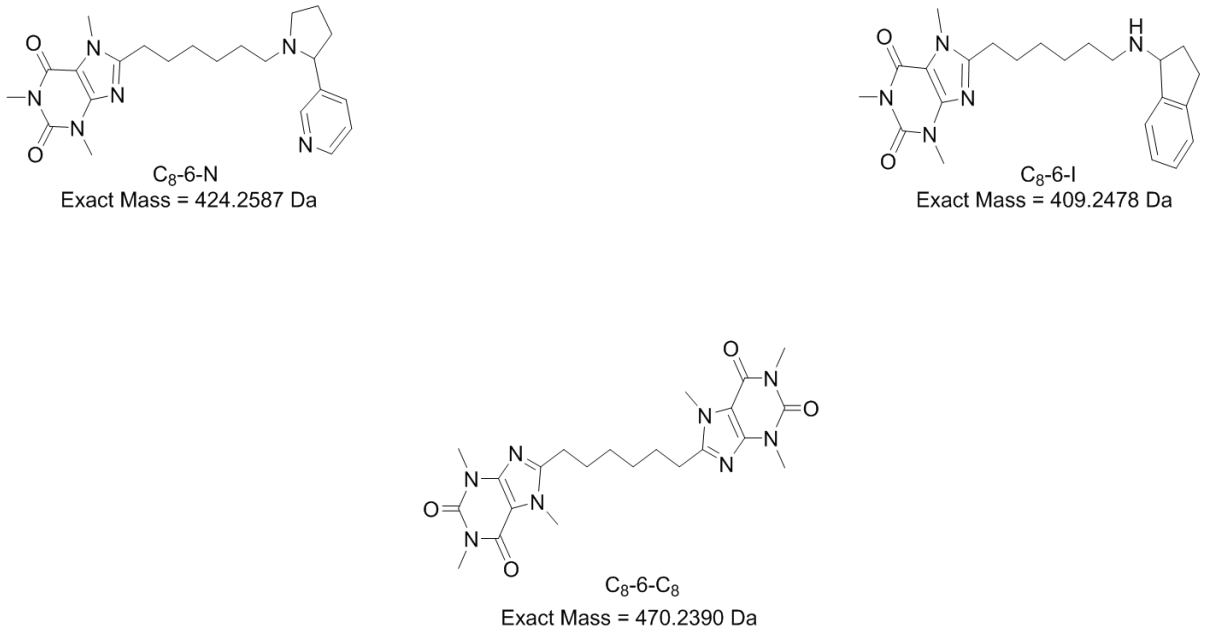

Figure 3.1 Structure of novel bifunctional compounds.

3.3 Material and Methods

3.3.1 Materials

C_8-6-I, C_8-6-N, and C_8-6-C_8 were synthesized according to a previously established protocol in our laboratory (123). Acetonitrile (HPLC grade purity), methanol (HPLC grade purity), chloroform, and formic acid (LC-MS grade purity) were purchased from Fisher

Scientific (Fairlawn, NJ) while water was filtered using a Millipore, MilliQ system with a Quantum EX cartridge (Mississauga, ON).

3.3.2 Sample preparation

Stock solutions of 0.1 mg/mL C_8-6-I and C_8-6-N were prepared in 100% methanol while 0.1 mg/mL C_8-6-C_8 was prepared in 100% chloroform and stored at -80^{o}C. Subsequently, stock solutions of C_8-6-I and C_8-6-N were diluted 1000x and 10x respectively in 50:50 acetonitrile/water containing 0.1% LC-MS formic acid while stock solutions of C_8-6-C_8 were diluted 5x in acetonitrile containing 0.1% LC-MS formic acid.

3.3.3 Mass spectrometric analysis

3.3.3.1 Single-stage MS analysis

Bifunctional compounds were analyzed using an AB SCIEX QSTAR XL quadrupole orthogonal time-of-flight hybrid mass spectrometer (QqToF-MS) equipped with electrospray ionization (ESI) source (AB SCIEX, Redwood City, CA, USA). Nitrogen was used as the ESI nebulizing and drying gas. The instrument was calibrated with a two-point external calibration using cesium iodide (CsI, *m/z* 132.9049, Sigma-Aldrich, Oakville, ON, Canada) and sex pheromone inhibitor iPD1 (*m/z* 829.5393, Bachem Bioscience Inc., PA, USA). Samples were directly infused into the mass spectrometer at a flow rate of 10 µL/min using an integrated Harvard syringe pump through a Turbo ionspray source with a needle voltage of 5500 V. The mass spectrometer was operated in the positive ion mode with declustering potential of 40 V and focusing potential of 120 V.

3.3.3.2 MS/MS analysis

Tandem mass spectrometric analysis was conducted using an AB SCIEX QTRAP 4000 hybrid triple quadrupole-linear ion trap mass spectrometer (QqLIT-MS) equipped with a

'Turbo V Ion spray' ESI source (AB SCIEX, Redwood City, CA, USA). Nitrogen was used as the collision gas for CID-MS/MS. The instrument was operated in the positive ion mode with an optimized declustering potential of 40 V for each compound. The collision energy (CE) was also optimized and set at 55 eV for C_8-6-C_8, 50 eV for C_8-6-N and 22 eV for C_8-6-I. The optimized CEs were sufficient to induce fragmentation while the precursor ion remained abundant. Subsequently, aliquots of the samples were directly infused into the instrument at a flow rate of 10 µL/min by using a Model 11 Plus Syringe Pump (Harvard Apparatus, Holliston, MA, USA). The ionspray voltage was set at 5500 V with the source temperature set at 200^{o}C.

The MS/MS analysis of each compound was also performed using the QSTAR. The MS/MS spectra obtained from both instruments is similar; however, the MS/MS spectra obtained from the QTRAP provided more information.

3.3.3.3 Multi-stage MS^3 analysis

MS^3 analysis of the selected product ions was performed on the AB SCIEX QTRAP 4000 instrument under the same optimized conditions described above. The excitation energy was optimized to obtain sufficient product ions. The excitation energy ranged from 150 V - 190 V for C_8-6-I, 130 V - 175 V for C_8-6-N, and 115 V - 185 V for C_8-6-C_8.

3.4 Results and Discussion

3.4.1 Single-stage MS analysis

The full scan ESI-QqToF-MS spectra (Figure A.1, Appendix A) of all three bifunctional compounds showed an abundant singly charged precursor ion $[M+H]^+$ (C_8-6-N: *m/z* 425.2660; C_8-6-I: *m/z* 410.2551; and C_8-6-C_8: *m/z* 471.2468). The exact mass measurement analysis revealed mass accuracies of less than 2 ppm (Table A.1, Appendix A), hence

confirming the expected molecular structures. These mass accuracies were comparable to the results obtained from previous structural work in which external calibration was utilized on the QSTAR system (193).

3.4.2 MS/MS analysis

Since all three investigated compounds contain a common backbone structure composed of caffeine with a six carbon alkyl linker attached through the C8 position of caffeine (Figure 3.2), we hypothesized that caffeine dissociation would be the driving force during MS/MS analysis of these bifunctional compounds; however, this was not the observed case. We noticed that all three bifunctional compounds have distinct fragmentation patterns and dissociation of the caffeine moiety is only a minor pathway in the fragmentation of C_8-6-N and C_8-6-I. Interestingly, the dissociation of the caffeine moieties of C_8-6-C_8 required a high CE of 55 eV compared to the relatively low CE required for the dissociation of C_8-6-N (50 eV) and C_8-6-I (22 eV). In fact, if CE of 55 eV is applied for C_8-6-N and C_8-6-I, the ion is completely depleted indicating differential stability among the bifunctional compounds. In other words, caffeine is more stable than nicotine and 1-aminoindan, so fragmentation of the nicotine and 1-aminoindan moieties is the driving force during MS/MS analysis of C_8-6-N and C_8-6-I respectively. Furthermore, the fragmentation pathway of C_8-6-N and C_8-6-I shows only a few product ions originating from caffeine dissociation. On the contrary, the fragmentation pathway of C_8-6-C_8 consists of only product ions originating from caffeine dissociation. This suggests to us that when incorporated into these bifunctional compounds, the caffeine moiety may be more stable to fragmentation than either the nicotine or 1-aminoindan moieties. The fragmentation of the nicotine and 1-aminoindan moieties occurs primarily in a saturated, unconjugated

region, whereas caffeine possesses more extensive conjugation. This extensive conjugation and accompanying resonance effects for caffeine may be responsible for attenuating fragmentation. Hence, in the presence of nicotine or 1-aminoindan, caffeine dissociation in these bifunctional compounds is minor.

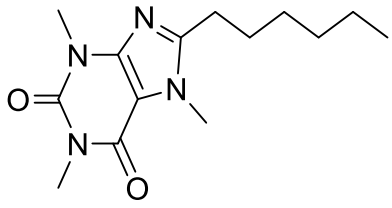

C_8-6

Exact Mass = 278.1743 Da

Figure 3.2 Backbone structure of all three bifunctional compounds.

Furthermore, MS^3 analysis (Figure A.2, Appendix A) revealed the genesis of the product ions observed in the MS/MS spectrum of the investigated bifunctional compounds. For ease of representation, the observed product ions were classified as initial product ions followed by ions designated as first, second, and third cohort ion groups. The first cohorts are product ions originating directly from the precursor ions, and subsequent dissociation (MS^3 analysis) of some of the first cohort ions gives rise to second cohort ions. MS^3 analysis of those designated as second cohort ions gives rise to third cohort ions. However, product ions not found on the MS^3 spectrum of the first, second, and third cohorts are called initial product ions.

Moreover, the fragmentation reaction mechanism for most of the product ions involves two or three steps with an intermediate product ion which undergoes further dissociation to give

the projected product ion. The intermediate product ions are also present in the MS/MS spectrum.

The following systematic method for identifying product ions is used in this study: the first cohort product ions are labeled with alphanumeric characters (for example **A2**), second cohort product ions with alphanumeric and numeric in superscript (for example **A2^{1}**), third cohort product ions with alphanumeric and numeric-plus sign in superscript (for example **A2^{1+}**), and those initial product ions that are not found in the MS^3 spectrum of the first, second, and third cohort product ions are labeled with numbers (for example **1**). The detailed tandem mass spectrometric fragmentation behaviour of these bifunctional compounds is described below.

3.4.2.1 MS/MS analysis of C_8-6-C_8

The MS/MS spectrum, as well as the proposed fragmentation pathway for C_8-6-C_8 are shown in Figure 3.3A and B.

A

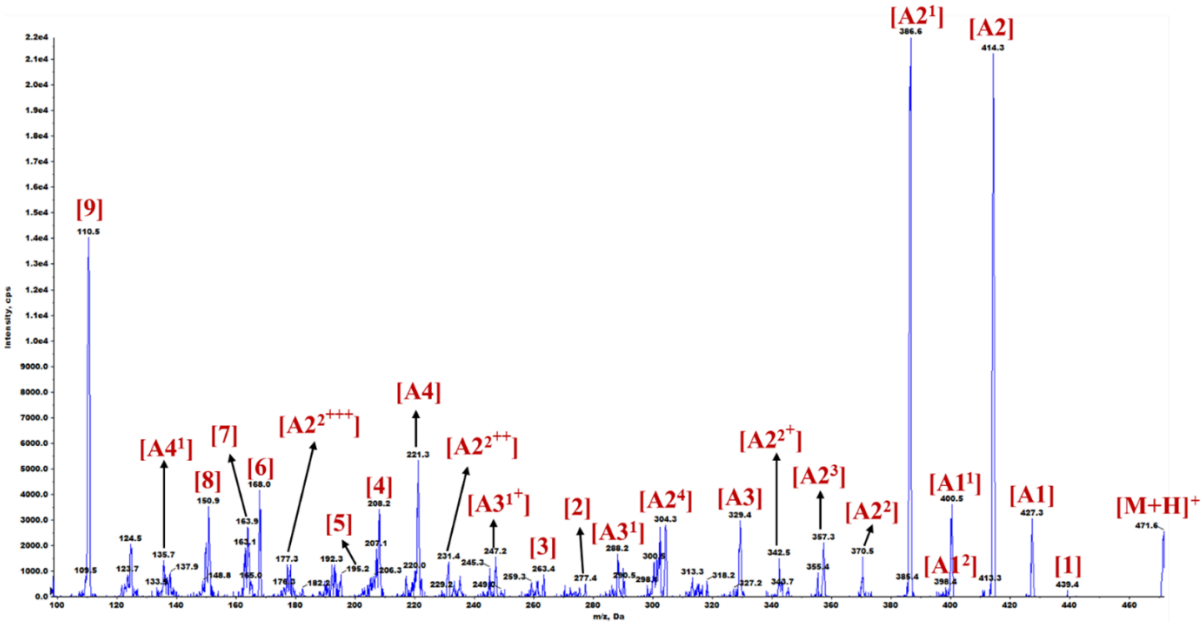
[A2¹]
386.6
[A2]
414.3
[9]
110.5
[A4¹]
[7]
[8]
[6]
[A2²⁺⁺⁺]
[A4]
[A2²⁺⁺]
[A3¹⁺]
[5]
[4]
[2]
[A3¹]
[3]
[A2⁴]
[A3]
[A2²⁺]
[A2³]
[A2²]
[A1¹]
[A1²]
[A1]
[1]
[M+H]⁺
471.6
Intensity, cps
m/z, Da

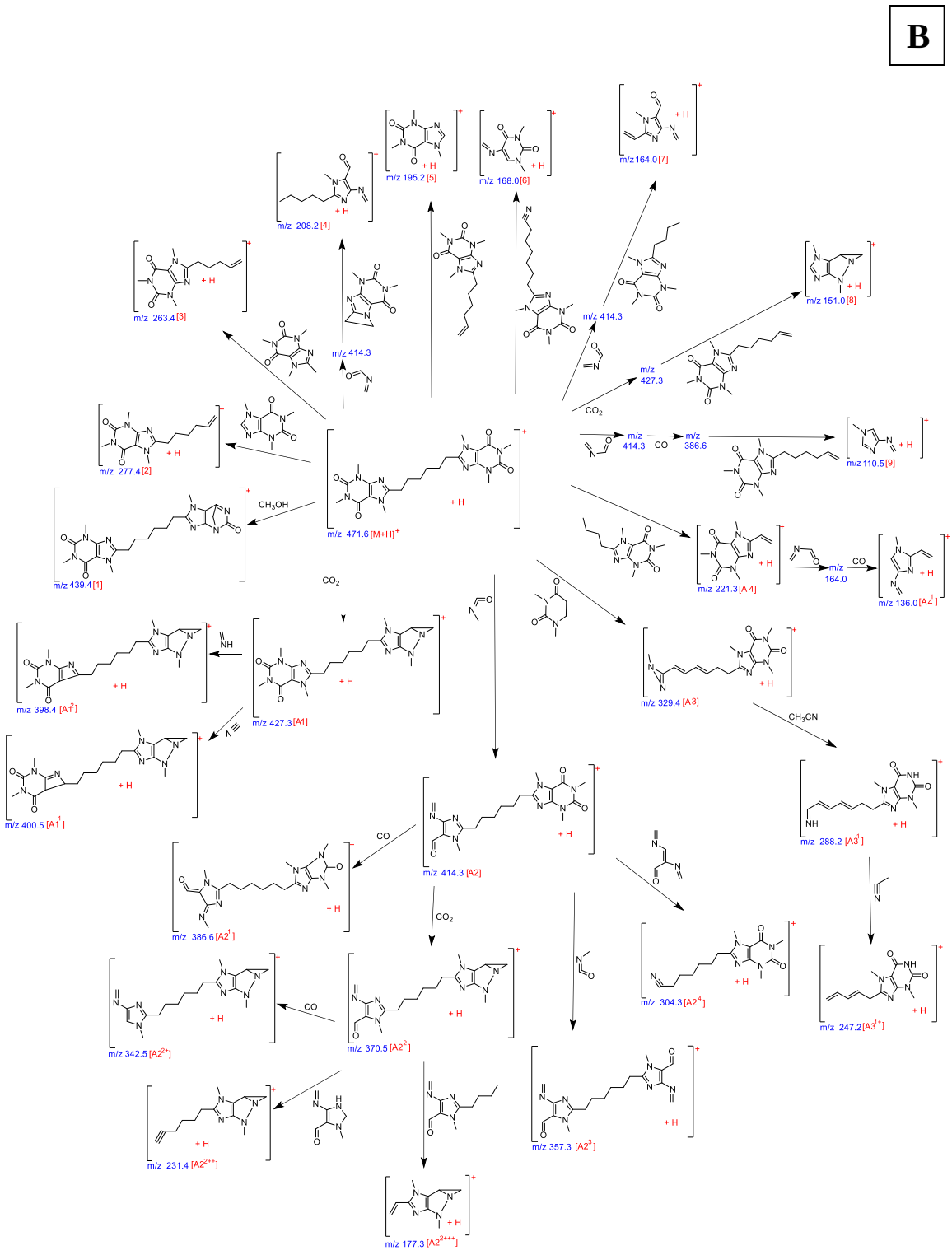

Figure 3.3 MS/MS spectrum of C_8-6-C_8 (A) and the proposed fragmentation pathway for C_8-6-C_8 (B).

The MS/MS analysis of the singly charged $[M+H]^+$ ion of C_8-6-C_8 gave rise to four first cohort product ions with each having their distinct dissociation pathway. Product ion **A1** (*m/z* 427.3) is derived from a ring contraction with a NL of carbon dioxide (CO_2, 44 Da). Interestingly, a previous study that investigated the fragmentation pattern of caffeine reported that a NL of acetaldehyde is associated with the ring contraction of caffeine (194). The loss of acetaldehyde is logical; however, our accurate mass measurement study suggests that the ring contraction of the caffeine moiety of C_8-6-C_8 is associated with a NL of carbon dioxide and the mass error of the corresponding product ion (**A1**) is 1.6384 ppm (Table A.2, Appendix A) compared to a mass error of -85.2020 ppm for the loss of acetaldehyde. Therefore, we proposed a new mechanism for the loss of carbon dioxide from the caffeine moiety of C_8-6-C_8 (Figure 3.4A). In the initial step, one of the O-carbonyl atoms attacks the carbonyl-C to form a carbamate along with ring opening and formation of an aziridine as shown in Figure 3.4A. Expulsion of carbon dioxide from the aziridine-carbamate occurs resulting in the observed product ion (**A1**). The theoretical mechanistic loss of acetaldehyde from the caffeine moiety of C_8-6-C_8 is shown in Figure 3.4B. Methyl migration to the carbonyl carbon occurs concurrently with hydrogen capture from N-CH_3 followed by bond formation between CH_2 and N, as well as N-N bond formation (Figure 3.4B).

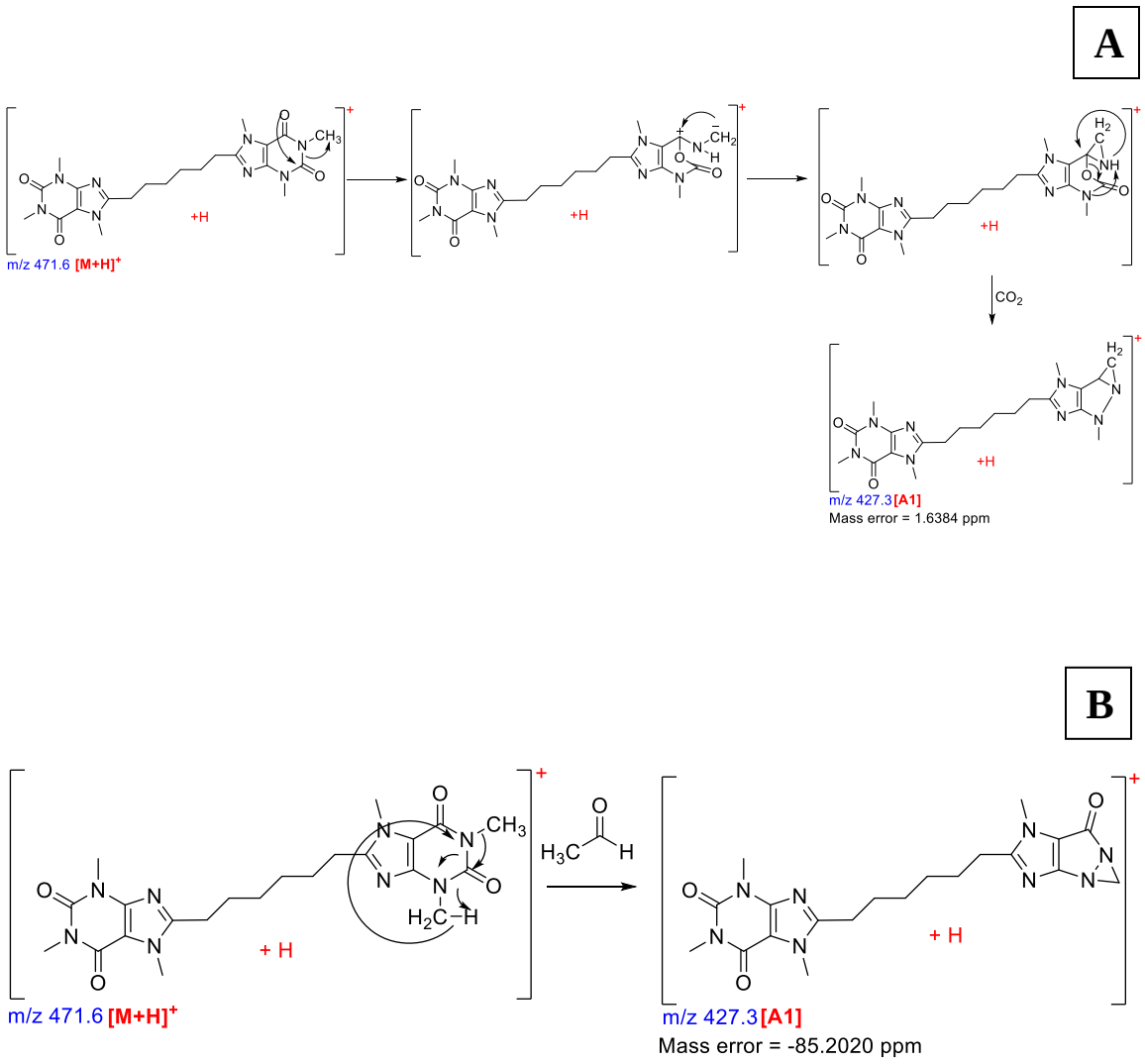

Figure 3.4 The proposed mechanism for the loss of carbon dioxide from C_8-6-C_8 (A) and loss of acetaldehyde from C_8-6-C_8 (B).

Product ion **A2** (*m/z* 414.3) is the result of a retro-Diels-Alder (RDA) rearrangement with a NL of methyl isocyanate (O=C=NCH_3, 57 Da), which is in agreement with the previously reported fragmentation mechanism of caffeine (194). Product ion **A3** (*m/z* 329.4) results from the NL of 1, 3-dimethyl-5, 6-dihydrouracil ($C_6H_{10}N_2O_2$, 142 Da) while product ion **A4** (*m/z* 221.3) arose from the NL of 8-butyl-1, 3, 7-trimethylpurine-2, 6-dione ($C_{12}H_{18}N_4O_2$, 250 Da) as shown in Figure 3.3B.

Product ions **A1**-**A4** each undergo additional dissociation which as confirmed by MS^3 analysis (Figure A.2A, Appendix A) give second cohort product ions. **A1** is further dissociated to form ions $\mathbf{A1^1}$ (*m/z* 400.5) and $\mathbf{A1^2}$ (*m/z* 398.4) due to the NL of hydrogen cyanide (27 Da) and methanimine (CH_3N, 29 Da), respectively. The elimination of carbon monoxide (CO, 28 Da) from **A2** (*m/z* 414.3) leads to the formation of $\mathbf{A2^1}$ (*m/z* 386.6) while the ion observed at *m/z* 370.5 ($\mathbf{A2^2}$) is the result of an inner ring breakage with the NL of carbon dioxide (CO_2, 44 Da) from **A2**, similar to the mechanism explained in Figure 3.4A. On the other hand, further dissociation of **A2** gives rise to the ions observed at *m/z* 357.3 ($\mathbf{A2^3}$) and *m/z* 304.3 ($\mathbf{A2^4}$) through an RDA with the concomitant loss of methyl isocyanate ($O=C=NCH_3$, 57 Da), and a NL of $C_5H_6N_2O$ (110 Da) respectively as shown in Figure 3.3B. In the case of **A3**, it dissociates at the end of the linker region and caffeine moiety eliminating acetonitrile (CH_3CN, 41 Da) to yield the ion observed at *m/z* 288.2 ($\mathbf{A3^1}$). The formation of $\mathbf{A4^1}$ from **A4** involves two steps: first, the rearrangement of **A4** through an RDA reaction results in the formation of the intermediate ion at *m/z* 164 (**7**) (Figure 3.3A) due to the NL of methyl isocyanate ($O=C=NCH_3$, 57 Da). This is followed by the elimination of carbon monoxide (CO, 28 Da) from the ion at *m/z* 164.0 (**7**) giving rise to the product ion at *m/z* 136.0 ($\mathbf{A4^1}$) as shown in Figure 3.3B.

Furthermore, some of the second cohort product ions undergo further dissociation to third cohort product ions. For example, the elimination of carbon monoxide (CO, 28 Da) from $\mathbf{A2^2}$ leads to the formation of the ion ($\mathbf{A2^{2+}}$) at *m/z* 342.5. While the loss of $C_6H_9N_3O$ (139 Da) from $\mathbf{A2^2}$ gives rise to the ion ($\mathbf{A2^{2++}}$) at *m/z* 231.4, the ion ($\mathbf{A2^{2+++}}$) at *m/z* 177.3 originated from the loss of $C_{10}H_{15}N_30$ (193 Da) from $\mathbf{A2^2}$. Additionally, the loss of

acetonitrile (C_2H_3N, 41 Da) from **A3^1** gives rise to the ion (**A3^{1+}**) at *m/z* 247.2. These losses are self-explanatory including repeating mechanisms and are shown in figure 3.3B.

The following product ions were found to originate directly from the precursor ion since they were not observed during MS^3 analysis (Figure A.2A, Appendix A). The product ion designated as **1** observed at *m/z* 439.4 is due to the NL of methanol (CH_3OH, 32 Da) from the precursor ion (Figure 3.3B), which is in agreement with a previously reported fragmentation mechanism for caffeine (194). We have proposed a mechanism for the loss of methanol from the caffeine moiety of C_8-6-C_8 (Figure 3.5). In the initial step, carbonyl oxygen captures an adjacent N-methyl followed by the capture of hydrogen from CH_3 with intramolecular cyclization. Furthermore, the ions labeled **2** and **3** with *m/z* 277.4 and 263.4 respectively are generated from the NL of caffeine ($C_8H_{10}N_4O_2$, 194 Da) and 1-methylcaffeine ($C_9H_{12}N_4O_2$, 208 Da) from the precursor ion respectively (Figure 3.3B).

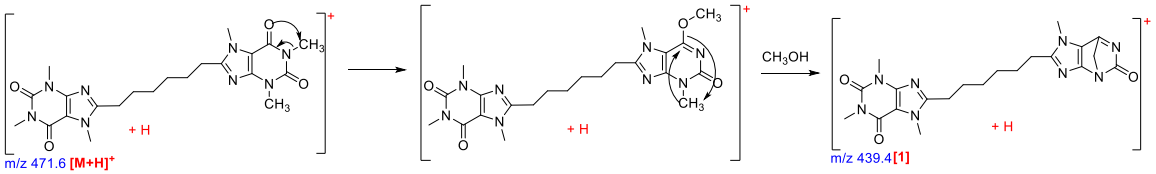

Figure 3.5 Proposed mechanism for the loss of methanol form C_8-6-C_8.

The NL of methyl isocyanate (O=C=NCH_3, 57 Da) from the precursor ion at *m/z* 471.6 gives an intermediate product ion observed at *m/z* 414.3 (**A2**) (Figure 3.3A). The subsequent loss of $C_9H_{10}N_4O_2$ (206 Da) from the intermediate product ion results in the formation of the product ion (**4**) with *m/z* 208.2 (Figure 3.3B). In addition, the ions designated **5** and **6** at *m/z* 195.2 and *m/z* 168.0 are derived from the elimination of the backbone structure ($C_{14}H_{22}N_4O_2$, 278 Da) and the backbone structure containing a cyanide

moiety ($C_{15}H_{21}N_5O_2$, 303 Da), respectively, from the precursor ion (Figure 3.3B). Three other dissociation mechanisms, each involving a two or three -step reaction generated ions with *m/z* 164.0 (**7**), 151.0 (**8**), and 110.5 (**9**). The ion (**7**) at *m/z* 164.0 is generated from the precursor ion at *m/z* 471.6 through an RDA rearrangement with the loss of methyl isocyanate ($O=C=NCH_3$, 57 Da) to give an intermediate product ion at *m/z* 414.3 (**A2**) (Figure 3.3A) followed by the loss of 8-butyl-1, 3, 7-trimethylpurine-2, 6-dione ($C_{12}H_{18}N_4O_2$, 250 Da) as shown in Figure 3.3B. Furthermore, the ion (**8**) at *m/z* 151.0 is directly derived from the precursor ion through the loss of carbon dioxide (CO_2, 44 Da) to give an intermediate product ion at *m/z* 427.3 (**A1**) (Figure 3.3A), followed by the loss of $C_{14}H_{20}N_4O_2$ (276 Da) from the intermediate product ion. The ion (**9**) at *m/z* 110.5 is generated from the precursor ion through an RDA rearrangement with the loss of methyl isocyanate ($O=C=NCH_3$, 57 Da) to give the first intermediate product ion with *m/z* 414.3 (**A2**) (Figure 3.3A), followed by the elimination of carbon monoxide (CO, 28 Da) to give a second intermediate product ion at *m/z* 386.6 (**A2^1**) (Figure 3.3A) and an additional loss of $C_{14}H_{20}N_4O_2$ (276 Da) as shown in Figure 3.3B. The diagnostic NLs associated with the dissociation of C_8-6-C_8 are shown in Table A.5, Appendix A.

3.4.2.2 MS/MS analysis of C_8-6-N

The MS/MS spectrum, as well as the proposed fragmentation pathway for C_8-6-N are shown in Figure 3.6A and B. The proposed structure of most of the product ions for C_8-6-N was confirmed using accurate mass measurement, showing a mass error of less than 9 ppm (Table A.3, Appendix A). The fragmentation of the singly charged $[M+H]^+$ ion of C_8-6-N gave rise to two first cohort product ions (Figure 3.6B) that emanated from the cleavage of the nicotine portion of C_8-6-N. **B1** and **B2** ions with *m/z* 346.4 and *m/z* 332.4

resulted from the NL of pyridine (C_5H_5N, 79 Da) and beta-picoline (C_6H_7N, 93 Da) respectively from the precursor ion as shown in Figure 3.6B. The NL of pyridine is in agreement with the previously reported fragmentation mechanism of nicotine (195). However, the authors did not observe a neutral loss of beta-picoline from the dissociation of nicotine (195). This may be because the authors used a different instrument, Linear Trap Quadrupole-Orbitrap hybrid mass spectrometer.

These two first cohort product ions undergo further dissociation to give second cohort product ions. The product ion at *m/z* 346.4 (**B1**: Figure 3.6A) gave rise to three other product ions at *m/z* 277.3 (**B1^1**), 275.3 (**B1^2**), and 207.2 (**B1^3**) (Figure 3.6A). While the ion (**B1^1**) at *m/z* 277.3 arose from the loss of 2, 3-dihydro-1H-pyrrole (C_4H_7N, 69 Da) from **B1** (Figure 3.6B), the ion (**B1^2**) at *m/z* 275.3 was derived from the loss of pyrrolidine (C_4H_9N, 71 Da) from **B1**. Finally, the loss of 1-pentyl-2, 3-dihydropyrrole ($C_9H_{17}N$, 139 Da) from **B1** yielded the product ion (**B1^3**) with *m/z* 207.2. The product ion at *m/z* 332.4 (**B2**) generated the product ion (**B2^1**) at *m/z* 263.2 as a result of the loss of C_4H_7N (69 Da), as shown in Figure 3.6B.

The other observed product ions originated directly from the fragmentation of the precursor ion at *m/z* 425.3 as they were not found in the MS^3 analysis (Figure A.2B, Appendix A) of the first, second, and third cohort product ions. The ion (**1**) at *m/z* 306.4 arose from the loss of 3-(1-propenyl) pyridine (C_8H_9N, 119 Da) from the precursor ion, while the loss of 3-(1-ethylpyrrolidin-2-yl) pyridine ($C_{11}H_{16}N_2$, 176 Da) from the precursor ion gave rise to the product ion (**2**) at *m/z* 249.3 (Figure 3.6B). The ion at *m/z* 220.4 (**3**) originated from a fragmentation reaction involving two steps: the loss of nornicotine ($C_9H_{12}N_2$, 148 Da) from the precursor ion to give an intermediate product ion at *m/z* 277.3 (**B1^1**) (Figure 3.6A)

followed by the loss of methyl isocyanate ($O=C=NCH_3$, 57 Da) through an RDA (Figure 3.6B). The ion (**4**) at *m/z* 195.1 originated from the loss of $C_{15}H_{22}N_2$ from the precursor ion as shown in Figure 3.6B. The other three product ions at *m/z* 168.2(**5**), 136.0(**6**), and 132.0(**7**) were derived from the precursor ion by the loss of $C_{16}H_{23}N_3$ (257 Da), $C_{14}H_{19}N_5O_2$ (289 Da), and $C_{14}H_{23}N_5O_2$ (293 Da), respectively. These losses are shown in Figure 3.6B. It is interesting to note that only (**3**) and (**5**) are derived from dissociation of caffeine, indicating that nicotine is the driving force in the dissociation of C_8-6-N. Furthermore, the ion (**8**) at *m/z* 130.0 was generated through a two-step process: loss of $C_{14}H_{23}N_5O_2$ (293 Da) from the precursor ion to generate an intermediate ion with *m/z* 132.0 (**7**) (Figure 3.6A) followed by the loss of molecular hydrogen (H_2, 2 Da) from the intermediate product ion (Figure 3.6B). Meanwhile, the major product ion (**9**) at *m/z* 120.0 (Figure 3.6A) was derived from the precursor ion by the loss of $C_{15}H_{23}N_5O_2$ (305 Da) while the ion (**10**) at *m/z* 110.5 originated from a two-step reaction involving the loss of pyridine (C_5H_5N, 79 Da) from the precursor ion to form an intermediate product ion at *m/z* 346.4 (**B1**) (Figure 3.6A) followed by the loss of 1, 3, 7-trimethyl-8-propylpurine-2, 6-dione ($C_{11}H_{16}N_4O_2$, 236 Da) from the intermediate product ion as shown in Figure 3.6B. The loss of $C_{16}H_{25}N_5O_2$ (319 Da) from the precursor ion gives rise to the product ion at *m/z* 106.0 (**11**). In agreement with our results, the product ions with *m/z* 132.0 (**7**), 130.0 (**8**), 120.0 (**9**), and 106.0 (**11**) (Figure 3.6A) have all been previously reported for the fragmentation of nicotine (195). The diagnostic NLs associated with the dissociation of C_8-6-N are shown in Table A.5, Appendix A.

A

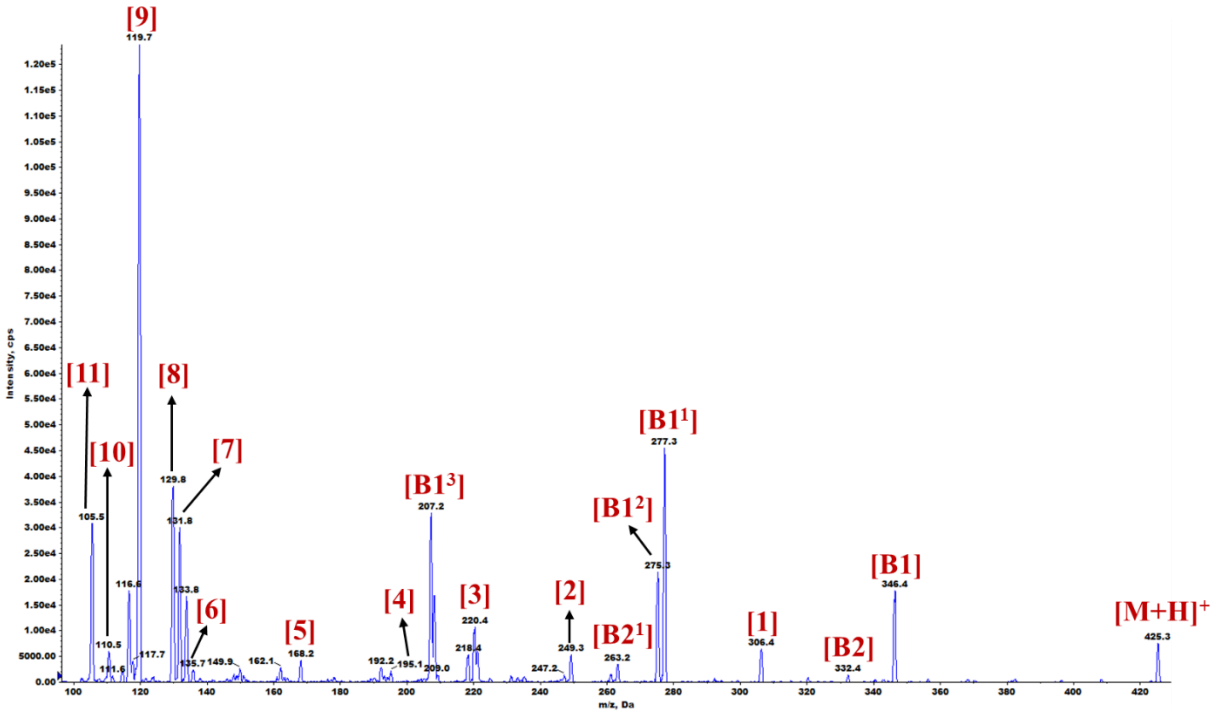
[9]
119.7
[11]
105.5
[8]
129.8
[10]
110.5
[7]
131.8
[B1³]
207.2
[B1¹]
277.3
[B1²]
275.3
[B1]
346.4
[M+H]⁺
425.3
[6]
[5]
168.2
[4]
[3]
220.4
[2]
249.3
[B2¹]
263.2
[1]
306.4
[B2]
332.4
Intensity, cps
m/z, Da

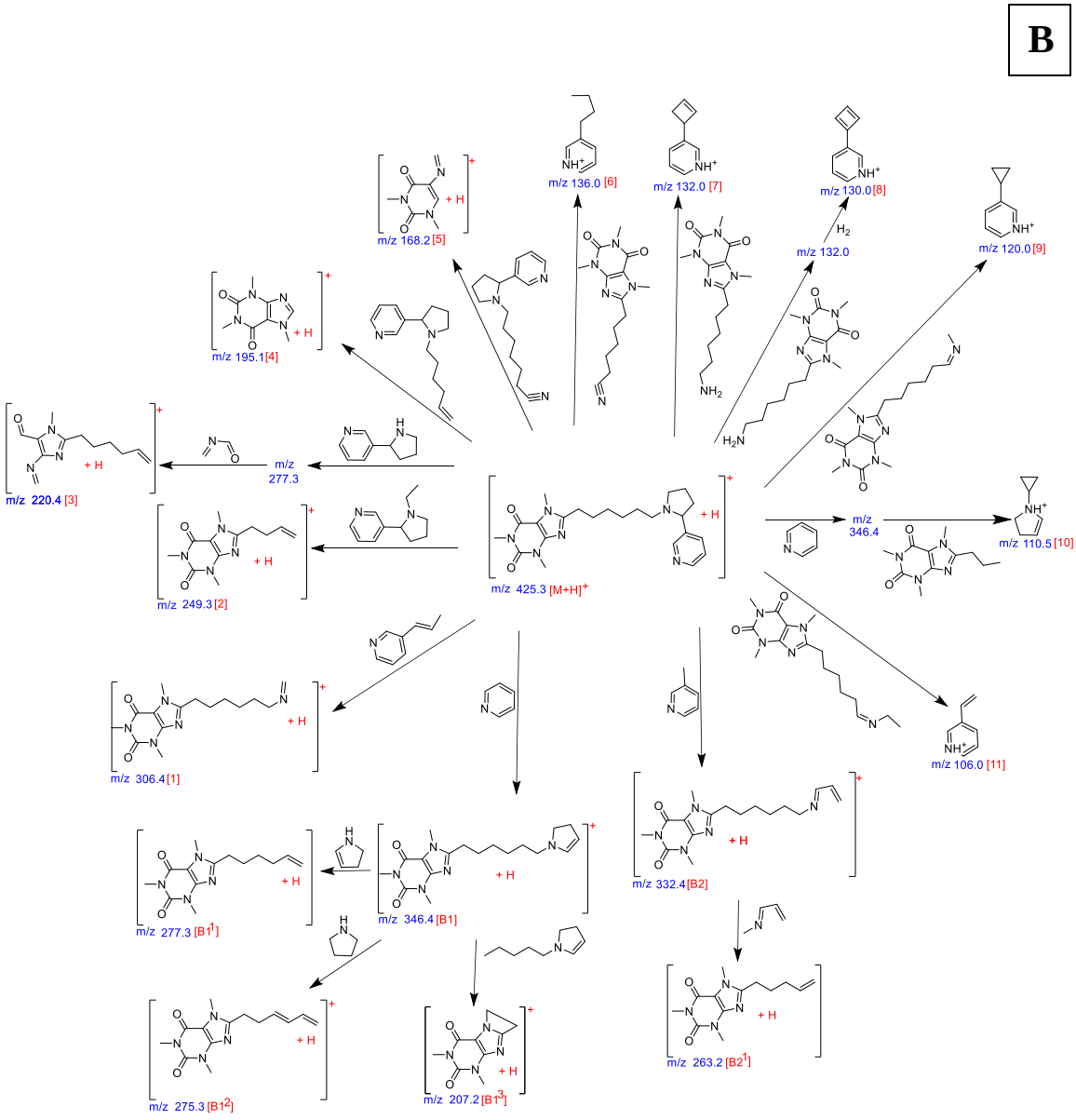

Figure 3.6 MS/MS spectrum of C_8-6-N (A) and the proposed fragmentation pathway for C_8-6-N (B).

3.4.2.3 MS/MS analysis of C_8-6-I

The MS/MS spectrum, as well as the proposed fragmentation pathway for C_8-6-I, are shown in Figure 3.7A and B. The fragmentation of the singly charged $[M+H]^+$ ion of C_8-

6-I gave rise to one first cohort product ion at *m/z* 294.4(**C1**) through the loss of an indene (C_9H_8, 116 Da) as shown in Figure 3.7B.

MS^3 analysis (Figure A.3A, Appendix A) of the product ion at *m/z* 294.4 (**C1**) revealed further dissociation to second cohort product ions. **C1** underwent additional dissociation with a NL of ammonia (NH_3, 17 Da), methylamine (CH_3NH_2, 31 Da), and methyl isocyanate ($O=C=NCH_3$, 57 Da) giving rise to the following second cohort product ions at *m/z* 277.2 (**C1^1**), *m/z* 263.2 (**C1^2**), and *m/z* 237.3 (**C1^3**) respectively as shown in Figure 3.7B. Interestingly, these product ions were not observed in the MS/MS analysis of C_8-6-I (Figure 3.7A).

Furthermore, MS^3 analysis of **C1^1** (Figure A.3B, Appendix A) indicates that subsequent dissociation of **C1^1** is associated with the formation of the product ions at: *m/z* 168.2 (**C1^{1+++}** : loss of 6-heptenitrile, $C_7H_{11}N$, 109.2 Da); *m/z* 207.1 (**C1^{1++}** : loss of 1-pentene, C_5H_{10}, 70.2 Da); and *m/z* 221.1 (**C1^{1+}** :loss of 2-butene, C_4H_8, 56.3 Da).

The product ion at *m/z* 117.0 (**1**) (protonated indene) originated directly from the precursor ion as it was not found in the MS^3 analysis (Figure A.2C, Appendix A). The ion designated **1** was generated by the loss of $C_{14}H_{23}N_5O_2$ (293 Da) from the precursor ion, and this product ion has previously been reported for the fragmentation of 1-aminoindan (196). The mass error of the MS/MS product ions of C_8-6-I is less than 5 ppm (Table A.4, Appendix A); however, QqToF-MS/MS analysis did not show the product ion at *m/z* 117.0 (**1**). The diagnostic NLs associated with the dissociation of C_8-6-I are shown in Table A.5, Appendix A.

A

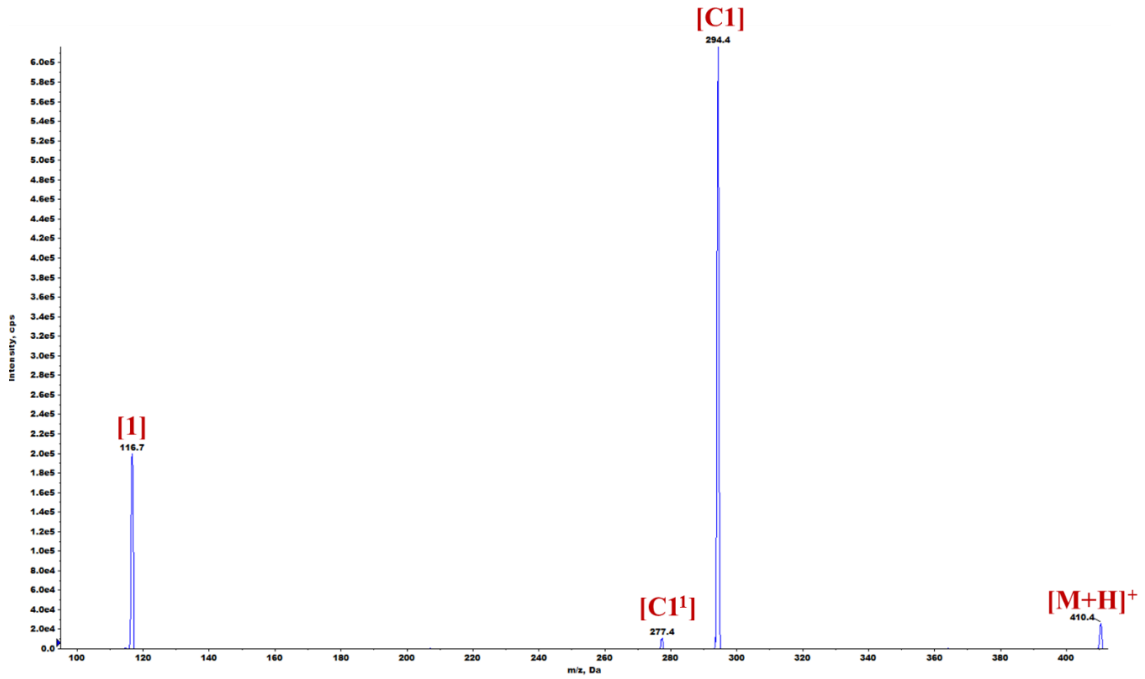

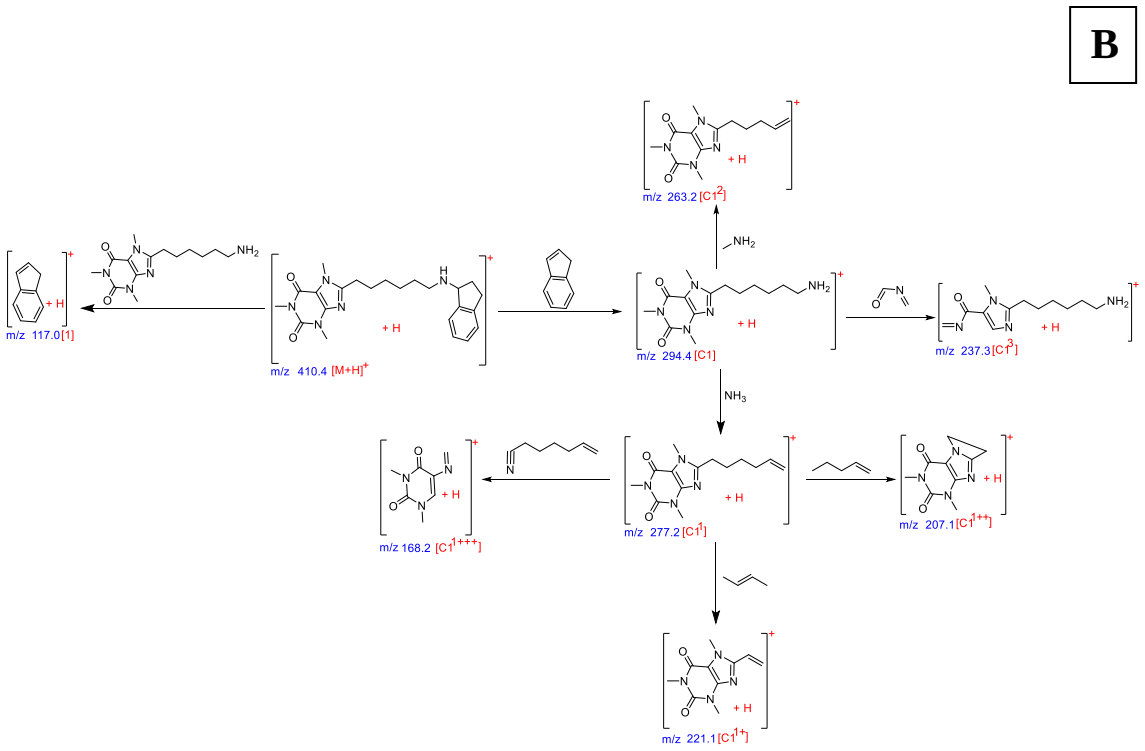

Figure 3.7 MS/MS spectrum of C_8-6-I (A) and the proposed fragmentation pathway for C_8-6-I (B).

3.5 Conclusion

In this study, we evaluated the CID-MS/MS fragmentation pattern of three novel bifunctional compounds for PD using ESI-QqToF-MS and ESI-QqLIT-MS/MS in the positive ion mode. Accurate mass measurement confirmed the molecular structure of the tested bifunctional compounds with a mass error of less than 2 ppm (Table A.1, Appendix A). Given that all three tested bifunctional compounds have a common scaffold consisting of caffeine linked to a six carbon alkyl chain through the C8 position of caffeine (C_8-6), it was expected that the dissociation of caffeine moiety would be the driving force in the fragmentation of C_8-6-C_8, C_8-6-N, and C_8-6-I; however, this was not consistent with our findings. We observed that all three bifunctional compounds have distinct fragmentation

patterns and the dissociation of caffeine moiety is only a minor pathway in the fragmentation of C_8-6-N and C_8-6-I. This suggests to us that when incorporated into these bifunctional compounds, the caffeine moiety may be more stable to fragmentation than either the nicotine or 1-aminoindan moieties. The fragmentation of the nicotine and 1-aminoindan moieties occurs primarily in a saturated, unconjugated region, whereas caffeine possesses more extensive conjugation. This extensive conjugation and accompanying resonance effects for caffeine may be responsible for attenuating fragmentation. Hence, in the presence of nicotine or 1-aminoindan, caffeine dissociation in these bifunctional compounds is minor.

A significant observation in the fragmentation of C_8-6-C_8 suggests that a previously reported loss of acetaldehyde during caffeine fragmentation (194) is instead a loss of CO_2. Through accurate mass measurement we observed that the ring contraction of the caffeine moiety of C_8-6-C_8 is associated with a NL of carbon dioxide, and the mass error of the corresponding product ion (**A1**) is 1.6384 ppm (Table A.2, Appendix A) compared to a mass error of -85.2020 ppm for the loss of acetaldehyde. We proposed a new mechanism for the loss of carbon dioxide from the caffeine moiety of C_8-6-C_8 (Figure 3.4A).

Finally, diagnostic product ions (Figure A.2, Appendix A) and distinct NLs (Table A.5, Appendix A) were observed for all three tested bifunctional compounds. While the second and third cohort product ions are potential ions for MRM^3 methods for targeted quantification, the diagnostic NLs can be used for targeted identification of these bifunctional compounds in biological matrices.

3.6 Acknowledgement

Chukwunonso Kingsley Nwabufo is a recipient of Pharmacy and Nutrition Graduate Student Scholarship and appreciates the College of Pharmacy and Nutrition, University of Saskatchewan for their financial support. We acknowledge Mr. Ken Thoms for his technical assistant and training on using the QSTAR MS, as well as Ms. Deborah Michel for providing Mr. Chukwunonso Kingsley Nwabufo training on the use of QTRAP MS instrument. We appreciate Kevin Allen and Paul Omozojie for synthesizing the bifunctional compounds. This research is funded by a Natural Sciences and Engineering Research Council of Canada (NSERC) Discovery Grant. The QTRAP 4000 instrument was obtained through a Canadian Foundation for Innovation (CFI) Grant.

4.0 Chapter Four: Metabolic Profile of Novel Bifunctional Compounds for Parkinson's Disease

Chukwunonso K. Nwabufo[1] and Ed S. Krol[1]*

1. Drug Discovery and Development Research Group, College of Pharmacy and Nutrition, University of Saskatchewan, Saskatoon, SK

*Author to whom correspondence should be addressed
Dr. Ed S. Krol
Drug Discovery and Development Research Group
College of Pharmacy and Nutrition
University of Saskatchewan
Saskatoon, SK
Ph: 306-966-2011
ed.krol@usask.ca

4.1 Abstract

The development of disease-modifying drugs and differential diagnostic agents are the main focus of research in Parkinson's disease (PD). Alpha-synuclein (AS) has been identified as a druggable target for the development of disease-modifying drugs and differential diagnostic agents for PD. Recently, we reported that two bifunctional compounds comprised of a caffeine scaffold attached to 1-aminoindan (C_8-6-I) and nicotine (C_8-6-N) are promising candidates in preventing the pathological pathway that leads to PD. We also observed that caffeine linked to caffeine (C_8-6-C_8) did not show any therapeutic potential, but displayed the strongest binding to AS and may be suitable for development as a diagnostic agent for PD. To better understand the *in vivo* properties of these compounds we are interested in preparing their ^{18}F labeled positron emission tomography (PET) imaging probes, but prior to developing these probes, it is imperative that we assess the *in vitro* metabolism of the bifunctional compounds. We investigated the *in vitro* metabolic profile of C_8-6-C_8, C_8-6-I, and C_8-6-N in human, mouse, and rat liver microsomes (HLM, MLM, and RLM) in parallel with positive and negative controls. Metabolites were identified and confirmed with accurate mass measurement and tandem mass spectrometry using liquid chromatography coupled with quadrupole/time of flight spectrometry (LC-QToF). While the caffeine scaffold in C_8-6-N, C_8-6-I, and C_8-6-C_8 was metabolically stable, the nicotine and 1-aminoindan moieties were either cleaved off (dealkylation) or hydroxylated in HLM, MLM, and RLM. This suggests that the caffeine moiety may be the preferable spot for the inclusion of ^{18}F radioisotope in these bifunctional compounds. Dealkylation and hydroxylation are the major metabolic pathways for C_8-6-I and C_8-6-N in HLM, MLM, and RLM. Given the similarity in the metabolic pathways,

mouse and rat may be useful surrogates for future animal studies of C_8-6-I, C_8-6-N, and C_8-6-C_8.

4.2 Introduction

Parkinson's disease (PD) is a neurodegenerative disorder that is characterized by the misfolding and aggregation of alpha-synuclein (AS) into fibrils, and the subsequent inclusion of the fibrils into cytoplasmic bodies known as Lewy bodies (4, 197-199). In addition to the challenges associated with the accurate diagnosis of PD (39, 42, 43, 174, 200-202), there is currently no cure for PD. Therefore, the development of disease-modifying drugs and differential diagnostic agents are the major focus of research in PD. Given its role in the pathophysiology of PD, AS may be a druggable target for the development of disease-modifying drugs and differential diagnostic probes for PD. In view of this new evidence, our laboratory has focused on developing novel compounds that can interact with AS and prevent the pathological pathway that leads to PD. Previous studies suggest that caffeine, nicotine, metformin, and 1-aminoindan may be neuroprotective (127-137). Recently, we confirmed that caffeine, nicotine, metformin, and 1-aminoindan exert their neuroprotective effects by binding to AS and preventing the initial misfolding pathway that leads to PD (32). To improve the efficacy of these compounds, we synthesized novel bifunctional compounds from a caffeine scaffold attached to 1-aminoindan (C_8-6-I), nicotine (C_8-6-N), and caffeine (C_8-6-C_8) (Figure 4.1) and determined their ability to bind to AS and prevent AS mediated toxicity in a yeast model of PD (123). The study concluded that C_8-6-I and C_8-6-N were the most promising candidates for preventing AS mediated toxicity in a yeast model of PD. Although C_8-6-C_8 did not show any therapeutic potential, it displayed the strongest binding to AS. In order to better understand the biodistribution of C_8-6-I, C_8-6-N and C_8-6-C_8 *in vivo*, we are developing methods to label the bifunctional compounds with ^{18}F to use in positron emission tomography (PET) imaging studies.

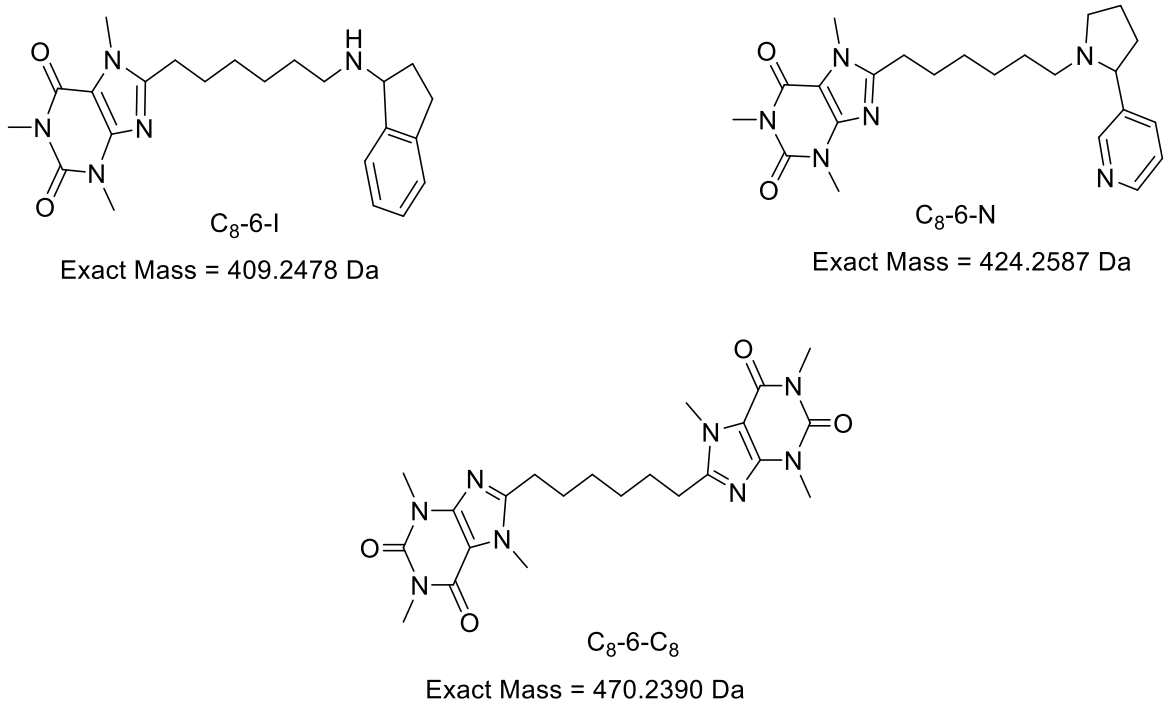

Figure 4.1 Structure of novel bifunctional compounds.

To develop these bifunctional compounds as therapeutics or diagnostics for PD, it is of great importance to determine their metabolic stability at this early stage of drug discovery and development. This initial drug metabolism studies serve as an appropriate screening mechanism to characterize drug metabolites, elucidate their metabolic pathways, and make suggestions for further *in vivo* studies with the overall goal of improving the safety and efficacy of these new chemical entities (NCEs) (203). Additionally, metabolism studies will provide useful information about metabolically stable locations to incorporate ^{18}F on the bifunctional compounds.

The liver is the major organ that is responsible for the metabolism of drugs and it contains drug metabolizing enzymes such as cytochrome P450 (P450) which mediates the oxidation, reduction, and hydrolysis (phase I) of drugs, as well as cytosolic enzymes which

catalyze several conjugation reactions such as glucuronidation, methylation, and sulfonation. Microsomes are one of the commonly used *in vitro* models for performing drug metabolism studies because they are rich in drug metabolizing enzymes (mainly P450) and are also economical. Another advantage of using microsomes as an *in vitro* drug metabolism model is the ability to focus on generating sufficient amount of presumptive P450-mediated phase I metabolites without interference from other competing processes such as phase II metabolism and transporter-mediated processes (204).

Liquid chromatography coupled with mass spectrometry (LC-MS) is an important analytical platform for the separation, detection, identification, and structural elucidation of metabolites. The identification and structural elucidation of metabolites using LC-MS is achieved through accurate mass measurement and tandem mass spectrometry. Therefore, it is essential to develop an LC method as well as a mass spectrometric method for NCEs in preparation for future preclinical studies. Recently, we established a tandem mass spectrometric fingerprint for C_8-6-C_8, C_8-6-I, and C_8-6-N for future development of qualitative and quantitative methods (manuscript in preparation).

The overall goal of this present study is to determine the metabolic profile of C_8-6-C_8, C_8-6-I, and C_8-6-N in human, mouse, and rat liver microsomes (HLM, MLM, and RLM). This is the first preclinical study to establish the metabolic profile of C_8-6-C_8, C_8-6-I, and C_8-6-N in HLM, MLM, and RLM. The information obtained from this study will contribute to the development of these bifunctional compounds as therapeutic or diagnostic agents for PD.

4.3 Materials and methods

4.3.1 Chemicals and standards

C_8-6-N, C_8-6-I, and C_8-6-C_8 were synthesized according to a previously established protocol in our laboratory (123) while 2, 2-di-(3-methoxy methyl phenyl) 1, 3-propanediol (MMPPD) was provided by Kevin Allen. Acetonitrile (HPLC grade purity), methanol (HPLC grade purity), chloroform, formic acid (LC/MS grade purity), magnesium chloride ($MgCl_2$) were purchased from Fisher Scientific (Fairlawn, NJ) while water was filtered using a Millipore, MilliQ system with a Quantum EX cartridge (Mississauga, ON). The following chemicals were purchased from Sigma-Aldrich (St. Louis, MO): sodium pyrophosphate decahydrate (SPP), chlorzoxazone, and dipotassium orthophosphate (K_2HPO_4). Potassium dihydrogen orthophosphate (KH_2P0_4) was purchased from BDH Chemicals (Toronto, ON) while reduced nicotinamide adenine dinucleotide (NADPH) was purchased from Roche Diagnostics (Indianapolis, IN). HLM, MLM, and RLM were purchased from Invitrogen (Life Technologies; Burlington, ON).

4.3.2 Microsomal incubation

A standard method for *in vitro* metabolism of novel bifunctional compounds using liver microsomes was developed and optimized in our laboratory. This method included incubation of chlorzoxazone as a positive control to determine the viability of the liver microsomes. The incubation mixture contained 5 mM $MgCl_2$, 10 mM SPP, 0.5 mg/mL liver microsomes (RLM, MLM and HLM), and 30 μM test compound. After 5-minute pre-incubation in a shaking water bath at 37^{o}C, 10 μL NADPH (1 mM final concentration) in pH 7.4 100 mM potassium phosphate buffer was added to initiate the reaction. The incubation mixtures were prepared in duplicate in parallel with two negative controls. The first negative control did not contain NADPH while the second negative control excluded

active liver microsomes. The reaction was terminated after 60 minutes by the addition of 200 µL of ice-cold acetonitrile containing 50 µM MMPPD as an internal standard.

The samples were vortexed for about 1 min and then centrifuged at 14000×g for 10 minutes. Subsequently, 200 µL of the supernatant was placed in an LC vial, and 50 µL were injected into the LC-QqToF instrument.

4.3.3 Non-targeted metabolite identification

The analysis of incubated samples was performed on an Agilent 1100 high-performance liquid chromatography (HPLC) (Agilent technologies; Mississauga, ON) coupled with an AB SCIEX QSTAR XL quadrupole orthogonal time-of-flight hybrid mass spectrometer (QqToF-MS) equipped with an electrospray ionization (ESI) source (AB SCIEX, Redwood City, CA, USA). The Agilent 1100 series HPLC was equipped with a degasser (G1379A), binary pump (G1312A), autosampler (G1329A), and diode array detector (G1315B), and the HPLC column was an Agilent Poroshell 120 EC-C_{18} column (4.6 ×50 mm, 2.7 µm). The binary solvent system used consisted of 0.1% LC-MS grade formic acid in water (mobile phase A) and 0.1% LC-MS grade formic acid in acetonitrile (mobile phase B), with a flow rate of 0.3 mL/min. A 20-minute gradient elution was set up to ensure separation of the metabolites and parent compounds. The gradient was programmed to start with an initial isocratic hold at 90% mobile phase A for 5 minutes, decreasing gradually to 10% mobile phase A and holding for 10 minutes before returning to the initial conditions at 21 minutes and equilibrating for 5 minutes. The mass spectrometer was operated in the positive ion mode, and nitrogen was used as the ESI nebulizing and drying gas. The instrument was calibrated with a two-point external calibration using cesium iodide (CsI, m/z 132.9049, Sigma-Aldrich, Oakville, ON, Canada) and sex pheromone inhibitor

iPD1(m/z 829.5393, Bachem Bioscience Inc., PA, USA). The ion source voltage was set at 5500 V while the source temperature was optimized and set at 400^{o}C. The declustering potential and focusing potential was set at 40 V and 120 V respectively. A scan range of 100-700 *m/z* was used for metabolite detection.

Identification of metabolites was made by observing unique peaks present in the reaction mixture samples in comparison to the negative control samples. Confirmation of metabolite structure was carried out using accurate mass measurement and tandem mass spectrometry. Tandem mass spectrometric analysis of the observed metabolite ions was performed under the same conditions and set to target the tentative metabolite ions and retention times in order to confirm their fragmentation pattern. The collision energy was optimized and was set at 25 eV (C_8-6-N), and 17 eV (C_8-6-I) to ensure sufficient fragmentation without depleting the precursor ion. Data analysis was done using Analyst QS 1.1.

Liquid-liquid extraction consisting of a mixture of chloroform-isopropanol (85:15, v/v) was previously used by Grant *et al*., (143) for extraction of caffeine and its metabolites from HLM. Therefore, we evaluated this mixture of solvents for extracting C_8-6-C_8, C_8-6-N, and C_8-6-I, as well as their corresponding metabolites from HLM, MLM, and RLM but found unacceptably high variation in the results. The variation with acetonitrile was acceptable and was selected as the solvent for protein precipitation.

4.4 Results and Discussion

4.4.1 Metabolite profiling

The determination of the major metabolic pathway of NCEs can provide useful information about its route of elimination from the body, and such information can be used in further structural optimization. Additionally, the biotransformation of PET imaging probes can alter the information obtained from biodistribution studies; therefore, it is important to perform metabolism studies of NCEs to determine the least metabolically labile spot for the attachment of a radioisotope as a guide for the development of novel PET imaging probes.

The goal of this study is to determine the metabolic fate of C_8-6-N, C_8-6-I, and C_8-6-C_8 in HLM, MLM, and RLM. This metabolism studies addressed three major questions: are C_8-6-N, C_8-6-I, and C_8-6-C_8 metabolized in HLM, MLM, and RLM; are the metabolic pathways of C_8-6-N, C_8-6-I, and C_8-6-C_8 the same in HLM, MLM and RLM; and what are the least metabolically labile positions for the inclusion of ^{18}F in C_8-6-N, C_8-6-I, and C_8-6-C_8.

Herein, we demonstrate the importance of combining accurate mass measurement and tandem mass spectrometric analysis in the identification and structural elucidation of the major presumptive P450 metabolites for C_8-6-N, C_8-6-I, and C_8-6-C_8 in HLM, MLM, and RLM. First, we confirmed the conversion of chlorzoxazone to 6-hydroxychlorzoxazone as an indication of microsomal viability. Subsequently, potential metabolites of the bifunctional compounds were selected by comparing the chromatograms of the reaction mixtures against those of the negative control samples (No NADPH and inactive liver microsomes) as shown in Figure 4.2. The negative control samples did not contain either

NADPH or active liver microsomes therefore, they would not metabolize the bifunctional compounds.

A

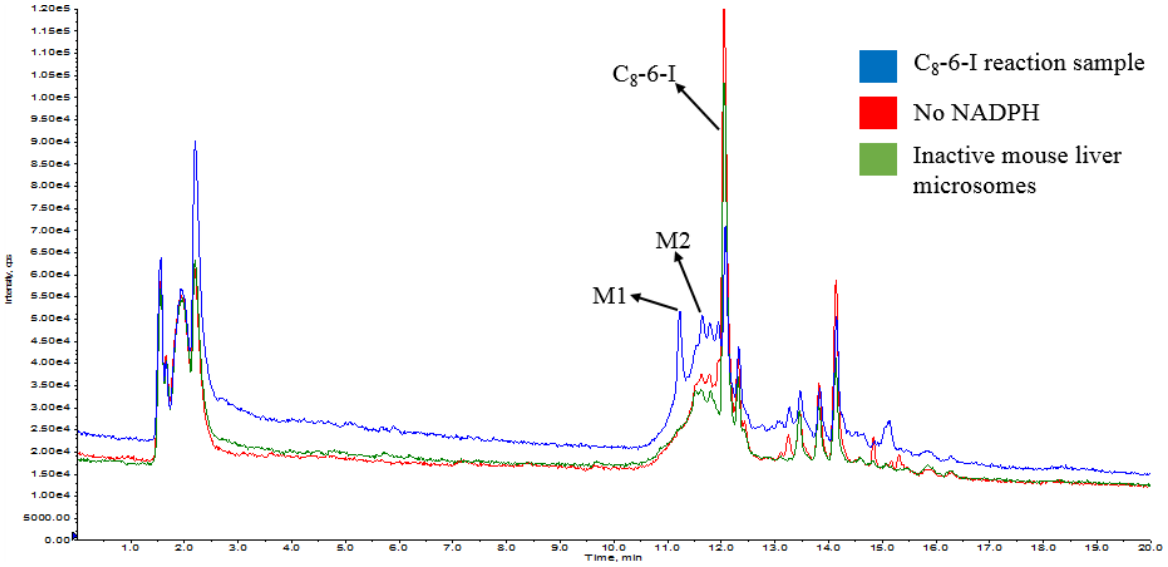

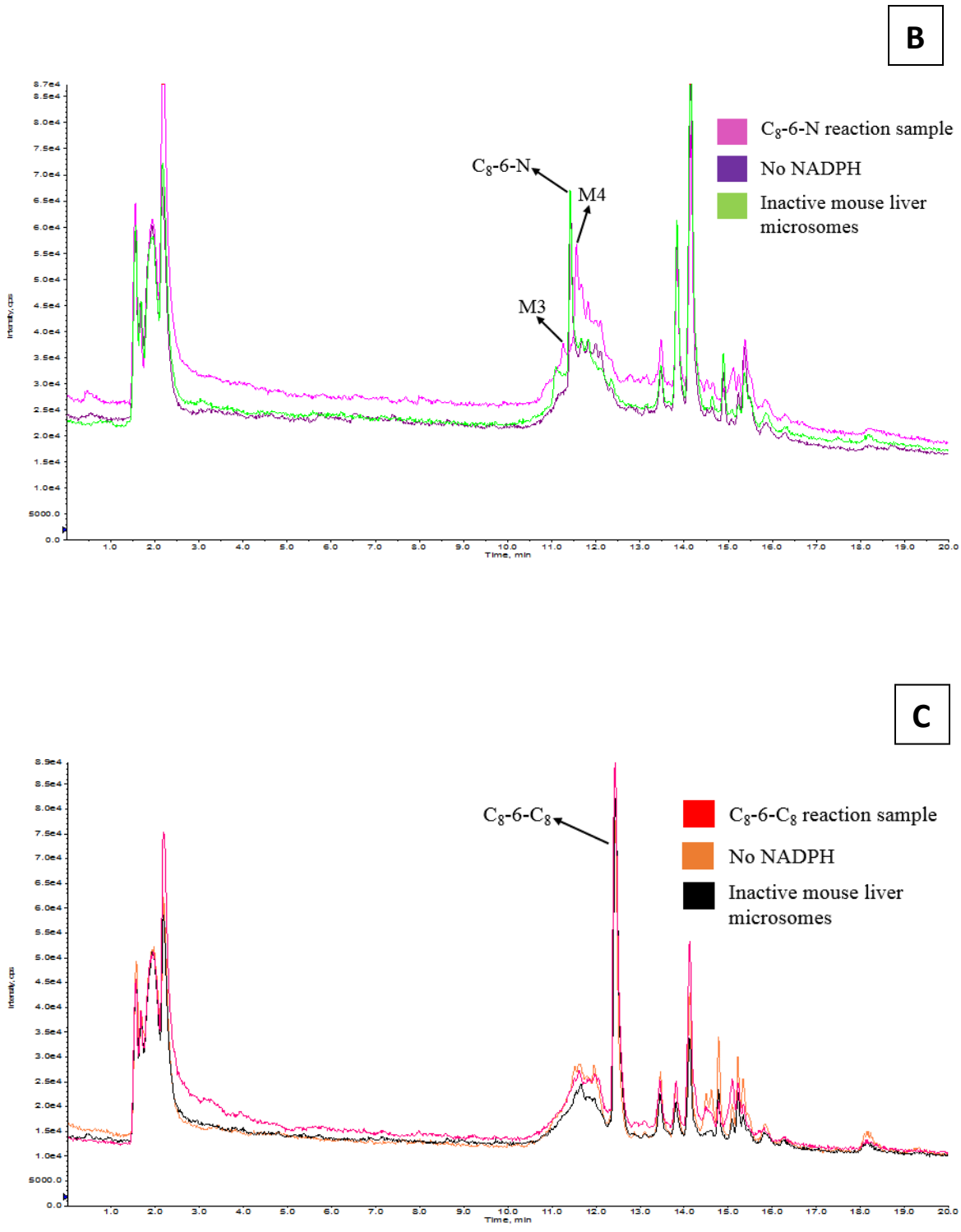

Figure 4.2 Total ion chromatogram (ESI in positive mode) of LC-MS analysis of a 50 μL injection of 15 μM samples from *in vitro* mouse liver microsomal metabolism of C_8-6-I (A), C_8-6-N (B), and C_8-6-C_8 (C).

Two metabolites (M1 and M2) were identified for C_8-6-I (Figure 4.2A), and two metabolites M3 and M4 were identified for C_8-6-N (Figure 4.2B). On the contrary, no metabolite was detected for C_8-6-C_8 (Figure 4.2C) in HLM, MLM, and RLM. We also observed that C_8-6-N undergoes extensive metabolism in HLM, MLM, and RLM as the parent compound was not detected in the reaction mixture after 60 minutes incubation (Figure 4.2B).

The metabolites were first identified using accurate mass measurement, and the mass error of each of the identified metabolites was less than 7 ppm (Table B.1, Appendix B), confirming the molecular structures. These mass accuracies were comparable to the results obtained from previous structural work in which external calibration was used (see chapter 3).

Furthermore, MS/MS analysis was performed to confirm the molecular structures of the identified metabolites and to examine how the fragmentation pattern of the identified metabolites relate to the previously established mass spectrometric pattern of C_8-6-N, C_8-6-I, and C_8-6-C_8 as described in chapter 3.4.2.

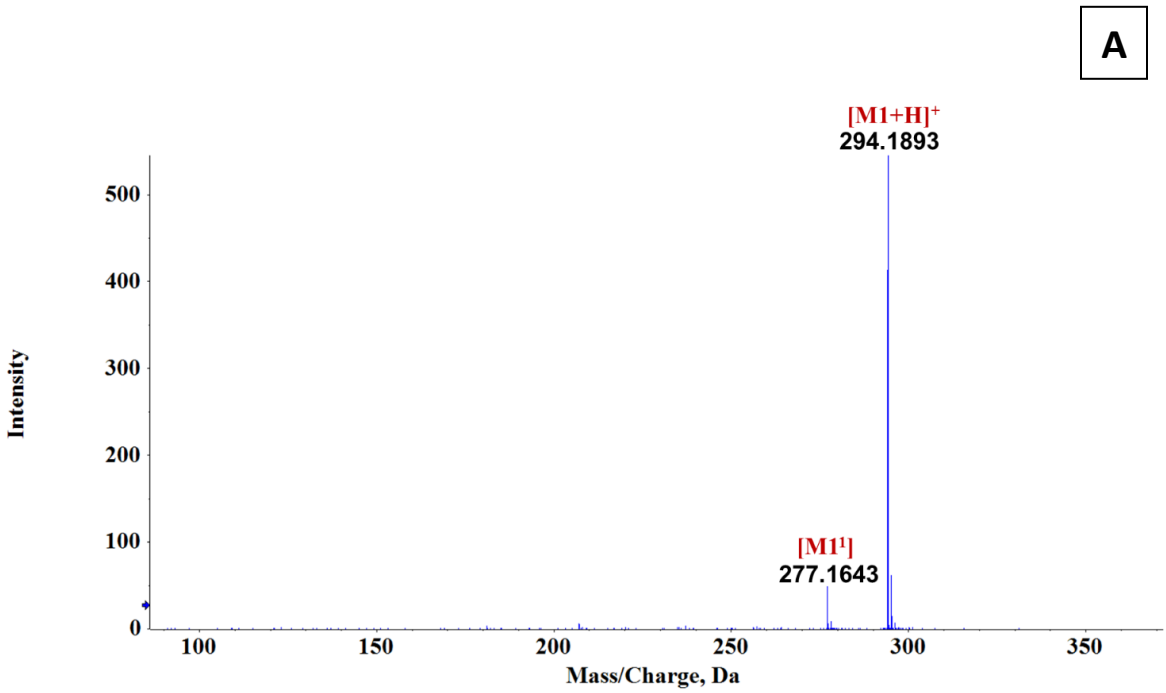
A
[M1+H]+
294.1893
[M1[1]]
277.1643
Intensity
500
400
300
200
100
0
100
150
200
250
300
350
Mass/Charge, Da

B

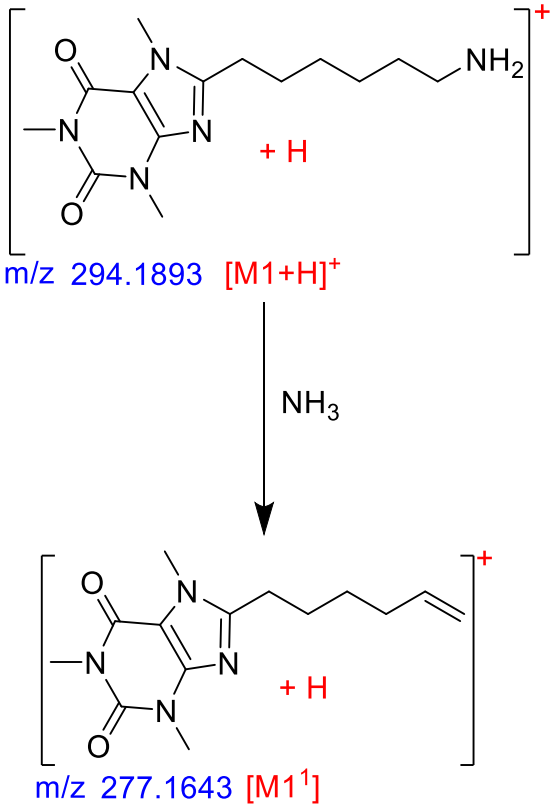

C

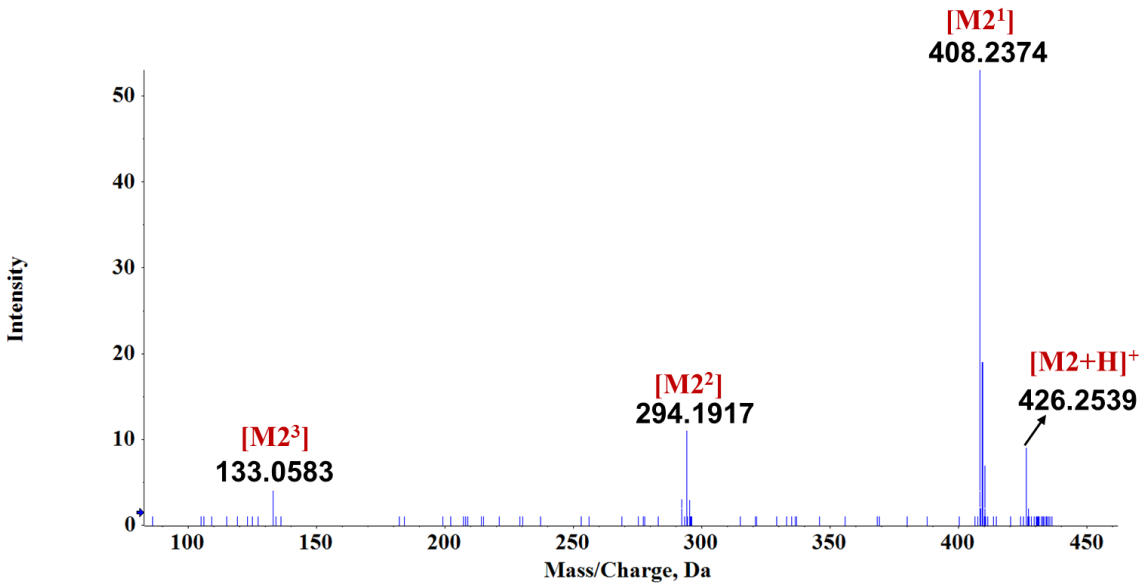
[M2¹]
408.2374
[M2+H]⁺
426.2539
[M2²]
294.1917
[M2³]
133.0583
Intensity
Mass/Charge, Da
0
10
20
30
40
50
100
150
200
250
300
350
400
450

D

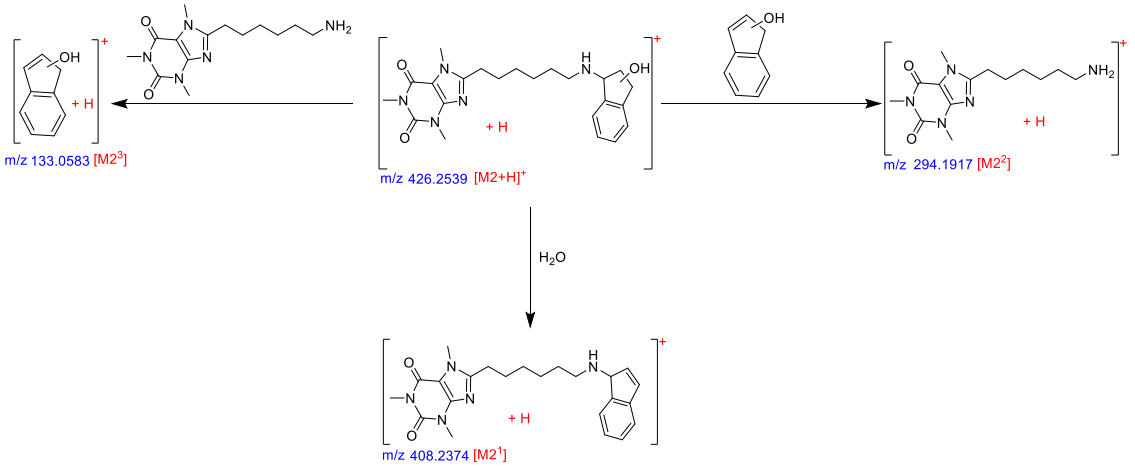
m/z 133.0583 [M2³]
m/z 426.2539 [M2+H]⁺
m/z 294.1917 [M2²]
m/z 408.2374 [M2¹]
H₂O
+ H
OH
NH₂

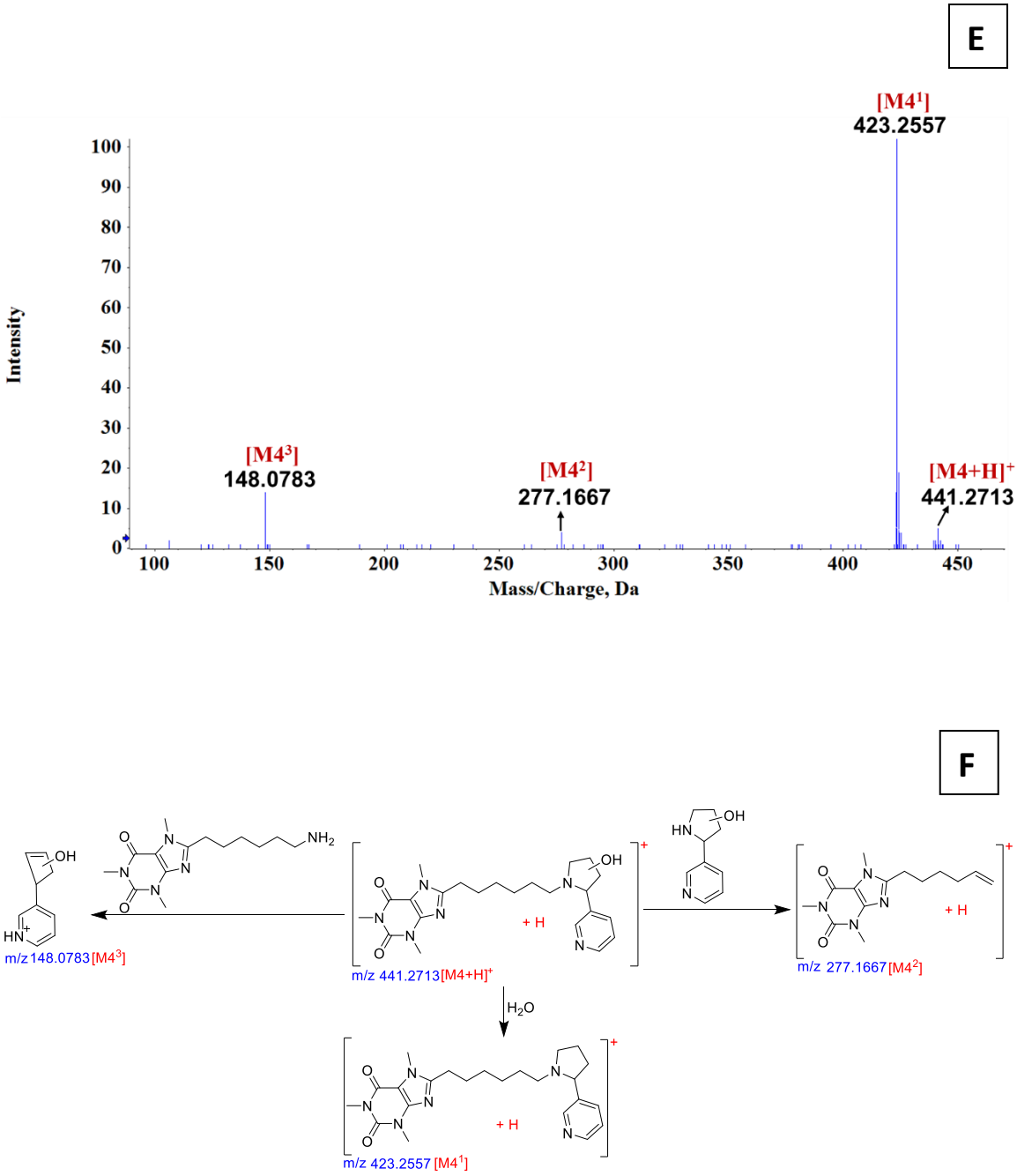

Figure 4.3 The ESI-QToF-MS/MS spectrum for M1(A), M2(C), M4(E), and the proposed fragmentation pathway for M1(B), M2(D), M4(F). ESI was performed in positive mode.

The MS/MS spectrum of M1 (Figure 4.3A) revealed a diagnostic product ion with *m/z* 277.1643 (**M1¹**) produced by the neutral loss of ammonia (17 Da) from the terminal amino

group of the precursor ion at *m/z* 294.1893 (Figure 4.3B). This fragmentation pattern correlates with the previously established fragmentation pathway for C_8-6-I in which fragmentation of C_8-6-I leads to the formation of the product ion with *m/z* 294.4, and subsequent fragmentation of this product ion (*m/z* 294.4) leads to the generation of the diagnostic product ion at *m/z* 277.4 with the concomitant loss of ammonia (see chapter 3.4.2.3). More so, accurate mass measurement revealed that the molecular formula of M1 is $C_{14}H_{24}N_50_2$ with a mass error of 0.000 ppm (Table B.1, Appendix B) which correlates with the proposed molecular structure of M1. Together the results obtained from the tandem mass spectrometric analysis and accurate mass measurement clearly confirmed the molecular structure of M1.

Metabolite M2 is 16 Da higher than the parent compound (C_8-6-I) consistent with the formation of a hydroxylated metabolite of C_8-6-I. The MS/MS spectrum (Figure 4.3C) of the precursor ion with *m/z* 426.2539 revealed an abundant diagnostic product ion at *m/z* 408.2374 (**M2^1**) corresponding to the loss of a water molecule (18 Da; Figure 4.3D) from the precursor ion, in agreement with the presence of a hydroxyl group on the precursor ion. The product ion with *m/z* 294.1917 (**M2^2**) is also diagnostic for the parent compound (C_8-6-I) (see chapter 3.4.2.3), indicating that the precursor ion $[M2+H]^+$ originated from C_8-6-I. **M2^2** is formed from the loss of hydroxyindan from the precursor ion $[M2+H]^+$ suggesting that the hydroxyl group is located on the indan moiety of M2 (Figure 4.3D). The neutral loss of $C_{14}H_{23}N_5O_2$ (293 Da) from $[M2+H]^+$ is associated with the formation of the product ion at *m/z* 133.0583 (**M2^3**) as shown in Figure 4.3D. A neutral loss of $C_{14}H_{23}N_5O_2$ (293 Da) from C_8-6-I is associated with the formation of a protonated indene (see chapter

3.4.2.3) and the protonated indene formed from this loss is only 16 Da higher than **M2^{3}** strongly indicating that the hydroxyl group is located on the indan moiety of M2.

Although the fragmentation pattern suggests that the hydroxyl group is located on the indan moiety of M2, it does not indicate the position in which it is located on the indan moiety. However, previous studies suggest that rasagiline (an antiparkinson drug) undergoes P450 mediated biotransformation to 1-aminoindan, and subsequent P450 mediated metabolism of 1-aminoindan leads to the formation of 3-hydroxy-1-aminoindan (161-163). This suggests that position 3 of the indan may be the location of the hydroxyl group on M2; however, further structural characterization studies will be necessary for the determination of the position of the hydroxyl group on the indan moiety of M2. Furthermore, accurate mass measurement revealed the molecular formula of M2 as $C_{23}H_{32}N_5O_3$ with a mass error of 6.8035 ppm (Table B.1, Appendix B), confirming the projected molecular structure.

The M3 metabolite of C_8-6-N has a similar fragmentation pathway as the M1 metabolite of C_8-6-I. The molecular formula and mass error of M1 and M3 are the same indicating that they both have the same molecular structure.

More so, M4 is 16 Da higher than the parent compound (C_8-6-N) indicating hydroxylation. Furthermore, the MS/MS spectrum of M4 (Figure 4.3E) shows an abundant diagnostic product ion at *m/z* 423.2557 (**M4^{1}**) originating from the neutral loss of water molecule from the precursor ion at *m/z* 441.2713 $[M4+H]^+$ (Figure 4.3F) indicating the presence of a hydroxyl group on the precursor ion $[M4+H]^+$. Subsequent fragmentation of $[M4+H]^+$ is linked to the neutral loss of $C_9H_{12}N_2O$ (164 Da) with the concomitant formation of the diagnostic product ion at *m/z* 277.1667 (**M4^{2}**) (Figure 4.3F). The diagnostic neutral loss of $C_9H_{12}N_2O$ (164 Da) suggests that the hydroxyl group is located on the nicotine moiety of

the M4. Additionally, **M4^2** is one of the product ions of C_8-6-N, and its presence in the MS/MS spectrum of M4 suggests that M4 originated from C_8-6-N. The diagnostic product ion at *m/z* 148.0783 (**M4^3**) is formed from the loss of $C_{14}H_{23}N_5O_2$ (293 Da; Figure 4.3F) from the precursor ion at *m/z* 441.2713 (Figure 4.3E). The presence of a hydroxyl group on **M4^3 s**trongly suggest that the hydroxyl group is located on the nicotine moiety of M4.

Interestingly, 2' and 5' phase I hydroxylated metabolites of nicotine have been reported (156, 205-207). This suggests that the 2' or 5' position of nicotine may be the location onto which the hydroxyl group is attached on M4; however, it is essential to conduct further structural characterization studies to determine the exact position in which the hydroxyl group is located on M4. Furthermore, accurate mass measurement revealed the molecular formula of M4 as $C_{23}H_{33}N_6O_3$ with a mass error of 6.1188 ppm (Table B.1, Appendix B), confirming the projected molecular structure.

4.4.2 Metabolic pathway

Two metabolic pathways were observed in HLM, MLM and RLM for each of C_8-6-I (dealkylation (M1) and hydroxylation (M2), Figure 4.4A) and C_8-6-N (dealkylation (M3) and hydroxylation (M4), Figure 4.4B). In contrast, no metabolite was detected for C_8-6-C_8 in HLM, MLM, and RLM (Figure 4.4C). Given that C_8-6-N, C_8-6-I, and C_8-6-C_8 have the same metabolic pathway in HLM, RLM, and MLM, mouse and rat may be useful models for future animal studies of these bifunctional compounds.

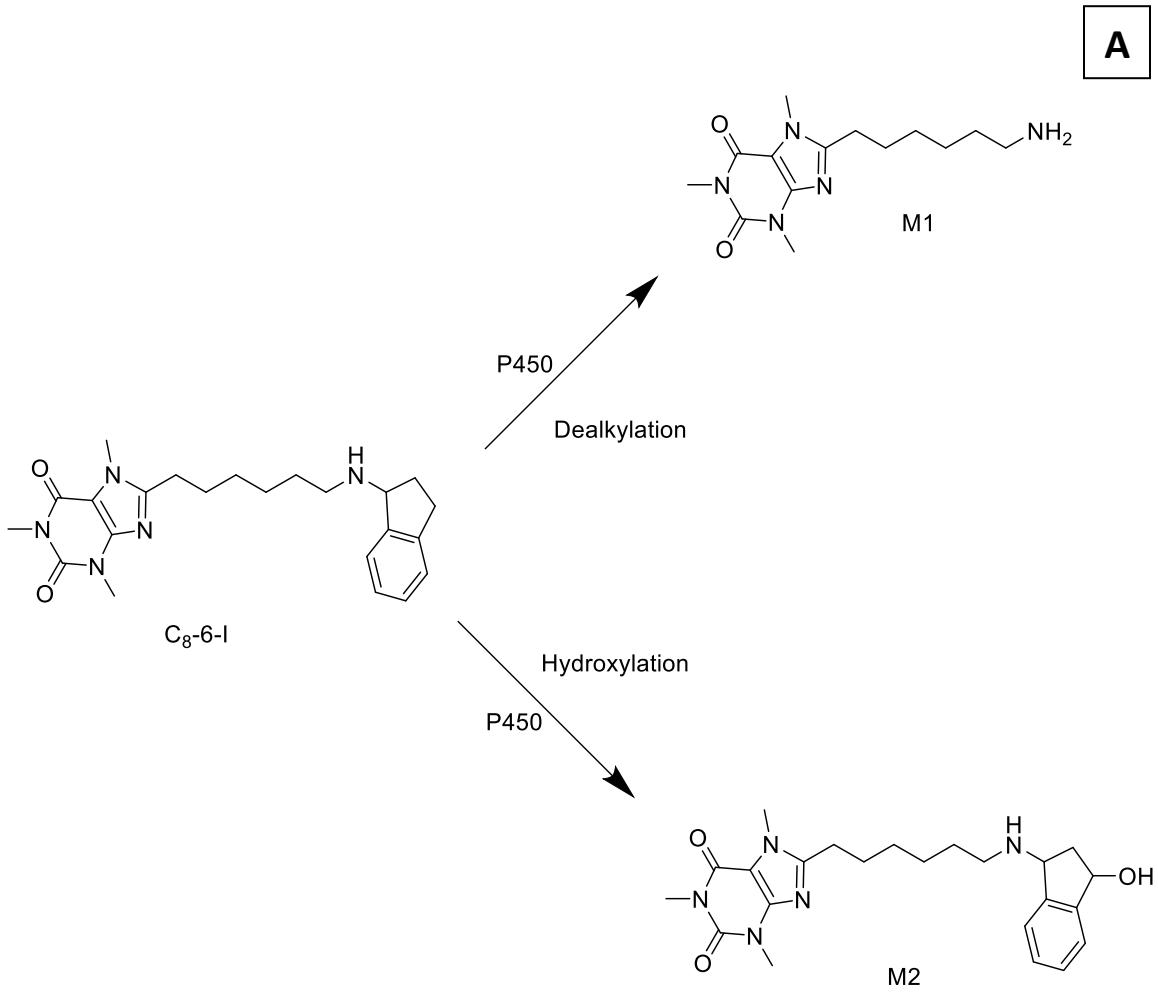
A
M1
P450
Dealkylation
C8-6-I
Hydroxylation
P450
M2

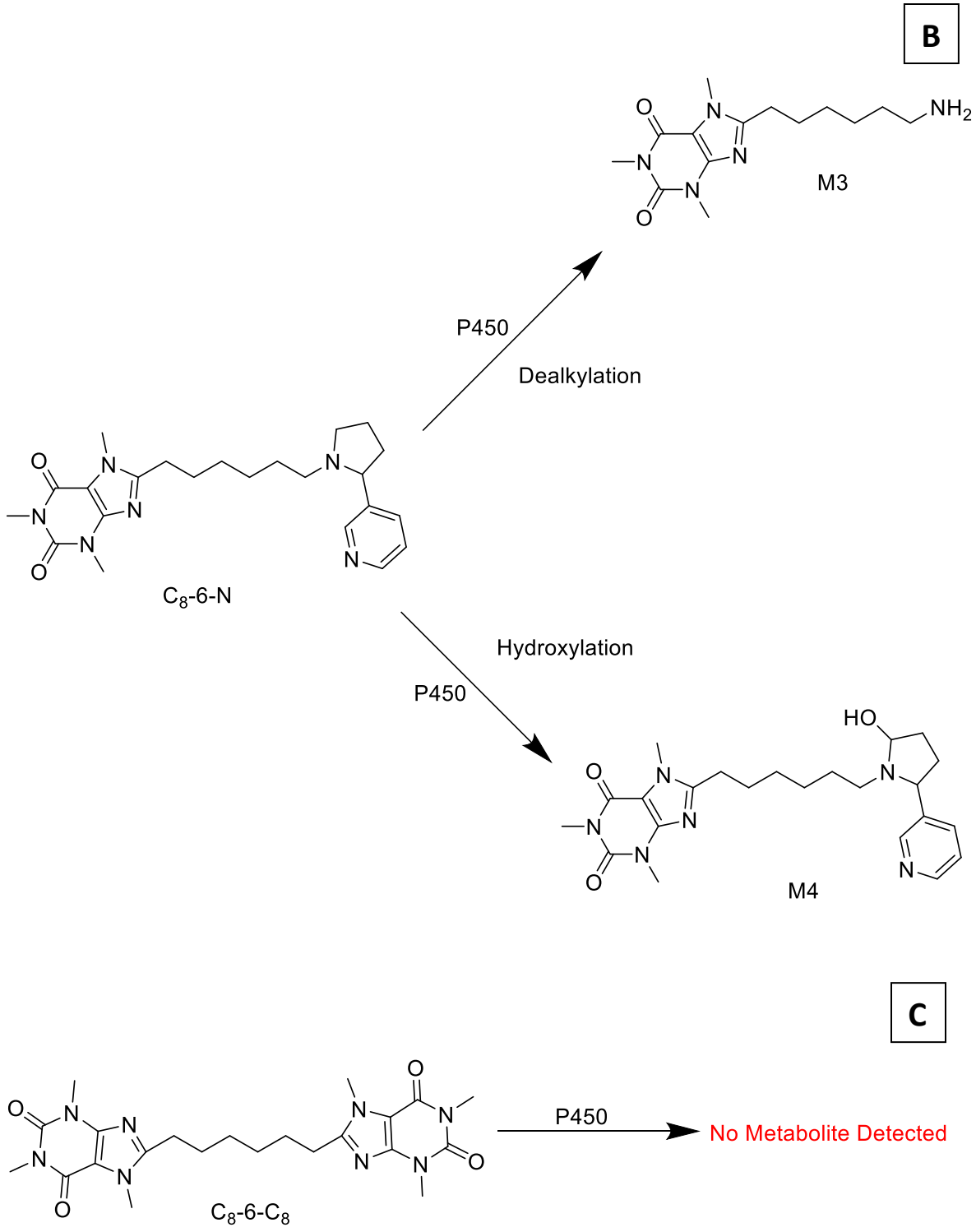

Figure 4.4 The proposed metabolic pathway for C_8-6-I (A), C_8-6-N (B), and C_8-6-C_8 (C) in human, mouse, and rat liver microsomes.

Given that C_8-6-N, C_8-6-I, and C_8-6-C_8 all have a common caffeine backbone structure, we expected that caffeine metabolism would be the common metabolic pathway for these bifunctional compounds; however, this was not the case. We observed that the caffeine moiety of these bifunctional compounds was conserved as no metabolite corresponding to the phase I biotransformation pathway of caffeine was observed. In fact, the conservation of the caffeine moiety was confirmed in C_8-6-C_8 as no corresponding metabolite was observed in HLM, MLM, and RLM. Interestingly, previous *in vitro* metabolism studies indicate that caffeine undergoes phase 1 metabolism to generate four primary metabolites: paraxanthine, theobromine, theophylline, and 1, 3, 7-trimethyluric acid which correspond to N3, N1, N7- demethylation, and C8-oxidation respectively (143, 208-210); however, none of these metabolites were observed for all investigated bifunctional compounds.

We speculate that dimerization of the caffeine monomer might have conferred energetic stability to C_8-6-C_8 hence making it metabolically stable to P450 metabolism. In fact, our tandem mass spectrometric analysis confirmed the energetic stability of C_8-6-C_8 as more collision energy was required for complete dissociation of C_8-6-C_8 compared to C_8-6-N and C_8-6-I (manuscript in preparation). Additionally, the low *in vitro* turnover rate of the enzymes involved in the metabolism of caffeine (143, 211) may be responsible for the metabolic stability of C_8-6-C_8, as well as the caffeine moiety of C_8-6-I and C_8-6-N. Intriguingly, Istradefylline, which is a caffeine analogue that is currently under development for treatment of the signs and symptoms of PD, was reported to be primarily eliminated by oxidative metabolism on the non-caffeine moiety, with the main metabolites (Figure 4.5) being M1 (4′-O-monodesmethylated) and M8 (1-β-hydroxylated) (data on file;

Kyowa Kirin Pharmaceutical Development, Inc.) suggesting that C8 functionalization of caffeine may confer metabolic stability.

Furthermore, we previously observed that C_8-6-C_8 did not protect yeast cells and may have been toxic, even though caffeine was found to prevent AS mediated toxicity in a yeast model of PD (123). Whether toxicity is the result of a lack of P450 metabolism leading to diminished clearance of C_8-6-C_8 is unknown.

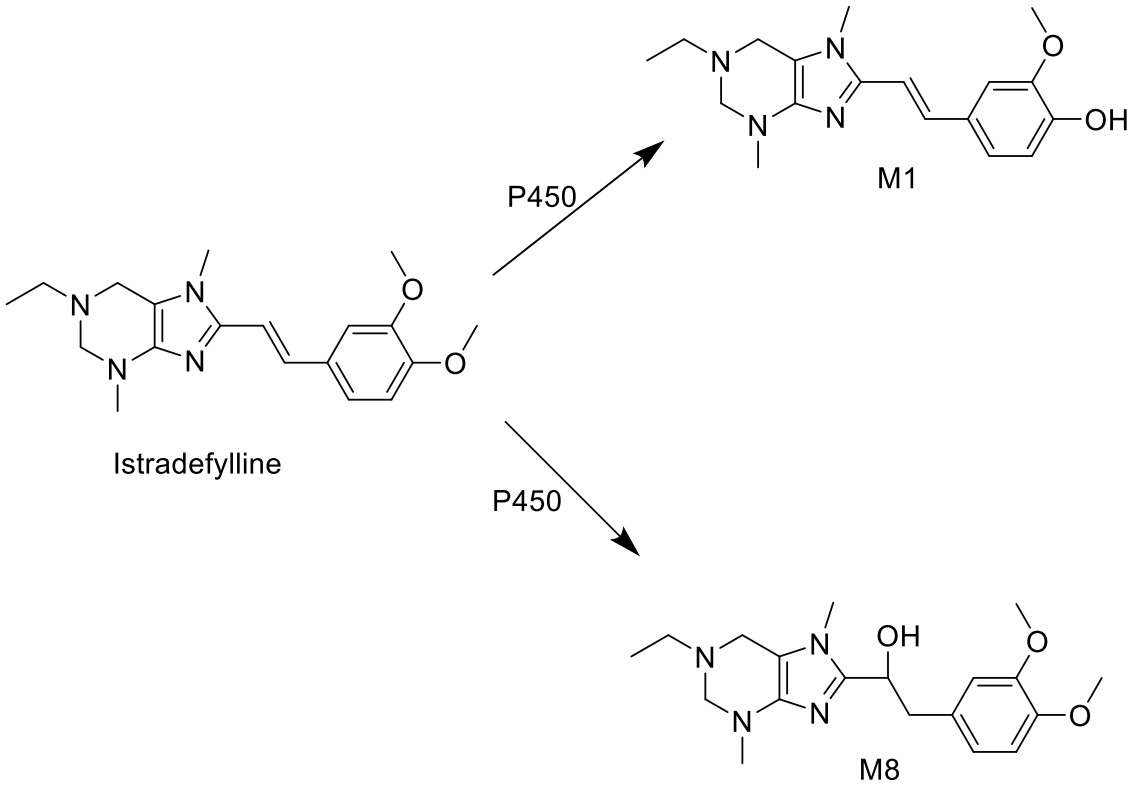

Figure 4.5 Primary phase I metabolic pathway of Istradefylline.

The 1-aminoindan moiety of C_8-6-I is a P450 metabolite of the antiparkinson drug, rasagiline which can be further metabolized to 3-hydroxy-1-aminoindan (161-163). Interestingly, we identified a hydroxylated metabolite of C_8-6-I and tandem mass spectrometric analysis suggests that the hydroxyl group is located on the 1-aminoindan

moiety; however, it is not clear as to the position in which the hydroxyl group is located on the 1-aminoindan moiety. We proposed a reaction mechanism for the dealkylation and hydroxylation of C_8-6-I (Figure 4.6). For the dealkylation reaction, we proposed an initial hydroxylation at the 1-position followed by a breakdown of the carbinolamine to form M1 with the concomitant loss of 1-oxoindan (Figure 4.6A), while the hydroxylation of C_8-6-I is more likely to occur at the benzylic 3-position to give M2 (Figure 4.6B). It has been suggested that 3-hydroxy-1-aminoindan may have neuroprotective effects (168); therefore M2 may also be neuroprotective. Additionally, given that M1 still contains the caffeine moiety, it may also have neuroprotective properties.

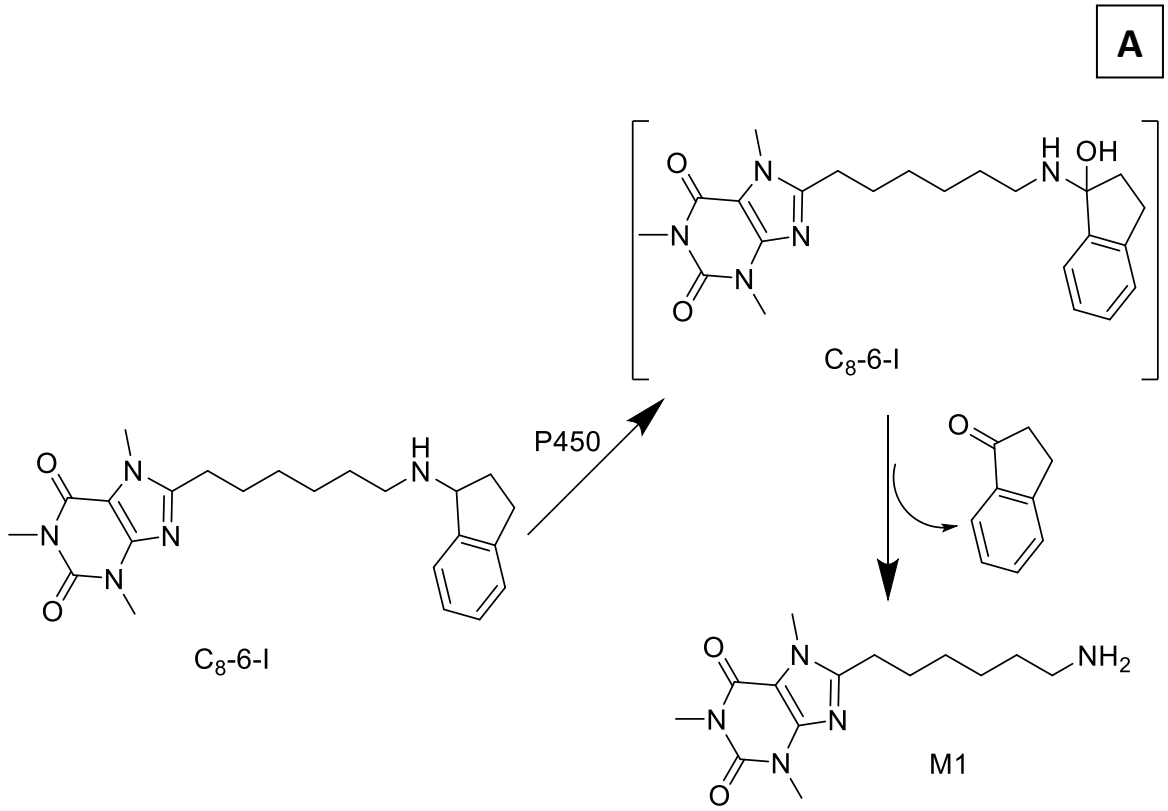

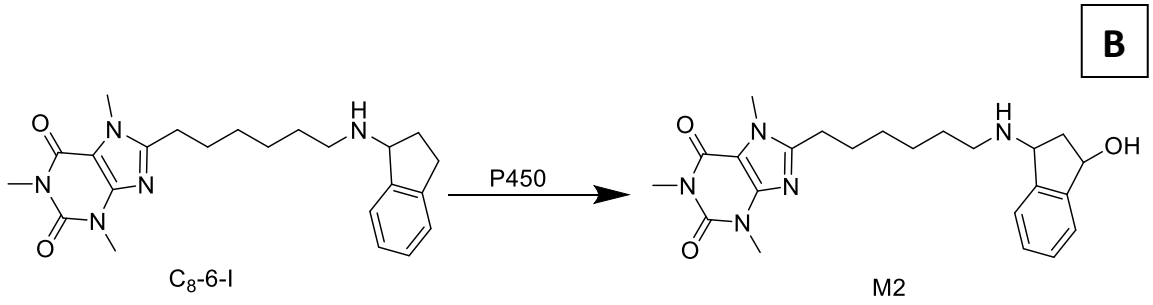

Figure 4.6 Proposed mechanism for dealkylation (A) and hydroxylation (B) of C_8-6-I in human, mouse, and rat liver microsomes.

Nicotine undergoes *in vitro* P450-mediated metabolism resulting in the following metabolites: nicotine-$\Delta^{1'(5')}$-iminium ion, 5'-hydroxynicotine, nornicotine, 2'-hydroxynicotine, 4-(methylamino)-1-(3- pyridyl)-1-butanone, 4-oxo-4-(3-pyridyl) butanoic acid and 4- hydroxy-4-(3-pyridyl) butanoic acid (148). We identified a hydroxylated metabolite (M4) for C_8-6-N, and tandem mass spectrometric analysis suggests that the hydroxyl group is located on the nicotine portion of C_8-6-N. Given that 70-80% of nicotine is biotransformed to cotinine and the 5'-hydroxylation pathway ultimately leads to the formation of cotinine by a cytoplasmic aldehyde oxidase-mediated reaction (148), we propose that the hydroxyl group on M4 is located on the 5'-position of the nicotine moiety (Figure 4.7B). Since microsomes do not contain cytoplasmic enzymes such as aldehyde oxidase, the 5'-hydroxylated metabolite cannot be converted to cotinine. We propose that the mechanism of formation of M3 is based on ring opening dealkylation which occurs at the 2'-hydroxy position followed by dealkylation at the 5'-hydroxy position resulting in loss of 4-oxo-4-pyridyl butanal (Figure 4.7A).

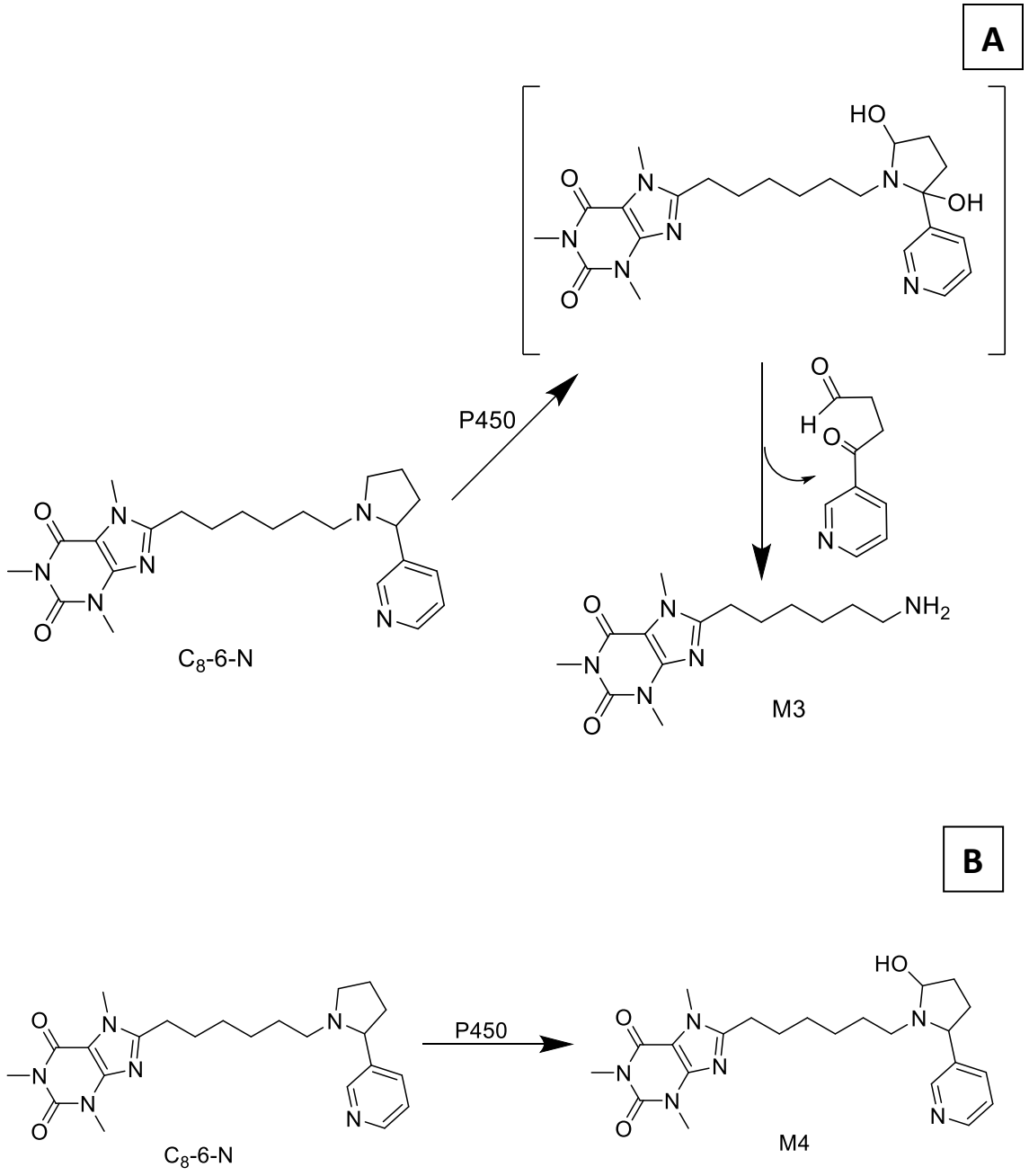

Figure 4.7 Proposed mechanism for dealkylation (A) and hydroxylation (B) of C_8-6-N in human, mouse, and rat liver microsomes.

In order for these novel bifunctional compounds to be developed as imaging probes with clinical translation for diagnosis of PD, they will be required to display high binding affinity to AS, high specificity to AS, high sensitivity, high contrast ratio, high *in vivo*

stability, low immunogenicity and toxicity (96). The metabolic stability of these compounds can alter their binding affinity, sensitivity, selectivity, and toxicity; however, the *in vitro* metabolism studies suggest that the caffeine scaffold of these bifunctional agents is stable and may be the optimal location for the attachment of the ^{18}F radioisotope.

This *in vitro* metabolism study serves as an initial screening mechanism to rule out any insignificant metabolic pathways and further direct *in vivo* testing (203). Certain factors for *in vivo* testing that are not accounted for in this study include the absence of cytosolic enzymes and cofactors to support the generation of phase II metabolites, as well as xenobiotic transporters.

4.5 Conclusion

In this study, we evaluated the metabolic stability of C_8-6-N, C_8-6-I, and C_8-6-C_8 in HLM, MLM, and RLM. Accurate mass measurement and tandem mass spectrometry were used to identify and elucidate the structure of the corresponding metabolites of C_8-6-N, C_8-6-I, and C_8-6-C_8 in HLM, MLM, and RLM. The caffeine moiety of all of the tested compounds was stable to *in vitro* Phase 1 metabolism, whereas the nicotine and aminoindan moieties underwent hydroxylation, presumably as a result of cytochrome P450 mediated metabolism. The same metabolites were observed for C_8-6-I and C_8-6-N in HLM, MLM, and RLM, suggesting that mouse and rat may be useful surrogates for future animal studies of these bifunctional compounds. These results suggest that placement of the ^{18}F radioisotope should be on the caffeine moiety of C_8-6-I, C_8-6-N, and C_8-6-C_8.

4.6 Acknowledgement

Chukwunonso Kingsley Nwabufo is a recipient of Pharmacy and Nutrition Graduate Student Scholarship and appreciates the College of Pharmacy and Nutrition, University of Saskatchewan for their financial support. We acknowledge Mr. Ken Thoms for his technical assistant and training on using the QSTAR MS. We appreciate Kevin Allen and Paul Omozojie for synthesizing the bifunctional compounds. This research is funded by a Natural Sciences and Engineering Research Council of Canada (NSERC) Discovery Grant.

5.0 Chapter Five: Bioanalytical Method Development and Validation for the Quantitative Determination of Novel Bifunctional Compounds in Human, Mouse, and Rat Liver Microsomes.

5.1 Introduction

The development of disease-modifying drugs and differential diagnostic agents are the main focus of research in Parkinson's disease (PD). Alpha-synuclein (AS) has been identified as a putative target for the development of disease-modifying drugs a nd differential diagnostic agents for PD. Recently, we reported that novel bifunctional compounds comprised of a caffeine scaffold attached to nicotine (C_8-6-N) and 1-aminoindan (C_8-6-I) were the most promising candidates in preventing AS mediated toxicity in a yeast model of PD (123). Additionally, caffeine linked to caffeine (C_8-6-C_8) did not show any therapeutic potentials, but it demonstrated the strongest binding to AS making it a good candidate for the development of positron emission tomography (PET) imaging probe. In order to better understand the *in vivo* biodistribution of C_8-6-I, C_8-6-N, and C_8-6-C_8, we are developing methods to label the bifunctional compounds with ^{18}F to use in PET imaging studies.

To develop these bifunctional compounds as therapeutics or diagnostics for PD, it will be necessary to conduct further preclinical studies to determine their safety and efficacy. To achieve this goal, we established a novel tandem mass spectrometric fingerprint for C_8-6-N, C_8-6-I, and C_8-6-C_8 for future application in qualitative and quantitative analysis of these bifunctional compounds in biological matrices (manuscript in preparation). Interestingly, we applied the established mass spectrometric pattern to the identification of the

metabolites of C_8-6-N, C_8-6-I, and C_8-6-C_8 in human, mouse, and rat liver microsomes (HLM, MLM, and RLM; manuscript in preparation).

It is important to determine the kinetics of the biotransformation of C_8-6-N, C_8-6-I, and C_8-6-C_8 in HLM, MLM, and RLM. The evaluation of the enzyme kinetics of these bifunctional compounds is beneficial for further understanding of their safety and efficacy. The metabolite formation approach has been used for the determination of the enzyme kinetics and pharmacokinetic parameters of NCEs (212). The major disadvantage associated with this approach is the need for authentic metabolite standards which are rarely available for NCEs whose corresponding metabolites have not been characterized. To circumvent this problem, the substrate depletion approach was adopted because this method does not require metabolite quantification (213-215) rather substrate depletion is monitored over time.

An appropriate analytical method is required for the quantification of NCEs in biological matrices. It is also important to validate the bioanalytical method according to stipulated regulatory guidelines. The goal of this research is to develop and validate a high-performance liquid chromatography (HPLC) ultraviolet detection method for the quantification of C_8-6-N, C_8-6-I, and C_8-6-C_8 in HLM, MLM, and RLM. The validated bioanalytical method will be applied to future quantification of C_8-6-N, C_8-6-I, and C_8-6-C_8 in HLM, MLM, and RLM for the determination of the associated metabolism kinetics.

5.2 Materials

C_8-6-N, C_8-6-I, and C_8-6-C_8 were synthesized according to a previously established protocol in our laboratory (123). Acetonitrile (HPLC grade purity), methanol (HPLC grade purity), chloroform, formic acid (LC-MS grade purity), magnesium chloride ($MgCl_2$) were

purchased from Fisher Scientific (Fairlawn, NJ) while water was filtered using a Millipore, MilliQ system with a Quantum EX cartridge (Mississauga, ON). The following chemicals were purchased from Sigma-Aldrich (St. Louis, MO): Sodium pyrophosphate decahydrate (SPP), and dipotassium orthophosphate (K_2HPO_4). Potassium dihydrogen orthophosphate (KH_2P0_4) was purchased from BDH Chemicals (Toronto, ON) while HLM, MLM, and RLM were purchased from Invitrogen (Life Technologies; Burlington, ON).

5.3 Methods

5.3.1 Chromatographic conditions

HPLC analysis was performed using an Agilent 1200 series HPLC (Agilent Technologies; Mississauga, ON) equipped with an online degasser (G1322A), quaternary pump (G1311A), autosampler (G1329A), diode array detector (G1315D), and the results were analysed using Open Lab CDS software (Agilent Technologies; Mississauga, ON). The maximum wavelength (λ) was set at 275 nm, and an Agilent Poroshell 120 EC-C_{18}, 4.6 × 50 mm, 2.7μm column was used for compound and metabolite separation. A linear gradient mobile phase system with solvent A comprising of water with 0.1% formic acid and solvent B comprising of acetonitrile with 0.1% formic acid was used to elute the analytes at a flow rate of 1 mL/min. The 18-minute gradient elution program started with an initial condition of 15% mobile phase B and was held isocratically for 6 minutes. It was then gradually decreased to 90% mobile phase B where it was held for 3 minutes before returning to the initial conditions at 13 minutes. The column was equilibrated in the initial conditions for 5 minutes before the start of another run.

5.3.2 Sample preparation

Stock standard solutions and quality control solutions (QCs) of C_8-6-C_8 (8 mg/mL) was prepared in chloroform while 50 mg/mL of C_8-6-I and C_8-6-N were separately prepared in

methanol and stored at -80°C. The standard working solutions were prepared by diluting the stock solution to yield the following concentrations: 0.04/0.4/1.6/2.4/3.2/4/5.6 mg/mL for C_8-6-C_8 and 0.2/0.4/4/8/16/24/32/ 40 mg/mL for C_8-6-I. The calibration standards were prepared by spiking 1 µL of standard working solutions into a 5 µL aliquot of control liver microsomes, and then 10 µL of $MgCl_2$ and 20 µL of SPP were added to the cocktail mixture. Subsequently, 164 µL of 100 mM potassium phosphate buffer was added to achieve a volume of 200 µL. Finally, 200 µL of cold acetonitrile was added to precipitate the proteins, and a final volume of 400 µL was considered to obtain the following final concentrations: 0.1/1/4/6/8/10/14 µg/mL for C_8-6-C_8, and 0.5/1/10/20/40/60/80/100 µg/mL for C_8-6-I. The medium cocktail was vortexed for 1 min followed by centrifugation in a VWR centrifuge at 14000×g for 10 min. Then 200 µL of the supernatant was placed in an HPLC vial, and 10 µL was injected into the HPLC.

5.3.3 Bioanalytical method validation

The bioanalytical method is being validated for specificity, linearity, accuracy, precision, recovery, and stability according to US Food and Drug Administration guideline (216).

5.3.3.1 Specificity

Specificity was assessed by analyzing pooled HLM, RLM, and MLM to determine the absence of endogenous substances with similar retention time as the analyte of interest.

5.3.3.2 Linearity

A standard curve was constructed by plotting known concentrations in the range of 0.1 µg/mL to 14 µg/mL for C_8-6-C_8, and 0.5 µg/mL to 100 µg/mL for C_8-6-I against the detector response peak area. The calibration standards also contain a blank sample (matrix

sample without analyte). Accuracy was set at ±15% for all standards except for the lower limit of quantification (LLOQ) which should be no more than ±20%.

The standard that is three times the signal to noise ratio should be considered as the limit of detection (LOD).

5.3.3.3 Accuracy and precision

The accuracy and precision of the bioanalytical method will be determined in terms of intermediate precision (intraday and interday). The QCs consisted of LLOQ, low quality control (LQC), middle quality control (MQC), and high quality control (HQC), and had the following concentrations, for C_8-6-C_8: 0.1 µg/mL (LLOQ), 0.2 µg/mL (LQC), 7 µg/mL (MQC), and 11 µg/mL (HQC) while for C_8-6-I: 0.5 µg/mL (LLOQ), 0.8 µg/mL (LQC), 50 µg/mL (MQC), and 85 µg/mL (HQC). The QCs will be analysed in sextuplicate during the same day (intraday) and on three consecutive days (interday). The accuracy was expressed as the difference in percentage between the measured concentration and the nominal concentration for each sample. Precision will be determined using the coefficient of variation (CV).

For accuracy, the mean value should be within ±15% of the nominal value, except LLOQ which should be no more than ±20%. The precision around the mean value should be within 15% of the CV, except for LLOQ where it should not deviate by more than 20% of the CV.

5.3.3.4 Recovery

The absolute recovery of C_8-6-C_8, C_8-6-I, and C_8-6-N will be determined in the triplicate analysis of control microsomes spiked with the LLOQ, LQC, MQC, and HQC. The recovery will be calculated by comparing the peak areas of the extracted standards with the unextracted standards at the same concentration.

5.3.3.5 Stability

The stability of samples at room temperature will be tested in triplicate by placing the LLOQ, LQC, MQC, and HQC at the bench top. Samples will be analysed at 12 and 24 hours by comparison with freshly prepared samples at the same concentration. Additionally, the stability of samples in the autosampler will be established by placing the LLOQ, LQC, MQC, and HQC in the autosampler for 12 and 24 hours. Analytes of interest will be considered stable if the determined concentrations are within ±15% of the nominal value except for the LLOQ which can be no more than ±20%.

5.4 Results and Discussion

5.4.1 Bioanalytical method development

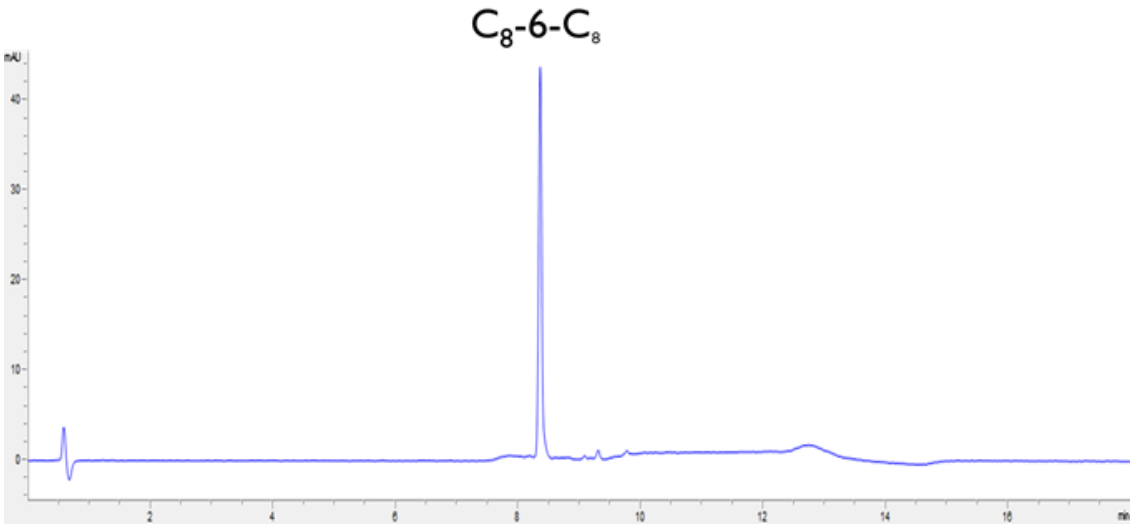

Figure 5.1 HPLC chromatogram of C_8-6-C_8.

5.4.1.1 Specificity

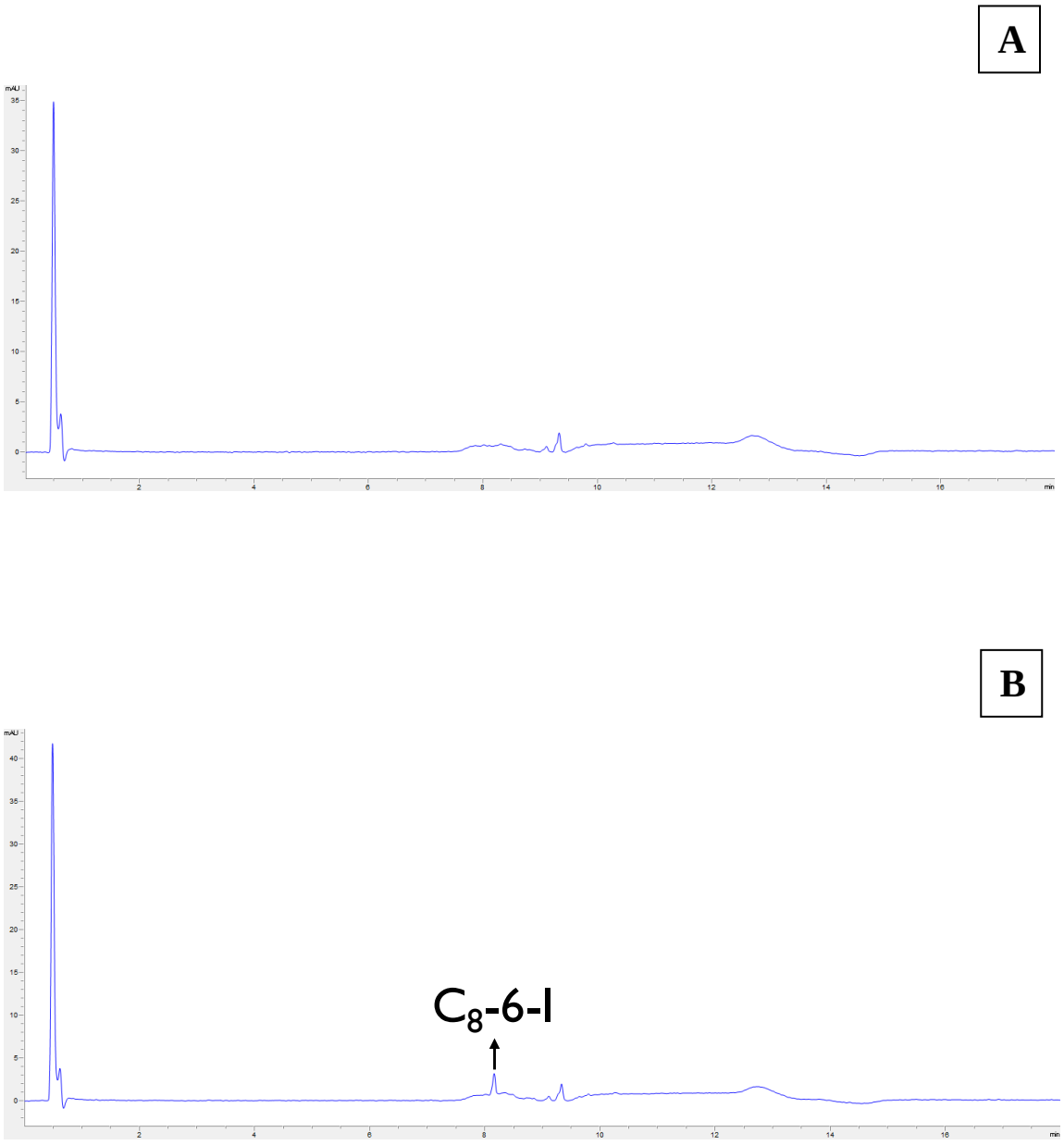

Figure 5.2 HPLC chromatograms of rat liver microsomes without C_8-6-I (A) and rat liver microsomes spiked with 0.5 µg/mL C_8-6-I (B).

5.4.1.2 Linearity

A

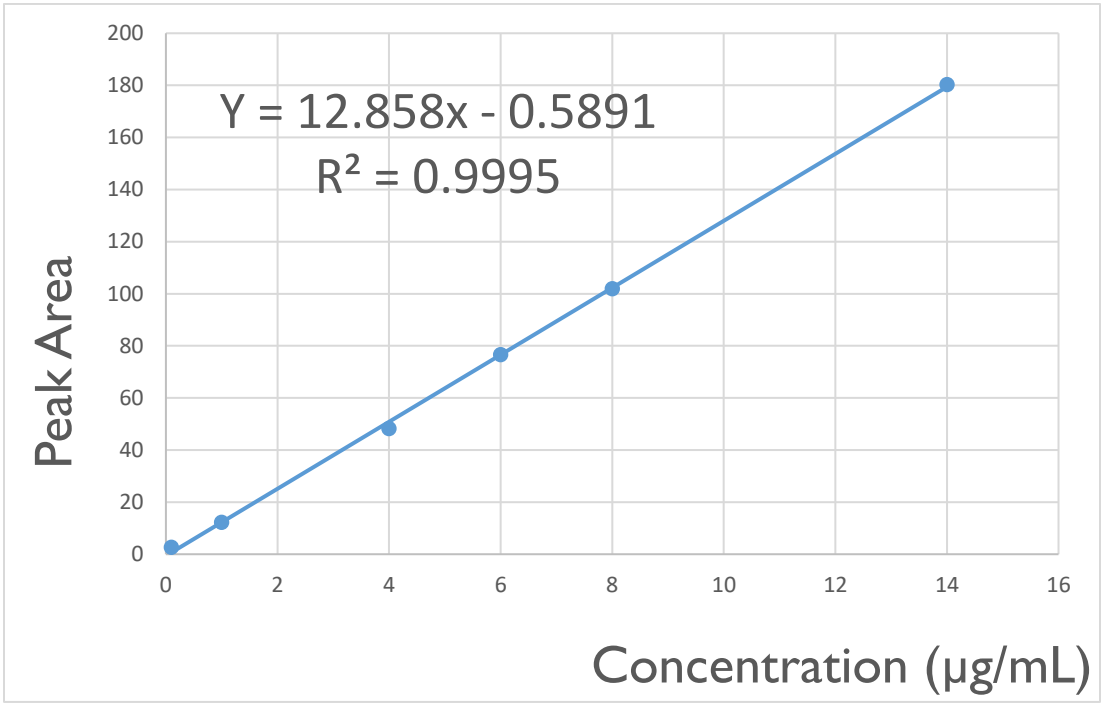

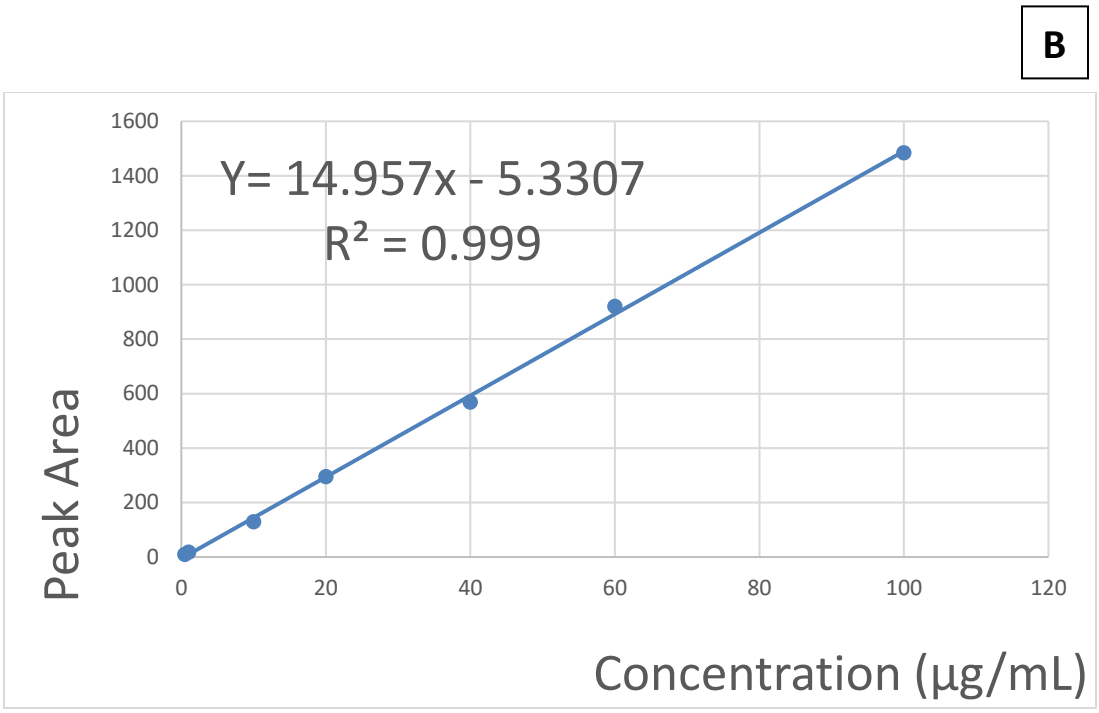

Figure 5.3 Calibration curve of C_8-6-C_8 in rat liver microsomes (A) and C_8-6-I in mouse liver microsomes (B).

The C_8-6-C_8 was linear from 0.1 µg/mL to 14 µg/mL while C_8-6-I was linear from 0.5 µg/mL to 100 µg/mL

An HPLC bioanalytical method has been developed and is currently being validated according to the US Food and Drug Administration guideline. Several challenges such as instrument problems and difficulty obtaining analytes prevented completion of the validation process. Future work will be focused on completing the bioanalytical method validation.

6.0 Chapter Six: General Discussion

In this study, I established a novel tandem mass spectrometric fingerprint for three novel bifunctional compounds (C_8-6-I, C_8-6-N, and C_8-6-C_8) that our laboratory discovered as potential therapeutics for PD. Subsequently, I used the established tandem mass spectrometric fingerprint to develop a novel LC-MS and LC-MS/MS method for the unambiguous identification and structural elucidation of the phase I metabolites of C_8-6-I, C_8-6-N, and C_8-6-C_8 in HLM, MLM, and RLM. This is the first preclinical study to evaluate the tandem mass spectrometric behaviour, as well as to establish the metabolic profile of C_8-6-I, C_8-6-N, and C_8-6-C_8 in HLM, MLM, and RLM. The elucidation of the metabolic pathway of these bifunctional compounds can provide information that can direct future studies towards the improvement of the safety and efficacy of these compounds. Furthermore, the characterization of the metabolites will provide useful information about the least metabolically labile location for the inclusion of the ^{18}F radioisotope on C_8-6-I, C_8-6-N, and C_8-6-C_8 as a guide for the development of PET imaging probes for diagnosis of PD. Comparison of the metabolic fate of C_8-6-I, C_8-6-N, and C_8-6-C_8 in HLM, MLM, and RLM will help us to determine the most appropriate animal model for future animal studies. In general, the outcome of this study will contribute to the development of predictive structural models to maximize biodistribution (high brain penetrance and AS selectivity) and minimize metabolic degradation (optimize lifetime).

6.1 Tandem mass spectrometric analysis

The tandem mass spectrometric analysis revealed the mass spectrometric behaviour of C_8-6-I, C_8-6-N, and C_8-6-C_8. For example, we realized that the CE required for complete dissociation increased from C_8-6-I, C_8-6-N, to C_8-6-C_8 reflecting the energetic stability of

these bifunctional compounds. Interestingly, I hypothesized that caffeine dissociation would be the driving force in the tandem mass spectrometric fragmentation of C_8-6-I, C_8-6-N, and C_8-6-C_8 but this was not the case as all three compounds had distinct fragmentation pathways and dissociation of caffeine moiety is only a minor pathway in the fragmentation of C_8-6-N and C_8-6-I. This suggests to us that when incorporated into these bifunctional compounds, the caffeine moiety may be more stable to fragmentation than either the nicotine or 1-aminoindan moieties. The fragmentation of the nicotine and 1-aminoindan moieties occurs primarily in a saturated, unconjugated region, whereas caffeine possesses more extensive conjugation. This extensive conjugation and accompanying resonance effects for caffeine may be responsible for attenuating fragmentation. Hence, in the presence of nicotine or 1-aminoindan, caffeine dissociation in these bifunctional compounds is minor. Furthermore, the fragmentation of C_8-6-I, C_8-6-N, and C_8-6-C_8 produced a sequence of diagnostic product ions which I classified as first, second, and third cohort ion groups, as well as initial product ions. The first cohorts are product ions originating directly from the precursor ions, and subsequent dissociation (MS^3 analysis) of some of the first cohorts gives rise to second cohorts. MS^3 analysis of the second cohorts gives rise to third cohorts and those product ions not found on the MS^3 spectrum of the first, second, and third cohorts are called initial product ions. The classification of these product ions provides useful information about their origin, and such information may serve as a guide when selecting diagnostic quantifier and qualifier ions for MRM methods. For example, a generalized MS/MS fingerprint was developed for a series of structurally similar novel drug delivery agents, namely gemini surfactants (187-189), and the established CID-MS/MS fingerprint was used to develop a targeted MS

method for the quantification of the gemini surfactants within a cellular lysate (190-192). Additionally, the second and third cohort of product ions may be useful for developing an MRM^3 method for the quantification of these bifunctional compounds in complex biological matrices. MRM^3 plays a critical role in enhancing analytical selectivity during the quantification of compounds in complex biological matrices where there is an increased possibility of matrix interference with conventional MRM transitions. For instance, a loss of analytical selectivity was observed for quantifying plasma normetanephrine and metanephrine when using conventional LC-MRM due to matrix interferences (217-220). To address the issue, Wright *et al*., developed a multi-stage fragmentation (MRM^3) for the measurement of plasma free metanephrine and normetanephrine (221). The developed MRM^3 method improved the analytical selectivity of plasma free metanephrine and normetanephrine quantification with sufficient analytical sensitivity (221).

Another interesting fact about the tandem mass spectrometric analysis is that through accurate mass measurement we discovered that a previously reported loss of acetaldehyde during caffeine fragmentation (194) is instead a loss of carbon dioxide. It was observed that the mass error of the product ion (**A1**) originating from the loss of acetaldehyde from C_8-6-C_8 is -85.2020 ppm, but when the NL is carbon dioxide, the mass error of **A1** is 1.6384 ppm (Table A.2, Appendix A). Interestingly, other product ions that originated from the loss of acetaldehyde had unacceptable mass errors, but when we proposed a new fragmentation mechanism involving the loss of carbon dioxide (Figure 3.4A), the mass error was found to be within the acceptable range (Table A.2, Appendix A).

The diagnostic NLs observed in the fragmentation pathways can be used for targeted identification of the three bifunctional compounds and their metabolites in biological

matrices. For example, Bourcier *et al*., used diagnostic NLs identified from the fragmentation of 28 neurotransmitters and related compounds (181-185) to identify expected and unexpected metabolites in biological fluids (181). Additionally, Bourcier *et al*., used diagnostic NLs for the unambiguous differentiation of isomers, as well as the identification and localization of functional groups(186).

Another instructive aspect of this work is that future MS/MS fragmentation of analogues containing caffeine moiety would be anticipated to occur elsewhere in the structure, and this is a powerful tool for identification in biological matrices. Conversely, bifunctional compounds without caffeine, for example, nicotine linked to 1-aminoindan (N-6-I), would also be expected to have a unique MS/MS fragmentation. For example, you could predict that fragmentation of N-6-I would occur exclusively at the 1-aminoindan moiety at a collision energy of 22 eV. This would be valuable for identifying the parent compound and also useful for identifying metabolites (for example, it can determine if a hydroxyl group is attached to nicotine or 1-aminoindan).

6.2 Metabolism studies

To determine the metabolic stability of C_8-6-I, C_8-6-N, and C_8-6-C_8 in HLM, MLM, and RLM, it was necessary to establish an LC-MS, as well as LC-MS/MS method for non-targeted identification and structural elucidation of the associated metabolites. Previous tandem mass spectrometric analysis of C_8-6-I, C_8-6-N, and C_8-6-C_8 guided our design of an LC-MS and LC-MS/MS method. The developed LC-high-resolution MS method allowed us to detect and identify the metabolites of C_8-6-I, C_8-6-N, and C_8-6-C_8 by characterizing distinct peaks present in the reaction mixtures but absent in the negative control samples as shown in Figure 4.2, and Figure C.1, Appendix C. The identified

metabolites have a mass error of less than 7 ppm (Table B.1, Appendix B) confirming the projected molecular structures. Additionally, the tandem mass spectrometric analysis confirmed the expected molecular structures of the identified metabolites. This clearly shows that tandem mass spectrometry and accurate mass measurement are important in the structural elucidation of unknown metabolites.

Two metabolites were each identified for C_8-6-I (Figure 4.2A) and C_8-6-N (Figure 4.2B) while no metabolites were detected for C_8-6-C_8 (Figure 4.2C) in HLM, MLM, and RLM. Upon characterization of the identified metabolites for C_8-6-I and C_8-6-N in HLM, MLM, and RLM, we realized that none of those metabolites originated from the caffeine moiety. This suggests that the caffeine moiety of these bifunctional compounds is metabolically stable *in vitro*. Interestingly, previous *in vitro* metabolism studies suggest that caffeine undergoes phase 1 metabolism to form the following metabolites: theobromine, theophylline, paraxanthine, and 1, 3, 7-trimethyluric acid (143, 208-210). Surprisingly, none of these metabolites was detected for C_8-6-C_8, as well as for the caffeine moiety of C_8-6-I and C_8-6-N. I speculated that the dimerization of caffeine would have conferred extra energetic stability to circumvent P450-mediated metabolism. Additionally, the low *in vitro* turnover rate of the enzymes involved in caffeine metabolism (143, 211) may be responsible for the metabolic stability of C_8-6-C_8, as well as the caffeine moiety of C_8-6-I and C_8-6-N. Interestingly, Istradefylline which is a caffeine analogue that is currently under development for treatment of the signs and symptoms of PD, was reported to undergo oxidative metabolism of the non-caffeine moiety, with the main metabolites (Figure 4.5) being M1 (4′-O-monodesmethylated) and M8 (1-β-hydroxylated) (data on file; Kyowa

Kirin Pharmaceutical Development, Inc.) suggesting that C8 functionalization of caffeine may confer metabolic stability.

Furthermore, our study revealed that dealkylation (M1 and M3) and hydroxylation (M2 and M4) are the common metabolic pathways for C_8-6-I and C_8-6-N in HLM, MLM, and RLM (Figure 4.4). Previous metabolism studies suggest that nicotine is metabolized to the following phase I metabolites: nicotine-$\Delta^{1'(5')}$-iminium ion, 5'-hydroxynicotine, nornicotine, 2'-hydroxynicotine, 4-(methylamino)-1-(3- pyridyl)-1-butanone, 4-oxo-4-(3-pyridyl) butanoic acid and 4- hydroxy-4-(3-pyridyl) butanoic acid(148); however, our study identified only a hydroxylated metabolite (M4) for the nicotine moiety of C_8-6-N. Given that the 2'-hydroxylation of nicotine is a minor pathway for nicotine metabolism, we propose the 5'-position of nicotine as the location of the hydroxyl group on M4 (Figure 4.7B) because the 5'-hydroxylation pathway leads to the formation of cotinine which is the main metabolite of nicotine (148). The formation of cotinine involves two steps: (i) CYP2A6-mediated metabolism of nicotine to form nicotine-$\Delta^{1'(5')}$-iminium ion which is in equilibrium with 5'-hydroxynicotine, and (ii) cytoplasmic aldehyde oxidase-mediated formation of cotinine (148). As microsomes do not contain cytoplasmic enzymes such as aldehyde oxidase, it is impossible to ascertain at this stage whether the hydroxyl group on M4 is further reduced to a ketone (cotinine).

Furthermore, previous studies suggest that nicotine and some of its metabolites (such as cotinine) have neurotherapeutic effects for PD (222). This suggests that M4 may have similar neuroprotective effect as the parent compound (C_8-6-N). More so, 2'-hydroxylation of nicotine is an important step in the formation of 4-(methylamino)-1-

(3- pyridyl)-1-butanone, 4-oxo-4-(3-pyridyl) butanoic acid and 4-hydroxy-4-(3-pyridyl) butanoic acid (156); however, this is a minor pathway in nicotine metabolism. In fact, this pathway is toxicologically significant since 4-(methylamino)-1-(3-pyridyl)-1-butanone can be biotransformed to carcinogenic NNK (148). Fortunately, this pathway was not observed in the biotransformation of C_8-6-N in HLM, RLM, and MLM.

In addition, 1-aminoindan is a metabolite of rasagiline, and subsequent metabolism of 1-aminoindan gives rise to 3-OH-AI (161-163). A hydroxylated metabolite of C_8-6-I was identified, and tandem mass spectrometry suggests that the hydroxyl group is located on the 1-aminoindan moiety of C_8-6-I. Given that 3-OH-AI is the only reported metabolite of 1-aminoindan, we propose that the hydroxyl group is located on the 3-position of M2 (Figure 4.6 B). As a derivative of 1-aminoindan, 3-OH-AI might also have neuroprotective effects (168); therefore M2 might be neuroprotective too. Additionally, as M1 and M3 contain a caffeine moiety, they might also have potential neuroprotective properties.

A major challenge encountered during the *in vitro* metabolism studies is the poor solubility of C_8-6-C_8. I discovered that C_8-6-C_8 had better solubility in chloroform than other organic solvents such as methanol, acetonitrile, and dimethyl sulfoxide. To ensure optimum P450 enzyme activity, the final organic solvent concentration in the samples was kept at 0.5%. Additionally, a recent study reported the negative impact of cytosolic contamination of liver microsomes on the interpretation of *in vitro* metabolism studies performed in microsomal fractions (223). Although there is a potential for cytosolic contamination of the liver microsomes used in this present

study, we did not observe any metabolite originating from aldehyde oxidase activity, such as the cotinine metabolite of C_8-6-N, or conjugation reactions.

6.3 Recommendation for development of PET Imaging probes for Parkinson's disease

Given the current challenges associated with the diagnosis of PD, PET imaging probes may be useful for early stage, as well as differential diagnosis of PD. Previous studies have used PET imaging probes to monitor the biochemical and neurological changes associated with PD. For example, Ouchi *et al*., used ^{11}C-PK11195 and ^{11}C-CFT (119) while Gerhard *et al*., used [^{11}C] (R)-PK11195 and [^{18}F]-DOPA(120) to monitor the alterations in neuroinflammatory reactions and the deletion of nerve terminals in the striatum as a measure of the integrity of dopaminergic neurons. Although the outcome of both studies provided useful information about the neuroanatomical changes associated with PD, it does not provide sufficient information that can help detect the onset of PD or aid in the differential diagnosis of PD in the presence of other neurodegenerative disorders.

The overall advantage of these bifunctional compounds resides in their ability to interact with AS; therefore, radiolabeled analogues of these bifunctional compounds can be used to monitor AS misfolding as an indication of the onset of PD even in the presence of other neurodegenerative disorders. This is better than monitoring neuroanatomical changes such as deletion of dopaminergic nerve terminals because clinical manifestation of neuroanatomical abnormalities is dependent on the severity of the disease; for example, previous studies have shown that patients diagnosed with PD have lost about 60 to 80% of dopaminergic neurons prior to the onset of symptoms (22-25).

To develop these novel bifunctional compounds as PET imaging probes with clinical translational for diagnosing PD, they should have high binding affinity to AS, high specificity to AS, high sensitivity, high contrast ratio, high *in vivo* stability, low immunogenicity and toxicity (96). To achieve high *in vivo* stability, the ^{18}F should be attached to the caffeine moiety of these bifunctional compounds because of its *in vitro* metabolic stability. Given the similarity in the metabolic pathways, mouse and rat may be useful surrogates for future animal studies of C_8-6-I, C_8-6-N, and C_8-6-C_8. Interestingly, our *in vivo* animal model for biodistribution studies is a mouse, and there is a good chance that the outcome of the biodistribution studies can be correlated to humans.

6.4 Conclusion

I established a novel tandem mass spectrometric fingerprint for C_8-6-I, C_8-6-N, and C_8-6-C_8, and determined their metabolic profile in HLM, MLM, and RLM. The diagnostic product ions and neutral losses identified from the tandem mass spectrometric analysis can be used for qualitative and quantitative analysis of C_8-6-I, C_8-6-N, and C_8-6-C_8 in biological matrices. While C_8-6-I and C_8-6-N are metabolized in HLM, MLM, and RLM, C_8-6-C_8 is not metabolized. Given the similarity in the metabolic pathways, mouse and rat may be useful surrogates for future animal studies of C_8-6-I, C_8-6-N, and C_8-6-C_8. To ensure optimum *in vivo* biodistribution and lifetime, the ^{18}F radioisotope should be attached to the caffeine moiety of C_8-6-I, C_8-6-N, and C_8-6-C_8. A rapid bioanalytical method has been developed for the quantification of C_8-6-I, C_8-6-N, and C_8-6-C_8 in HLM, MLM, and RLM. I have set up a validation protocol according to the US Food and Drug Administration guideline, and I achieved linearity of 0.1 µg/mL to 14 µg/mL for C_8-6-C_8 and 0.5 µg/mL to 100 µg/mL for C_8-6-I. Upon completion of validation, the method will

be used for the determination of the kinetic parameters of the *in vitro* metabolism of C_8-6-I, C_8-6-N, and C_8-6-C_8 in HLM, MLM, and RLM.

6.5 Future work

Although previous studies have established the binding of C_8-6-I, C_8-6-N, and C_8-6-C_8 to AS (123), it is important to determine whether these bifunctional compounds also bind to the oligomeric, fibrillated, and phosphorylated forms of AS. Given the implication of the phosphorylated, oligomeric, and fibrillated forms of AS in the pathogenesis of PD, developing PET probes that can bind to these forms of AS will be important in determining the onset of PD. Interestingly, previous studies suggest that authentic phosphorylation of AS at serine-129 leads to an increase in fibril formation(13-17) and 90% of insoluble AS in Lewy bodies is phosphorylated (14, 224); therefore, if C_8-6-I, C_8-6-N, and C_8-6-C_8 bind to the phosphorylated, oligomeric, and fibrillated forms of AS, their radiolabeled forms may be used for detecting the onset of PD and also for monitoring disease progression. A good next step would be to determine the amino acids that define the binding region of C_8-6-I, C_8-6-N, and C_8-6-C_8 on AS. Such information would be used to modify the structure of C_8-6-I, C_8-6-N, and C_8-6-C_8 if binding to the oligomeric, fibrillated, and phosphorylated forms of AS becomes challenging.

Furthermore, previous studies suggest that the metabolites of 1-aminoindan (168) and nicotine (222) might also have neuroprotective effects. Thus, future studies should be directed toward evaluating the neurotherapeutic properties of M1, M2, M3, and M4. Although evaluating the neurotherapeutic potentials of the metabolites of C_8-6-I, C_8-6-N, and C_8-6-C_8 is beneficial, it is also imperative to determine their toxicity profile especially at this early stage of drug discovery and development.

Additionally, as the present study did not determine the effect of cytosolic enzymes in the biotransformation of C_8-6-I, C_8-6-N, and C_8-6-C_8 in HLM, MLM, and RLM, it is necessary to determine the phase II metabolic profile of C_8-6-I, C_8-6-N, and C_8-6-C_8, as well as the neurotherapeutic effects of the corresponding metabolites. Also, it is important to determine the P450 enzymes, as well as the conjugation enzymes involved in the *in vitro* metabolism of C_8-6-I, C_8-6-N, and C_8-6-C_8. Such reaction phenotyping studies can help predict and avoid pharmacokinetic variability and adverse drug reactions by indicating whether the P450 isoform is highly inducible (for example, CYP2B6) or polymorphically expressed (for instance, CYP2D6) (203). However, an appropriate analytical method is critical to the success of reaction phenotyping studies.

Although the present study developed an HPLC method for the quantification of C_8-6-I, C_8-6-N, and C_8-6-C_8 in HLM, MLM, and RLM, it is important to mention that LC-MRM offers superior quantitative capabilities, high selectivity, and sensitivity through MRM mode. The developed HPLC method can be used for the determination of the enzyme kinetics of the *in vitro* metabolism of C_8-6-I, C_8-6-N, and C_8-6-C_8 in HLM, MLM, and RLM. Future studies for the quantification of C_8-6-I, C_8-6-N, and C_8-6-C_8 in complex biological matrices such as blood and plasma for determination of their pharmacokinetic parameters should utilize the established mass spectrometric fingerprint to develop an LC-MRM-based analytical method. Such pharmacokinetic studies usually monitor very low concentrations of the test compounds which may not be achieved using an HPLC-ultraviolet detection. A major challenge with quantification using LC-MRM is the need to develop isotopically labeled forms of the test compounds as internal standards; however,

the cost associated with developing isotopically labeled forms of C_8-6-I, C_8-6-N, and C_8-6-C_8 can be circumvented by using differential isotopic labeling.

Moreover, the effect of membrane transporters should be evaluated at this early stage of drug discovery to ascertain whether to modify the structure of these bifunctional compounds without affecting their efficacy. P-glycoprotein (P-gp) and breast cancer resistance protein (BCRP) are two important efflux transporters that play a critical role in limiting the CNS activity of some neurotherapeutic agents by preventing their penetration across the BBB (225). In fact, P-gp and BCRP are also implicated in the neuropathology of PD (226, 227). Hence, it is important to ascertain the effect of these transporters in the disposition of C_8-6-I, C_8-6-N, and C_8-6-C_8 using a PD-pathological BBB model, as well as a non-PD-pathological BBB model. There are several case studies implicating either P-gp, BCRP or both in the low CNS activity of neurotherapeutic agents and a typical example is the novel anti-PD candidate drug FLZ (N-2-(4-hydroxy-phenyl)-ethyl]-2-(2,5-dimethoxy-phenyl)-3-(3-methoxy-4-hydroxy-phenyl)-acrylamide) which showed low BBB penetration in rat brain (225). Given the role of P-gp and BCRP in both efflux of substrates across the BBB, as well as neuropathology of PD, a study was conducted to determine whether P-gp and BCRP play a role in the low BBB permeability of FLZ and also to examine the influence of PD-pathological BBB in the transport of FLZ (228). The study found greater expression of P-gp and BCRP in the PD-pathological BBB model associated with reduced *in vitro* BBB permeability of FLZ compared to the non-PD-pathological BBB model. The study concluded that P-gp but not BCRP is responsible for the low BBB permeability of FLZ (228). One way to address this challenge would be to co-administer P-gp inhibitors such as haloperidol or the use of novel drug delivery P-gp bypass systems

and pharmaceutical excipients such as chemosensitizers, natural and synthetic polymers, and formulation excipients used as P-gp inhibitors (229)

References

1. Klockgether T. Parkinson's disease: clinical aspects. Cell Tissue Res. 2004;318(1):115-20.
2. de Lau LM, Breteler MM. Epidemiology of Parkinson's disease. Lancet Neurol. 2006;5(6):525-35.
3. Ayano G. Parkinson's Disease: A Concise Overview of Etiology, Epidemiology, Diagnosis, Comorbidity and Management. Journal of Neurological Disorders. 2016.
4. Samii A, Nutt JG, Ransom BR. Parkinson's disease. Lancet. 2004;363(9423):1783-93.
5. Schrag A. Epidemiology of movement disorders. Tolosa E, Jankovic J, editors. Hagerstown, Maryland: Lippincott Williams & Wilkins; 2007.
6. Lesage S, Brice A. Parkinson's disease: from monogenic forms to genetic susceptibility factors. Hum Mol Genet. 2009;18(R1):R48-59.
7. Greggio E, Bisaglia M, Civiero L, Bubacco L. Leucine-rich repeat kinase 2 and alpha-synuclein: intersecting pathways in the pathogenesis of Parkinson's disease? Mol Neurodegener. 2011;6(1):6.
8. Maekawa T, Sasaoka T, Azuma S, Ichikawa T, Melrose HL, Farrer MJ, et al. Leucine-rich repeat kinase 2 (LRRK2) regulates alpha-synuclein clearance in microglia. BMC Neurosci. 2016;17(1):77.
9. Farrer M, Kachergus J, Forno L, Lincoln S, Wang DS, Hulihan M, et al. Comparison of kindreds with parkinsonism and alpha-synuclein genomic multiplications. Ann Neurol. 2004;55(2):174-9.
10. Goedert M. Familial Parkinson's disease. The awakening of alpha-synuclein. Nature. 1997;388(6639):232-3.
11. Polymeropoulos MH, Lavedan C, Leroy E, Ide SE, Dehejia A, Dutra A, et al. Mutation in the alpha-synuclein gene identified in families with Parkinson's disease. Science. 1997;276(5321):2045-7.
12. Trinh J, Guella I, Farrer MJ. Disease penetrance of late-onset parkinsonism: a meta-analysis. JAMA Neurol. 2014;71(12):1535-9.
13. Arawaka S, Wada M, Goto S, Karube H, Sakamoto M, Ren CH, et al. The role of G-protein-coupled receptor kinase 5 in pathogenesis of sporadic Parkinson's disease. J Neurosci. 2006;26(36):9227-38.
14. Fujiwara H, Hasegawa M, Dohmae N, Kawashima A, Masliah E, Goldberg MS, et al. alpha-Synuclein is phosphorylated in synucleinopathy lesions. Nat Cell Biol. 2002;4(2):160-4.
15. Smith WW, Margolis RL, Li X, Troncoso JC, Lee MK, Dawson VL, et al. Alpha-synuclein phosphorylation enhances eosinophilic cytoplasmic inclusion formation in SH-SY5Y cells. J Neurosci. 2005;25(23):5544-52.
16. Takahashi M, Ko LW, Kulathingal J, Jiang P, Sevlever D, Yen SH. Oxidative stress-induced phosphorylation, degradation and aggregation of alpha-synuclein are linked to upregulated CK2 and cathepsin D. Eur J Neurosci. 2007;26(4):863-74.
17. Wu B, Liu Q, Duan C, Li Y, Yu S, Chan P, et al. Phosphorylation of alpha-synuclein upregulates tyrosine hydroxylase activity in MN9D cells. Acta Histochem. 2011;113(1):32-5.

18. Paleologou KE, Schmid AW, Rospigliosi CC, Kim HY, Lamberto GR, Fredenburg RA, et al. Phosphorylation at Ser-129 but not the phosphomimics S129E/D inhibits the fibrillation of alpha-synuclein. J Biol Chem. 2008;283(24):16895-905.
19. Schreurs S, Gerard M, Derua R, Waelkens E, Taymans JM, Baekelandt V, et al. In vitro phosphorylation does not influence the aggregation kinetics of WT alpha-synuclein in contrast to its phosphorylation mutants. Int J Mol Sci. 2014;15(1):1040-67.
20. Greggio E, Jain S, Kingsbury A, Bandopadhyay R, Lewis P, Kaganovich A, et al. Kinase activity is required for the toxic effects of mutant LRRK2/dardarin. Neurobiol Dis. 2006;23(2):329-41.
21. Qing H, Wong W, McGeer EG, McGeer PL. Lrrk2 phosphorylates alpha synuclein at serine 129: Parkinson disease implications. Biochem Biophys Res Commun. 2009;387(1):149-52.
22. Hollerman JR, Schultz W. Dopamine neurons report an error in the temporal prediction of reward during learning. Nat Neurosci. 1998;1(4):304-9.
23. Ljungberg T, Apicella P, Schultz W. Responses of monkey dopamine neurons during learning of behavioral reactions. J Neurophysiol. 1992;67(1):145-63.
24. Schultz W, Dayan P, Montague PR. A neural substrate of prediction and reward. Science. 1997;275(5306):1593-9.
25. Waelti P, Dickinson A, Schultz W. Dopamine responses comply with basic assumptions of formal learning theory. Nature. 2001;412(6842):43-8.
26. contributors. W. MPTP: Wikipedia, The free Encyclopedia; 2017 [updated June 17, 2017. Available from: https://en.wikipedia.org/w/index.php?title=MPTP&oldid=786163490.
27. Callaghan RC, Cunningham JK, Sykes J, Kish SJ. Increased risk of Parkinson's disease in individuals hospitalized with conditions related to the use of methamphetamine or other amphetamine-type drugs. Drug Alcohol Depend. 2012;120(1-3):35-40.
28. Curtin K, Fleckenstein AE, Robison RJ, Crookston MJ, Smith KR, Hanson GR. Methamphetamine/amphetamine abuse and risk of Parkinson's disease in Utah: a population-based assessment. Drug Alcohol Depend. 2015;146:30-8.
29. Kamel F. Epidemiology. Paths from pesticides to Parkinson's. Science. 2013;341(6147):722-3.
30. Kuter K, Nowak P, Golembiowska K, Ossowska K. Increased reactive oxygen species production in the brain after repeated low-dose pesticide paraquat exposure in rats. A comparison with peripheral tissues. Neurochem Res. 2010;35(8):1121-30.
31. Wang A, Costello S, Cockburn M, Zhang X, Bronstein J, Ritz B. Parkinson's disease risk from ambient exposure to pesticides. Eur J Epidemiol. 2011;26(7):547-55.
32. Kakish J, Lee D, Lee JS. Drugs That Bind to alpha-Synuclein: Neuroprotective or Neurotoxic? ACS Chem Neurosci. 2015;6(12):1930-40.
33. Atik A, Stewart T, Zhang J. Alpha-Synuclein as a Biomarker for Parkinson's Disease. Brain Pathol. 2016;26(3):410-8.
34. Jankovic J. Parkinson's disease and movement disorders: moving forward. Lancet Neurol. 2008;7(1):9-11.

35. Shulman JM, De Jager PL, Feany MB. Parkinson's disease: genetics and pathogenesis. Annu Rev Pathol. 2011;6:193-222.
36. Tolosa E, Wenning G, Poewe W. The diagnosis of Parkinson's disease. Lancet Neurol. 2006;5(1):75-86.
37. Moore DJ, West AB, Dawson VL, Dawson TM. Molecular pathophysiology of Parkinson's disease. Annu Rev Neurosci. 2005;28:57-87.
38. Sollinger AB, Goldstein FC, Lah JJ, Levey AI, Factor SA. Mild cognitive impairment in Parkinson's disease: subtypes and motor characteristics. Parkinsonism Relat Disord. 2010;16(3):177-80.
39. Schrag A, Ben-Shlomo Y, Quinn N. How valid is the clinical diagnosis of Parkinson's disease in the community? J Neurol Neurosurg Psychiatry. 2002;73(5):529-34.
40. Hughes AJ, Ben-Shlomo Y, Daniel SE, Lees AJ. What features improve the accuracy of clinical diagnosis in Parkinson's disease: A clinicopathologic study. Neurology. 2001;57(10):S34-S8.
41. Hughes AJ, Daniel SE, Lees AJ. Improved accuracy of clinical diagnosis of Lewy body Parkinson's disease. Neurology. 2001;57(8):1497-9.
42. Litvan I, MacIntyre A, Goetz CG, Wenning GK, Jellinger K, Verny M, et al. Accuracy of the clinical diagnoses of Lewy body disease, Parkinson disease, and dementia with Lewy bodies: a clinicopathologic study. Arch Neurol. 1998;55(7):969-78.
43. Rajput AH, Rozdilsky B, Rajput A. Accuracy of clinical diagnosis in parkinsonism--a prospective study. Can J Neurol Sci. 1991;18(3):275-8.
44. Aarsland D, Kurz MW. The epidemiology of dementia associated with Parkinson disease. J Neurol Sci. 2010;289(1-2):18-22.
45. Aarsland D, Zaccai J, Brayne C. A systematic review of prevalence studies of dementia in Parkinson's disease. Mov Disord. 2005;20(10):1255-63.
46. Ahn TB, Kim SY, Kim JY, Park SS, Lee DS, Min HJ, et al. alpha-Synuclein gene duplication is present in sporadic Parkinson disease. Neurology. 2008;70(1):43-9.
47. Miller DW, Hague SM, Clarimon J, Baptista M, Gwinn-Hardy K, Cookson MR, et al. Alpha-synuclein in blood and brain from familial Parkinson disease with SNCA locus triplication. Neurology. 2004;62(10):1835-8.
48. Lee HJ, Patel S, Lee SJ. Intravesicular localization and exocytosis of alpha-synuclein and its aggregates. J Neurosci. 2005;25(25):6016-24.
49. Marques O, Outeiro TF. Alpha-synuclein: from secretion to dysfunction and death. Cell Death Dis. 2012;3:e350.
50. Nakai M, Fujita M, Waragai M, Sugama S, Wei J, Akatsu H, et al. Expression of alpha-synuclein, a presynaptic protein implicated in Parkinson's disease, in erythropoietic lineage. Biochem Biophys Res Commun. 2007;358(1):104-10.
51. Braak H, Del Tredici K, Rub U, de Vos RA, Jansen Steur EN, Braak E. Staging of brain pathology related to sporadic Parkinson's disease. Neurobiol Aging. 2003;24(2):197-211.
52. Iwanaga K, Wakabayashi K, Yoshimoto M, Tomita I, Satoh H, Takashima H, et al. Lewy body-type degeneration in cardiac plexus in Parkinson's and incidental Lewy body diseases. Neurology. 1999;52(6):1269-71.

53. Beach TG, White CL, 3rd, Hladik CL, Sabbagh MN, Connor DJ, Shill HA, et al. Olfactory bulb alpha-synucleinopathy has high specificity and sensitivity for Lewy body disorders. Acta Neuropathol. 2009;117(2):169-74.
54. Braak H, de Vos RA, Bohl J, Del Tredici K. Gastric alpha-synuclein immunoreactive inclusions in Meissner's and Auerbach's plexuses in cases staged for Parkinson's disease-related brain pathology. Neurosci Lett. 2006;396(1):67-72.
55. Lebouvier T, Chaumette T, Damier P, Coron E, Touchefeu Y, Vrignaud S, et al. Pathological lesions in colonic biopsies during Parkinson's disease. Gut. 2008;57(12):1741-3.
56. Lebouvier T, Neunlist M, Bruley des Varannes S, Coron E, Drouard A, N'Guyen JM, et al. Colonic biopsies to assess the neuropathology of Parkinson's disease and its relationship with symptoms. PLoS One. 2010;5(9):e12728.
57. Pouclet H, Lebouvier T, Coron E, Des Varannes SB, Neunlist M, Derkinderen P. A comparison between colonic submucosa and mucosa to detect Lewy pathology in Parkinson's disease. Neurogastroenterol Motil. 2012;24(4):e202-5.
58. Pouclet H, Lebouvier T, Coron E, des Varannes SB, Rouaud T, Roy M, et al. A comparison between rectal and colonic biopsies to detect Lewy pathology in Parkinson's disease. Neurobiol Dis. 2012;45(1):305-9.
59. Shannon KM, Keshavarzian A, Mutlu E, Dodiya HB, Daian D, Jaglin JA, et al. Alpha-synuclein in colonic submucosa in early untreated Parkinson's disease. Mov Disord. 2012;27(6):709-15.
60. Orimo S, Uchihara T, Nakamura A, Mori F, Kakita A, Wakabayashi K, et al. Axonal alpha-synuclein aggregates herald centripetal degeneration of cardiac sympathetic nerve in Parkinson's disease. Brain. 2008;131(Pt 3):642-50.
61. Fujishiro H, Frigerio R, Burnett M, Klos KJ, Josephs KA, Delledonne A, et al. Cardiac sympathetic denervation correlates with clinical and pathologic stages of Parkinson's disease. Mov Disord. 2008;23(8):1085-92.
62. Ghebremedhin E, Del Tredici K, Langston JW, Braak H. Diminished tyrosine hydroxylase immunoreactivity in the cardiac conduction system and myocardium in Parkinson's disease: an anatomical study. Acta Neuropathol. 2009;118(6):777-84.
63. Beach TG, Adler CH, Dugger BN, Serrano G, Hidalgo J, Henry-Watson J, et al. Submandibular gland biopsy for the diagnosis of Parkinson disease. J Neuropathol Exp Neurol. 2013;72(2):130-6.
64. Cersosimo MG, Perandones C, Micheli FE, Raina GB, Beron AM, Nasswetter G, et al. Alpha-synuclein immunoreactivity in minor salivary gland biopsies of Parkinson's disease patients. Mov Disord. 2011;26(1):188-90.
65. Del Tredici K, Hawkes CH, Ghebremedhin E, Braak H. Lewy pathology in the submandibular gland of individuals with incidental Lewy body disease and sporadic Parkinson's disease. Acta Neuropathol. 2010;119(6):703-13.
66. Mu L, Sobotka S, Chen J, Su H, Sanders I, Nyirenda T, et al. Parkinson disease affects peripheral sensory nerves in the pharynx. J Neuropathol Exp Neurol. 2013;72(7):614-23.
67. Shi M, Zabetian CP, Hancock AM, Ginghina C, Hong Z, Yearout D, et al. Significance and confounders of peripheral DJ-1 and alpha-synuclein in Parkinson's disease. Neurosci Lett. 2010;480(1):78-82.

68. Hong Z, Shi M, Chung KA, Quinn JF, Peskind ER, Galasko D, et al. DJ-1 and alpha-synuclein in human cerebrospinal fluid as biomarkers of Parkinson's disease. Brain. 2010;133(Pt 3):713-26.
69. Mollenhauer B, Locascio JJ, Schulz-Schaeffer W, Sixel-Doring F, Trenkwalder C, Schlossmacher MG. alpha-Synuclein and tau concentrations in cerebrospinal fluid of patients presenting with parkinsonism: a cohort study. Lancet Neurol. 2011;10(3):230-40.
70. Parnetti L, Chiasserini D, Persichetti E, Eusebi P, Varghese S, Qureshi MM, et al. Cerebrospinal fluid lysosomal enzymes and alpha-synuclein in Parkinson's disease. Mov Disord. 2014;29(8):1019-27.
71. Wang Y, Shi M, Chung KA, Zabetian CP, Leverenz JB, Berg D, et al. Phosphorylated alpha-synuclein in Parkinson's disease. Sci Transl Med. 2012;4(121):121ra20.
72. Borghi R, Marchese R, Negro A, Marinelli L, Forloni G, Zaccheo D, et al. Full length alpha-synuclein is present in cerebrospinal fluid from Parkinson's disease and normal subjects. Neurosci Lett. 2000;287(1):65-7.
73. Jakowec MW, Petzinger GM, Sastry S, Donaldson DM, McCormack A, Langston JW. The native form of alpha-synuclein is not found in the cerebrospinal fluid of patients with Parkinson's disease or normal controls. Neurosci Lett. 1998;253(1):13-6.
74. Park MJ, Cheon SM, Bae HR, Kim SH, Kim JW. Elevated levels of alpha-synuclein oligomer in the cerebrospinal fluid of drug-naive patients with Parkinson's disease. J Clin Neurol. 2011;7(4):215-22.
75. Tokuda T, Qureshi MM, Ardah MT, Varghese S, Shehab SA, Kasai T, et al. Detection of elevated levels of alpha-synuclein oligomers in CSF from patients with Parkinson disease. Neurology. 2010;75(20):1766-72.
76. Stewart T, Sossi V, Aasly JO, Wszolek ZK, Uitti RJ, Hasegawa K, et al. Phosphorylated alpha-synuclein in Parkinson's disease: correlation depends on disease severity. Acta Neuropathol Commun. 2015;3:7.
77. Shi M, Bradner J, Hancock AM, Chung KA, Quinn JF, Peskind ER, et al. Cerebrospinal fluid biomarkers for Parkinson disease diagnosis and progression. Ann Neurol. 2011;69(3):570-80.
78. Toledo JB, Korff A, Shaw LM, Trojanowski JQ, Zhang J. CSF alpha-synuclein improves diagnostic and prognostic performance of CSF tau and Abeta in Alzheimer's disease. Acta Neuropathol. 2013;126(5):683-97.
79. Smith LM, Schiess MC, Coffey MP, Klaver AC, Loeffler DA. alpha-Synuclein and anti-alpha-synuclein antibodies in Parkinson's disease, atypical Parkinson syndromes, REM sleep behavior disorder, and healthy controls. PLoS One. 2012;7(12):e52285.
80. Besong-Agbo D, Wolf E, Jessen F, Oechsner M, Hametner E, Poewe W, et al. Naturally occurring alpha-synuclein autoantibody levels are lower in patients with Parkinson disease. Neurology. 2013;80(2):169-75.
81. Duran R, Barrero FJ, Morales B, Luna JD, Ramirez M, Vives F. Plasma alpha-synuclein in patients with Parkinson's disease with and without treatment. Mov Disord. 2010;25(4):489-93.

82. Foulds PG, Mitchell JD, Parker A, Turner R, Green G, Diggle P, et al. Phosphorylated alpha-synuclein can be detected in blood plasma and is potentially a useful biomarker for Parkinson's disease. FASEB J. 2011;25(12):4127-37.
83. Lee PH, Lee G, Park HJ, Bang OY, Joo IS, Huh K. The plasma alpha-synuclein levels in patients with Parkinson's disease and multiple system atrophy. J Neural Transm (Vienna). 2006;113(10):1435-9.
84. Li QX, Mok SS, Laughton KM, McLean CA, Cappai R, Masters CL, et al. Plasma alpha-synuclein is decreased in subjects with Parkinson's disease. Exp Neurol. 2007;204(2):583-8.
85. Mata IF, Shi M, Agarwal P, Chung KA, Edwards KL, Factor SA, et al. SNCA variant associated with Parkinson disease and plasma alpha-synuclein level. Arch Neurol. 2010;67(11):1350-6.
86. Gorostidi A, Bergareche A, Ruiz-Martinez J, Marti-Masso JF, Cruz M, Varghese S, et al. Alphalpha-synuclein levels in blood plasma from LRRK2 mutation carriers. PLoS One. 2012;7(12):e52312.
87. Shi M, Liu C, Cook TJ, Bullock KM, Zhao Y, Ginghina C, et al. Plasma exosomal alpha-synuclein is likely CNS-derived and increased in Parkinson's disease. Acta Neuropathol. 2014;128(5):639-50.
88. El-Agnaf OM, Salem SA, Paleologou KE, Curran MD, Gibson MJ, Court JA, et al. Detection of oligomeric forms of alpha-synuclein protein in human plasma as a potential biomarker for Parkinson's disease. FASEB J. 2006;20(3):419-25.
89. Yanamandra K, Gruden MA, Casaite V, Meskys R, Forsgren L, Morozova-Roche LA. alpha-synuclein reactive antibodies as diagnostic biomarkers in blood sera of Parkinson's disease patients. PLoS One. 2011;6(4):e18513.
90. Abd-Elhadi S, Honig A, Simhi-Haham D, Schechter M, Linetsky E, Ben-Hur T, et al. Total and Proteinase K-Resistant alpha-Synuclein Levels in Erythrocytes, Determined by their Ability to Bind Phospholipids, Associate with Parkinson's Disease. Sci Rep. 2015;5:11120.
91. Devic I, Hwang H, Edgar JS, Izutsu K, Presland R, Pan C, et al. Salivary alpha-synuclein and DJ-1: potential biomarkers for Parkinson's disease. Brain. 2011;134(Pt 7):e178.
92. Al-Nimer MS, Mshatat SF, Abdulla HI. Saliva alpha-Synuclein and A High Extinction Coefficient Protein: A Novel Approach in Assessment Biomarkers of Parkinson's Disease. N Am J Med Sci. 2014;6(12):633-7.
93. Lu FM, Yuan Z. PET/SPECT molecular imaging in clinical neuroscience: recent advances in the investigation of CNS diseases. Quant Imaging Med Surg. 2015;5(3):433-47.
94. Massoud TF, Gambhir SS. Molecular imaging in living subjects: seeing fundamental biological processes in a new light. Genes Dev. 2003;17(5):545-80.
95. Weissleder R, Mahmood U. Molecular imaging. Radiology. 2001;219(2):316-33.
96. Chen K, Chen X. Design and development of molecular imaging probes. Curr Top Med Chem. 2010;10(12):1227-36.
97. Kim E, Howes OD, Kapur S. Molecular imaging as a guide for the treatment of central nervous system disorders. Dialogues Clin Neurosci. 2013;15(3):315-28.
98. Phelps ME. Positron emission tomography provides molecular imaging of biological processes. Proc Natl Acad Sci U S A. 2000;97(16):9226-33.

99. Halldin C, Gulyas B, Langer O, Farde L. Brain radioligands--state of the art and new trends. Q J Nucl Med. 2001;45(2):139-52.
100. Strijckmans K. The isochronous cyclotron: principles and recent developments. Comput Med Imaging Graph. 2001;25(2):69-78.
101. Shoghi-Jadid K, Small GW, Agdeppa ED, Kepe V, Ercoli LM, Siddarth P, et al. Localization of neurofibrillary tangles and beta-amyloid plaques in the brains of living patients with Alzheimer disease. Am J Geriatr Psychiatry. 2002;10(1):24-35.
102. Brooks DJ, Ibanez V, Sawle GV, Quinn N, Lees AJ, Mathias CJ, et al. Differing patterns of striatal 18F-dopa uptake in Parkinson's disease, multiple system atrophy, and progressive supranuclear palsy. Ann Neurol. 1990;28(4):547-55.
103. Klunk WE, Engler H, Nordberg A, Wang Y, Blomqvist G, Holt DP, et al. Imaging brain amyloid in Alzheimer's disease with Pittsburgh Compound-B. Ann Neurol. 2004;55(3):306-19.
104. Mintun MA, Larossa GN, Sheline YI, Dence CS, Lee SY, Mach RH, et al. [11C]PIB in a nondemented population: potential antecedent marker of Alzheimer disease. Neurology. 2006;67(3):446-52.
105. Farde L, Wiesel FA, Stone-Elander S, Halldin C, Nordstrom AL, Hall H, et al. D2 dopamine receptors in neuroleptic-naive schizophrenic patients. A positron emission tomography study with [11C]raclopride. Arch Gen Psychiatry. 1990;47(3):213-9.
106. Hirvonen J, Karlsson H, Kajander J, Markkula J, Rasi-Hakala H, Nagren K, et al. Striatal dopamine D2 receptors in medication-naive patients with major depressive disorder as assessed with [11C]raclopride PET. Psychopharmacology (Berl). 2008;197(4):581-90.
107. Banati RB, Newcombe J, Gunn RN, Cagnin A, Turkheimer F, Heppner F, et al. The peripheral benzodiazepine binding site in the brain in multiple sclerosis: quantitative in vivo imaging of microglia as a measure of disease activity. Brain. 2000;123 (Pt 11):2321-37.
108. Groom GN, Junck L, Foster NL, Frey KA, Kuhl DE. PET of peripheral benzodiazepine binding sites in the microgliosis of Alzheimer's disease. J Nucl Med. 1995;36(12):2207-10.
109. Savic I, Thorell JO, Roland P. [11C]flumazenil positron emission tomography visualizes frontal epileptogenic regions. Epilepsia. 1995;36(12):1225-32.
110. Kadir A, Almkvist O, Wall A, Langstrom B, Nordberg A. PET imaging of cortical 11C-nicotine binding correlates with the cognitive function of attention in Alzheimer's disease. Psychopharmacology (Berl). 2006;188(4):509-20.
111. Pavese N, Brooks DJ. Imaging neurodegeneration in Parkinson's disease. Biochim Biophys Acta. 2009;1792(7):722-9.
112. Wang L, Zhang Q, Li H, Zhang H. SPECT molecular imaging in Parkinson's disease. J Biomed Biotechnol. 2012;2012:412486.
113. Gao HM, Jiang J, Wilson B, Zhang W, Hong JS, Liu B. Microglial activation-mediated delayed and progressive degeneration of rat nigral dopaminergic neurons: relevance to Parkinson's disease. J Neurochem. 2002;81(6):1285-97.
114. Mirza B, Hadberg H, Thomsen P, Moos T. The absence of reactive astrocytosis is indicative of a unique inflammatory process in Parkinson's disease. Neuroscience. 2000;95(2):425-32.

115. Sherer TB, Betarbet R, Kim JH, Greenamyre JT. Selective microglial activation in the rat rotenone model of Parkinson's disease. Neurosci Lett. 2003;341(2):87-90.
116. Sugama S, Yang L, Cho BP, DeGiorgio LA, Lorenzl S, Albers DS, et al. Age-related microglial activation in 1-methyl-4-phenyl-1,2,3,6-tetrahydropyridine (MPTP)-induced dopaminergic neurodegeneration in C57BL/6 mice. Brain Res. 2003;964(2):288-94.
117. Vila M, Jackson-Lewis V, Guegan C, Wu DC, Teismann P, Choi DK, et al. The role of glial cells in Parkinson's disease. Curr Opin Neurol. 2001;14(4):483-9.
118. Kreutzberg GW. Microglia: a sensor for pathological events in the CNS. Trends Neurosci. 1996;19(8):312-8.
119. Ouchi Y, Yoshikawa E, Sekine Y, Futatsubashi M, Kanno T, Ogusu T, et al. Microglial activation and dopamine terminal loss in early Parkinson's disease. Ann Neurol. 2005;57(2):168-75.
120. Gerhard A, Pavese N, Hotton G, Turkheimer F, Es M, Hammers A, et al. In vivo imaging of microglial activation with [11C](R)-PK11195 PET in idiopathic Parkinson's disease. Neurobiol Dis. 2006;21(2):404-12.
121. Cumming P, Borghammer P. Molecular imaging and the neuropathologies of Parkinson's disease. Curr Top Behav Neurosci. 2012;11:117-48.
122. Pedrosa DJ, Timmermann L. Review: management of Parkinson's disease. Neuropsychiatr Dis Treat. 2013;9:321-40.
123. Kakish J, Allen KJ, Harkness TA, Krol ES, Lee JS. Novel Dimer Compounds That Bind alpha-Synuclein Can Rescue Cell Growth in a Yeast Model Overexpressing alpha-Synuclein. A Possible Prevention Strategy for Parkinson's Disease. ACS Chem Neurosci. 2016;7(12):1671-80.
124. Feany MB, Pallanck LJ. Parkin: a multipurpose neuroprotective agent? Neuron. 2003;38(1):13-6.
125. Klein C, Westenberger A. Genetics of Parkinson's disease. Cold Spring Harb Perspect Med. 2012;2(1):a008888.
126. Youle RJ, Narendra DP. Mechanisms of mitophagy. Nat Rev Mol Cell Biol. 2011;12(1):9-14.
127. Bar Am O, Amit T, Youdim MB. Contrasting neuroprotective and neurotoxic actions of respective metabolites of anti-Parkinson drugs rasagiline and selegiline. Neurosci Lett. 2004;355(3):169-72.
128. Bar-Am O, Weinreb O, Amit T, Youdim MB. The neuroprotective mechanism of 1-(R)-aminoindan, the major metabolite of the anti-parkinsonian drug rasagiline. J Neurochem. 2010;112(5):1131-7.
129. Chau KY, Cooper JM, Schapira AH. Rasagiline protects against alpha-synuclein induced sensitivity to oxidative stress in dopaminergic cells. Neurochem Int. 2010;57(5):525-9.
130. Dimpfel W, Hoffmann JA. Effects of rasagiline, its metabolite aminoindan and selegiline on glutamate receptor mediated signalling in the rat hippocampus slice in vitro. BMC Pharmacol. 2011;11:2.
131. Patil SP, Jain PD, Ghumatkar PJ, Tambe R, Sathaye S. Neuroprotective effect of metformin in MPTP-induced Parkinson's disease in mice. Neuroscience. 2014;277:747-54.

132. Postuma RB, Lang AE, Munhoz RP, Charland K, Pelletier A, Moscovich M, et al. Caffeine for treatment of Parkinson disease: a randomized controlled trial. Neurology. 2012;79(7):651-8.
133. Prediger RD. Effects of caffeine in Parkinson's disease: from neuroprotection to the management of motor and non-motor symptoms. J Alzheimers Dis. 2010;20 Suppl 1:S205-20.
134. Quik M. Smoking, nicotine and Parkinson's disease. Trends Neurosci. 2004;27(9):561-8.
135. Quik M, Perez XA, Bordia T. Nicotine as a potential neuroprotective agent for Parkinson's disease. Mov Disord. 2012;27(8):947-57.
136. Ross GW, Petrovitch H. Current evidence for neuroprotective effects of nicotine and caffeine against Parkinson's disease. Drugs Aging. 2001;18(11):797-806.
137. Wahlqvist ML, Lee MS, Hsu CC, Chuang SY, Lee JT, Tsai HN. Metformin-inclusive sulfonylurea therapy reduces the risk of Parkinson's disease occurring with Type 2 diabetes in a Taiwanese population cohort. Parkinsonism Relat Disord. 2012;18(6):753-8.
138. Dufty BM, Warner LR, Hou ST, Jiang SX, Gomez-Isla T, Leenhouts KM, et al. Calpain-cleavage of alpha-synuclein: connecting proteolytic processing to disease-linked aggregation. Am J Pathol. 2007;170(5):1725-38.
139. Games D, Valera E, Spencer B, Rockenstein E, Mante M, Adame A, et al. Reducing C-terminal-truncated alpha-synuclein by immunotherapy attenuates neurodegeneration and propagation in Parkinson's disease-like models. J Neurosci. 2014;34(28):9441-54.
140. Contributors W. Drug Metabolism: Wikipedia, The Free Encyclopedia; 2017 [updated September 16, 2017. Available from: https://en.wikipedia.org/w/index.php?title=Drug_metabolism&oldid=800933953.
141. Croom E. Metabolism of xenobiotics of human environments. Prog Mol Biol Transl Sci. 2012;112:31-88.
142. Thorn CF, Aklillu E, McDonagh EM, Klein TE, Altman RB. PharmGKB summary: caffeine pathway. Pharmacogenet Genomics. 2012;22(5):389-95.
143. Grant DM, Campbell ME, Tang BK, Kalow W. Biotransformation of caffeine by microsomes from human liver. Kinetics and inhibition studies. Biochem Pharmacol. 1987;36(8):1251-60.
144. Begas E, Kouvaras E, Tsakalof A, Papakosta S, Asprodini EK. In vivo evaluation of CYP1A2, CYP2A6, NAT-2 and xanthine oxidase activities in a Greek population sample by the RP-HPLC monitoring of caffeine metabolic ratios. Biomed Chromatogr. 2007;21(2):190-200.
145. Gu L, Gonzalez FJ, Kalow W, Tang BK. Biotransformation of caffeine, paraxanthine, theobromine and theophylline by cDNA-expressed human CYP1A2 and CYP2E1. Pharmacogenetics. 1992;2(2):73-7.
146. Kot M, Daniel WA. The relative contribution of human cytochrome P450 isoforms to the four caffeine oxidation pathways: an in vitro comparative study with cDNA-expressed P450s including CYP2C isoforms. Biochem Pharmacol. 2008;76(4):543-51.
147. Kot M, Daniel WA. Caffeine as a marker substrate for testing cytochrome P450 activity in human and rat. Pharmacol Rep. 2008;60(6):789-97.

148. Benowitz NL, Hukkanen J, Jacob P, 3rd. Nicotine chemistry, metabolism, kinetics and biomarkers. Handb Exp Pharmacol. 2009(192):29-60.
149. Cashman JR, Park SB, Yang ZC, Wrighton SA, Jacob P, 3rd, Benowitz NL. Metabolism of nicotine by human liver microsomes: stereoselective formation of trans-nicotine N'-oxide. Chem Res Toxicol. 1992;5(5):639-46.
150. Shigenaga MK, Trevor AJ, Castagnoli N, Jr. Metabolism-dependent covalent binding of (S)-[5-3H]nicotine to liver and lung microsomal macromolecules. Drug Metab Dispos. 1988;16(3):397-402.
151. Benowitz NL, Jacob P, 3rd, Fong I, Gupta S. Nicotine metabolic profile in man: comparison of cigarette smoking and transdermal nicotine. J Pharmacol Exp Ther. 1994;268(1):296-303.
152. Park SB, Jacob P, 3rd, Benowitz NL, Cashman JR. Stereoselective metabolism of (S)-(-)-nicotine in humans: formation of trans-(S)-(-)-nicotine N-1'-oxide. Chem Res Toxicol. 1993;6(6):880-8.
153. Byrd GD, Uhrig MS, deBethizy JD, Caldwell WS, Crooks PA, Ravard A, et al. Direct determination of cotinine-N-glucuronide in urine using thermospray liquid chromatography/mass spectrometry. Biol Mass Spectrom. 1994;23(2):103-7.
154. Jacob P, 3rd, Shulgin AT, Benowitz NL. Synthesis of (3'R,5'S)-trans-3'-hydroxycotinine, a major metabolite of nicotine. Metabolic formation of 3'-hydroxycotinine in humans is highly stereoselective. J Med Chem. 1990;33(7):1888-91.
155. Voncken P, Rustemeier K, Schepers G. Identification of cis-3'-hydroxycotinine as a urinary nicotine metabolite. Xenobiotica. 1990;20(12):1353-6.
156. Hecht SS, Hochalter JB, Villalta PW, Murphy SE. 2'-Hydroxylation of nicotine by cytochrome P450 2A6 and human liver microsomes: formation of a lung carcinogen precursor. Proc Natl Acad Sci U S A. 2000;97(23):12493-7.
157. Hecht SS, Carmella SG, Chen M, Dor Koch JF, Miller AT, Murphy SE, et al. Quantitation of urinary metabolites of a tobacco-specific lung carcinogen after smoking cessation. Cancer Res. 1999;59(3):590-6.
158. Wang T, Yang L, Hua J, Xie H, Jiang X, Wang L. Simultaneous bioanalysis of rasagiline and its major metabolites in human plasma by LC-MS/MS: Application to a clinical pharmacokinetic study. J Pharm Biomed Anal. 2016;125:280-5.
159. Binda C, Hubalek F, Li M, Herzig Y, Sterling J, Edmondson DE, et al. Binding of rasagiline-related inhibitors to human monoamine oxidases: a kinetic and crystallographic analysis. J Med Chem. 2005;48(26):8148-54.
160. Olanow CW, Rascol O, Hauser R, Feigin PD, Jankovic J, Lang A, et al. A double-blind, delayed-start trial of rasagiline in Parkinson's disease. N Engl J Med. 2009;361(13):1268-78.
161. Agundez JA, Garcia-Martin E, Alonso-Navarro H, Jimenez-Jimenez FJ. Anti-Parkinson's disease drugs and pharmacogenetic considerations. Expert Opin Drug Metab Toxicol. 2013;9(7):859-74.
162. de Biase S, Merlino G, Lorenzut S, Valente M, Gigli GL. ADMET considerations when prescribing novel therapeutics to treat restless legs syndrome. Expert Opin Drug Metab Toxicol. 2014;10(10):1365-80.

163. Deftereos SN, Dodou E, Andronis C, Persidis A. From depression to neurodegeneration and heart failure: re-examining the potential of MAO inhibitors. Expert Rev Clin Pharmacol. 2012;5(4):413-25.
164. Bahar E, Frenkel A, Piryatinsky V. Deuterium enriched rasagiline. Google Patents; 2012.
165. Dimpfel W, Hoffmann JA. Electropharmacograms of rasagiline, its metabolite aminoindan and selegiline in the freely moving rat. Neuropsychobiology. 2010;62(4):213-20.
166. Ou XM, Lu D, Johnson C, Chen K, Youdim MB, Rajkowska G, et al. Glyceraldehyde-3-phosphate dehydrogenase-monoamine oxidase B-mediated cell death-induced by ethanol is prevented by rasagiline and 1-R-aminoindan. Neurotox Res. 2009;16(2):148-59.
167. Tazik S, Johnson S, Lu D, Johnson C, Youdim MB, Stockmeier CA, et al. Comparative neuroprotective effects of rasagiline and aminoindan with selegiline on dexamethasone-induced brain cell apoptosis. Neurotox Res. 2009;15(3):284-90.
168. Sterling J, Veinberg A, Lerner D, Goldenberg W, Levy R, Youdim M, et al. (R)(+)-N-propargyl-1-aminoindan (rasagiline) and derivatives: highly selective and potent inhibitors of monoamine oxidase B. J Neural Transm Suppl. 1998;52:301-5.
169. Bergman H, Deuschl G. Pathophysiology of Parkinson's disease: from clinical neurology to basic neuroscience and back. Mov Disord. 2002;17 Suppl 3:S28-40.
170. Brooks DJ. The early diagnosis of Parkinson's disease. Ann Neurol. 1998;44(3 Suppl 1):S10-8.
171. Gibrat C, Saint-Pierre M, Bousquet M, Levesque D, Rouillard C, Cicchetti F. Differences between subacute and chronic MPTP mice models: investigation of dopaminergic neuronal degeneration and alpha-synuclein inclusions. J Neurochem. 2009;109(5):1469-82.
172. Michel PP, Hirsch EC, Hunot S. Understanding Dopaminergic Cell Death Pathways in Parkinson Disease. Neuron. 2016;90(4):675-91.
173. Dauer W, Przedborski S. Parkinson's disease: mechanisms and models. Neuron. 2003;39(6):889-909.
174. Rizzo G, Copetti M, Arcuti S, Martino D, Fontana A, Logroscino G. Accuracy of clinical diagnosis of Parkinson disease: A systematic review and meta-analysis. Neurology. 2016;86(6):566-76.
175. Grebe SK, Singh RJ. LC-MS/MS in the Clinical Laboratory - Where to From Here? Clin Biochem Rev. 2011;32(1):5-31.
176. Himmelsbach M. 10 years of MS instrumental developments--impact on LC-MS/MS in clinical chemistry. J Chromatogr B Analyt Technol Biomed Life Sci. 2012;883-884:3-17.
177. Honour JW. Development and validation of a quantitative assay based on tandem mass spectrometry. Ann Clin Biochem. 2011;48(Pt 2):97-111.
178. Hsieh YS, Korfmacher W. The Role of Hyphenated Chromatography-Mass Spectrometry Techniques in Exploratory Drug Metabolism and Pharmacokinetics. Curr Pharm Design. 2009;15(19):2251-61.
179. Korfmacher W. Mass Spectrometry: The Premier Analytical Tool for DMPK Scientists in a Drug Discovery Environment. Spectroscopy-Us. 2013;28(3):46-53.

180. Liu X, Jia L. The conduct of drug metabolism studies considered good practice (I): analytical systems and in vivo studies. Curr Drug Metab. 2007;8(8):815-21.
181. Bourcier S, Benoist JF, Clerc F, Rigal O, Taghi M, Hoppilliard Y. Detection of 28 neurotransmitters and related compounds in biological fluids by liquid chromatography/tandem mass spectrometry. Rapid Commun Mass Sp. 2006;20(9):1405-21.
182. Bourcier S, Hoppilliard Y. Fragmentation mechanisms of protonated benzylamines. Electrospray ionisation-tandem mass spectrometry study and ab initio molecular orbital calculations. Eur J Mass Spectrom. 2003;9(4):351-60.
183. El Aribi H, Orlova G, Hopkinson AC, Siu KWM. Gas-phase fragmentation reactions of protonated aromatic amino acids: concomitant and consecutive neutral eliminations and radical cation formations. J Phys Chem A. 2004;108(17):3844-53.
184. Rogalewicz F, Bourcier S, Hoppilliard Y. Decomposition of protonated noradrenaline and normetanephrine assisted by NH2 migration studied by electrospray tandem mass spectrometry and molecular orbital calculations. Rapid Commun Mass Sp. 2005;19(6):743-51.
185. Rogalewicz F, Hoppilliard Y, Ohanessian G. Fragmentation mechanisms of alpha-amino acids protonated under electrospray ionization: a collisional activation and ab initio theoretical study. Int J Mass Spectrom. 2000;195:565-90.
186. Bourcier S, Hoppilliard Y. Use of diagnostic neutral losses for structural information on unknown aromatic metabolites: an experimental and theoretical study. Rapid Commun Mass Sp. 2009;23(1):93-103.
187. Al-Dulaymi M, El-Aneed A. Tandem mass spectrometric analysis of novel peptide-modified gemini surfactants used as gene delivery vectors. J Mass Spectrom. 2017;52(6):353-66.
188. Buse J, Badea I, Verrall RE, El-Aneed A. Tandem mass spectrometric analysis of novel diquaternary ammonium gemini surfactants and their bromide adducts in electrospray-positive ion mode ionization. J Mass Spectrom. 2011;46(10):1060-70.
189. Donkuru M, Chitanda JM, Verrall RE, El-Aneed A. Multi-stage tandem mass spectrometric analysis of novel beta-cyclodextrin-substituted and novel bis-pyridinium gemini surfactants designed as nanomedical drug delivery agents. Rapid Commun Mass Sp. 2014;28(7):757-72.
190. Buse J, Badea I, Verrall RE, El-Aneed A. A general liquid chromatography tandem mass spectrometry method for the quantitative determination of diquaternary ammonium gemini surfactant drug delivery agents in mouse keratinocytes' cellular lysate. J Chromatogr A. 2013;1294:98-105.
191. Buse J, Purves RW, Verrall RE, Badea I, Zhang HX, Mulligan CC, et al. The development and assessment of high-throughput mass spectrometry-based methods for the quantification of a nanoparticle drug delivery agent in cellular lysate. J Mass Spectrom. 2014;49(11):1171-80.
192. Donkuru M, Michel D, Awad H, Katselis G, El-Aneed A. Hydrophilic interaction liquid chromatography-tandem mass spectrometry quantitative method for the cellular analysis of varying structures of gemini surfactants designed as nanomaterial drug carriers. J Chromatogr A. 2016;1446:114-24.

193. Awad H, Das U, Dimmock J, El-Aneed A. Establishment of tandem mass spectrometric fingerprint of novel antineoplastic curcumin analogues using electrospray ionization. Rapid Commun Mass Sp. 2015;29(14):1307-16.
194. Bianco G, Abate S, Labella C, Cataldi TR. Identification and fragmentation pathways of caffeine metabolites in urine samples via liquid chromatography with positive electrospray ionization coupled to a hybrid quadrupole linear ion trap (LTQ) and Fourier transform ion cyclotron resonance mass spectrometry and tandem mass spectrometry. Rapid Commun Mass Spectrom. 2009;23(7):1065-74.
195. Medana C, Santoro V, Dal Bello F, Sala C, Pazzi M, Sarro M, et al. Mass spectrometric fragmentation and photocatalytic transformation of nicotine and cotinine. Rapid Commun Mass Sp. 2016;30(24):2617-27.
196. Wang T, Yang LT, Hua J, Xie HR, Jiang XH, Wang L. Simultaneous bioanalysis of rasagiline and its major metabolites in human plasma by LC-MS/MS: Application to a clinical pharmacokinetic study. J Pharmaceut Biomed. 2016;125:280-5.
197. Davie CA. A review of Parkinson's disease. Br Med Bull. 2008;86:109-27.
198. Forno LS. Neuropathology of Parkinson's disease. J Neuropathol Exp Neurol. 1996;55(3):259-72.
199. Uversky VN. Alpha-synuclein misfolding and neurodegenerative diseases. Curr Protein Pept Sci. 2008;9(5):507-40.
200. Hughes AJ, Ben-Shlomo Y, Daniel SE, Lees AJ. What features improve the accuracy of clinical diagnosis in Parkinson's disease: a clinicopathologic study. Neurology. 1992;42(6):1142-6.
201. Hughes AJ, Daniel SE, Lees AJ. Improved accuracy of clinical diagnosis of Lewy body Parkinson's disease. Neurology. 2001;57(8):1497-9.
202. Tolosa E, Gaig C, Santamaria J, Compta Y. Diagnosis and the premotor phase of Parkinson disease. Neurology. 2009;72(7 Suppl):S12-20.
203. Jia L, Liu X. The conduct of drug metabolism studies considered good practice (II): in vitro experiments. Curr Drug Metab. 2007;8(8):822-9.
204. Temporal KH, Scott KS, Mohr ALA, Logan BK. Metabolic Profile Determination of NBOMe Compounds Using Human Liver Microsomes and Comparison with Findings in Authentic Human Blood and Urine. J Anal Toxicol. 2017;41(7):646-57.
205. Brandange S, Lindblom L. Enzyme Aldehyde Oxidase Is an Iminium Oxidase - Reaction with Nicotine Delta-1'(5')Iminium Ion. Biochem Bioph Res Co. 1979;91(3):991-6.
206. Murphy PJ. Enzymatic oxidation of nicotine to nicotine 1'(5') iminium ion. A newly discovered intermediate in the metabolism of nicotine. J Biol Chem. 1973;248(8):2796-800.
207. Peterson LA, Trevor A, Castagnoli N, Jr. Stereochemical studies on the cytochrome P-450 catalyzed oxidation of (S)-nicotine to the (S)-nicotine delta 1'(5')-iminium species. J Med Chem. 1987;30(2):249-54.
208. Berthou F, Ratanasavanh D, Riche C, Picart D, Voirin T, Guillouzo A. Comparison of caffeine metabolism by slices, microsomes and hepatocyte cultures from adult human liver. Xenobiotica. 1989;19(4):401-17.
209. Campbell ME, Grant DM, Inaba T, Kalow W. Biotransformation of caffeine, paraxanthine, theophylline, and theobromine by polycyclic aromatic hydrocarbon-

inducible cytochrome(s) P-450 in human liver microsomes. Drug Metab Dispos. 1987;15(2):237-49.
210. Ferrero JL, Neims AH. Metabolism of caffeine by mouse liver microsomes: GSH or cytosol causes a shift in products from 1,3,7-trimethylurate to a substituted diaminouracil. Life Sci. 1983;33(12):1173-8.
211. Berthou F, Ratanasavanh D, Alix D, Carlhant D, Riche C, Guillouzo A. Caffeine and theophylline metabolism in newborn and adult human hepatocytes; comparison with adult rat hepatocytes. Biochem Pharmacol. 1988;37(19):3691-700.
212. Obach RS, Reed-Hagen AE. Measurement of Michaelis constants for cytochrome P450-mediated biotransformation reactions using a substrate depletion approach. Drug Metab Dispos. 2002;30(7):831-7.
213. Foster JA, Houston JB, Hallifax D. Comparison of intrinsic clearances in human liver microsomes and suspended hepatocytes from the same donor livers: clearance-dependent relationship and implications for prediction of in vivo clearance. Xenobiotica. 2011;41(2):124-36.
214. Kajbaf M, Ricci R, Zambon S, Fontana S. Contribution of rat intestinal metabolism to the xenobiotics clearance. Eur J Drug Metab Pharmacokinet. 2013;38(1):33-41.
215. Youdim K, Dodia R. Comparison between recombinant P450s and human liver microsomes in the determination of cytochrome P450 Michaelis-Menten constants. Xenobiotica. 2010;40(4):235-44.
216. US-FDA. Guidance for Industry : Bioanalytical Method Validation. US Department of Health and Human Services, Food and Drug Administration, Centre For Drug Evaluation and Research. May 2018.
217. Dasgupta A. Impact of interferences including metabolite crossreactivity on therapeutic drug monitoring results. Ther Drug Monit. 2012;34(5):496-506.
218. Dunand M, Donzelli M, Rickli A, Hysek CM, Liechti ME, Grouzmann E. Analytical interference of 4-hydroxy-3-methoxymethamphetamine with the measurement of plasma free normetanephrine by ultra-high pressure liquid chromatography-tandem mass spectrometry. Clin Biochem. 2014;47(12):1121-3.
219. Petteys BJ, Graham KS, Parnas ML, Holt C, Frank EL. Performance characteristics of an LC-MS/MS method for the determination of plasma metanephrines. Clin Chim Acta. 2012;413(19-20):1459-65.
220. Vogeser M, Seger C. Pitfalls Associated with the Use of Liquid Chromatography-Tandem Mass Spectrometry in the Clinical Laboratory. Clin Chem. 2010;56(8):1234-44.
221. Wright MJ, Thomas RL, Stanford PE, Horvath AR. Multiple reaction monitoring with multistage fragmentation (MRM3) detection enhances selectivity for LC-MS/MS analysis of plasma free metanephrines. Clin Chem. 2015;61(3):505-13.
222. Barreto GE, Iarkov A, Moran VE. Beneficial effects of nicotine, cotinine and its metabolites as potential agents for Parkinson's disease. Front Aging Neurosci. 2015;6.
223. Xie J, Saburulla NF, Chen S, Wong SY, Yap ZP, Zhang LH, et al. Evaluation of Carbazeran 4-Oxidation and O (6)-Benzylguanine 8-Oxidation as Catalytic Markers of Human Aldehyde Oxidase: Impact of Cytosolic Contamination of Liver Microsomes. Drug Metab Dispos. 2019;47(1):26-37.

224. Chen L, Feany MB. Alpha-synuclein phosphorylation controls neurotoxicity and inclusion formation in a Drosophila model of Parkinson disease. Nat Neurosci. 2005;8(5):657-63.
225. Hou J, Qu F, Wu C, Ren Q, Zhang J. Quantitative determination and pharmacokinetic study of the novel anti-Parkinson's disease candidate drug FLZ in rat brain by high performance liquid chromatography-tandem mass spectrometry. J Pharm Biomed Anal. 2012;66:232-9.
226. Bartels AL, Willemsen ATM, Kortekaas R, de Jong BM, de Vries R, de Klerk O, et al. Decreased blood-brain barrier P-glycoprotein function in the progression of Parkinson's disease, PSP and MSA. J Neural Transm. 2008;115(7):1001-9.
227. Zlokovic BV. The blood-brain barrier in health and chronic neurodegenerative disorders. Neuron. 2008;57(2):178-201.
228. Liu Q, Hou J, Chen X, Liu G, Zhang D, Sun H, et al. P-glycoprotein mediated efflux limits the transport of the novel anti-Parkinson's disease candidate drug FLZ across the physiological and PD pathological in vitro BBB models. PLoS One. 2014;9(7):e102442.
229. Hoosain FG, Choonara YE, Tomar LK, Kumar P, Tyagi C, du Toit LC, et al. Bypassing P-Glycoprotein Drug Efflux Mechanisms: Possible Applications in Pharmacoresistant Schizophrenia Therapy. Biomed Res Int. 2015;2015:484963.

Appendix A

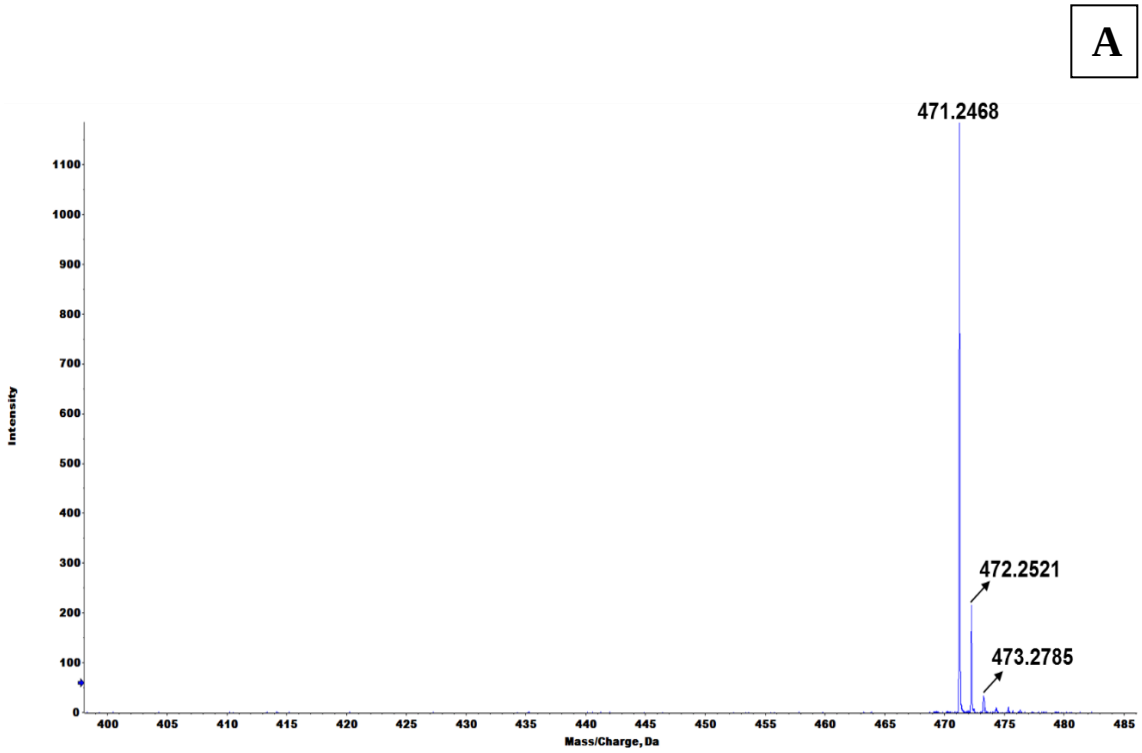
A
471.2468
472.2521
473.2785
Intensity
Mass/Charge, Da
0
100
200
300
400
500
600
700
800
900
1000
1100
400
405
410
415
420
425
430
435
440
445
450
455
460
465
470
475
480
485

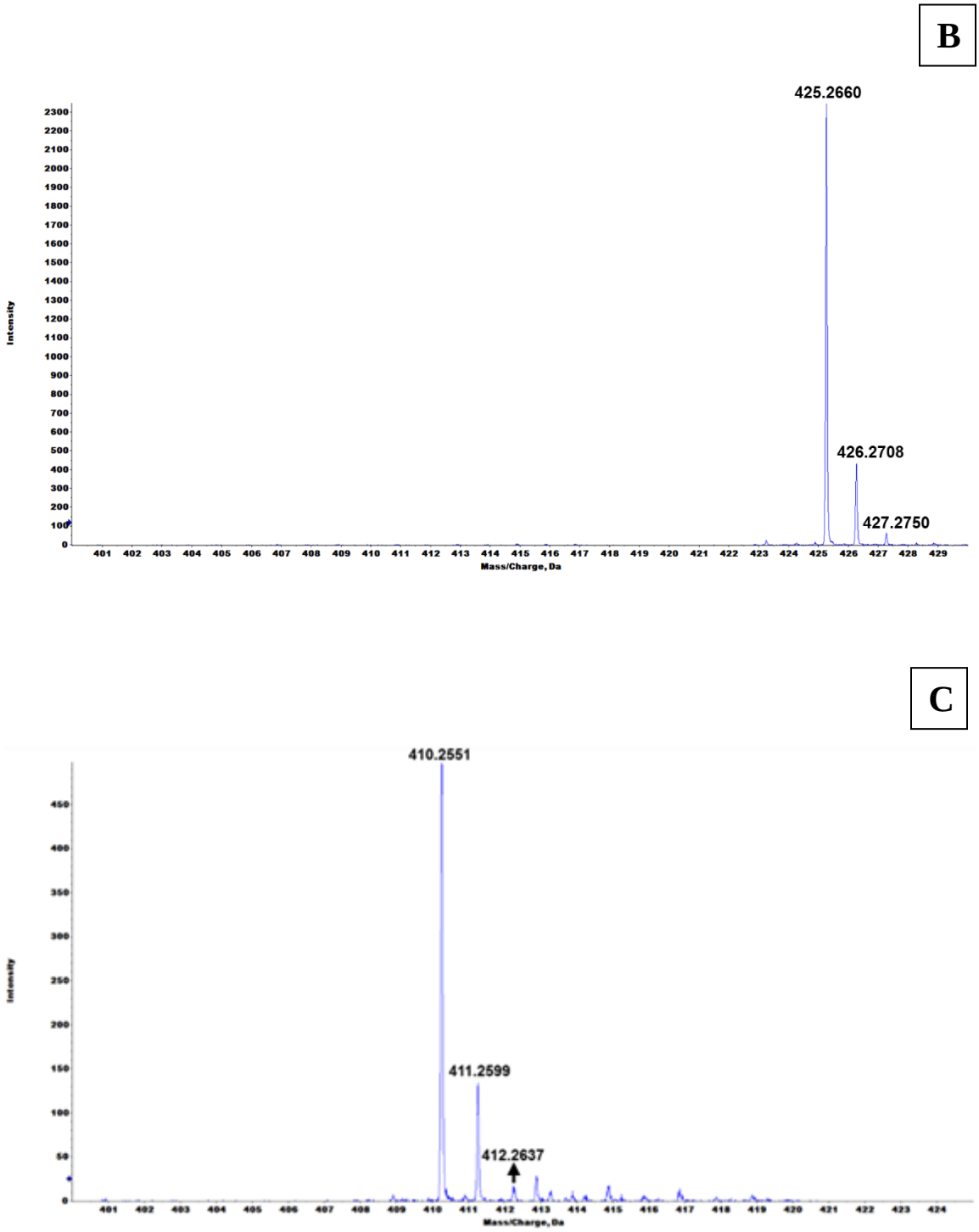

Figure A.1 The ESI-QqToF-MS spectrum of C_8-6-C_8 (A), C_8-6-N (B), and C_8-6-I(C).

Table A.1 Mass accuracies of C_8-6-C_8, C_8-6-N, and C_8-6-I obtained during single stage ESI-QqToF-MS analysis.

Compound	Molecular Formula	Theoretical, *m/z*	Observed, *m/z*	Mass Accuracy (ppm)
C_8-6-C_8	$C_{22}H_{31}N_8O_4$	471.2462	471.2468	1.2732
C_8-6-N	$C_{23}H_{33}N_6O_2$	425.2659	425.2660	0.2351
C_8-6-I	$C_{23}H_{32}N_5O_2$	410.2550	410.2551	0.2438

Table A.2 Mass accuracies of the MS/MS product ions of C_8-6-C_8 obtained during ESI-QqToF-MS/MS analysis.

MS/MS Product ions, *m/z*	Molecular Formula	Theoretical, *m/z*	Observed, *m/z*	Mass Accuracy (ppm)
[A1]	$C_{21}H_{31}N_8O_2$	427.2564	427.2571	1.6384
[A1^1]	$C_{20}H_{30}N_7O_2$	400.2455	400.2466	2.7483
[A2]	$C_{20}H_{28}N_7O_3$	414.2248	414.2230	-4.3455
[A2^1]	$C_{19}H_{28}N_7O_2$	386.2298	386.2293	-1.2946
[A2^2]	$C_{19}H_{28}N_7O$	370.2349	370.2382	8.9132
[A2^{2+}]	$C_{18}H_{28}N_7$	342.2400	342.2401	0.2922
[A2^{2++}]	$C_{13}H_{19}N_4$	231.1604	231.1619	6.4890
[A2^3]	$C_{18}H_{25}N_6O_2$	357.2033	357.2055	6.1589
[A2^4]	$C_{15}H_{22}N_5O_2$	304.1768	304.1789	6.9038
[A4]	$C_{10}H_{13}N_4O_2$	221.1033	221.1048	6.7841

Table A.3 Mass accuracies of the MS/MS product ions of C_8-6-N obtained during ESI-QqToF-MS/MS analysis.

MS/MS Product ions Designation	Molecular Formula	Theoretical, *m/z*	Observed, *m/z*	Mass Accuracy (ppm)
[B1]	$C_{18}H_{28}N_5O_2$	346.2237	346.2243	1.7330
[B1^1]	$C_{14}H_{21}N_4O_2$	277.1659	277.1666	2.5256
[B1^2]	$C_{14}H_{19}N_4O_2$	275.1502	275.1516	5.0881
[B1^3]	$C_9H_{11}N_4O_2$	207.0876	207.0891	7.2433
[B2]	$C_{17}H_{26}N_5O_2$	332.2081	332.2074	-2.1071
[B2^1]	$C_{13}H_{19}N_4O_2$	263.1502	263.1500	-0.7600
[1]	$C_{15}H_{24}N_5O_2$	306.1924	306.1942	5.8786
[3]	$C_{12}H_{18}N_3O$	220.1444	220.1451	3.1797
[5]	$C_7H_{10}N_3O_2$	168.0767	168.0781	8.3295
[8]	C_9H_8N	130.0651	130.0659	6.1507

Table A.4 Mass accuracies of the MS/MS product ions of C_8-6-I obtained during ESI-QqToF-MS/MS analysis.

MS/MS Product ions, *m/z*	Molecular Formula	Theoretical, *m/z*	Observed, *m/z*	Mass Accuracy (ppm)
294.4 [C1]	$C_{14}H_{24}N_5O_2$	294.1924	294.1912	-4.0790
277.4 [C1[1]]	$C_{14}H_{21}N_4O_2$	277.1659	277.1660	0.3608

Table A.5 Neutral losses observed from the fragmentation of all three bifunctional compounds.

	C_8-6-C_8	**C_8-6-N**	**C_8-6-I**
Neutral losses (Da)	44 (CO_2)	79 (C_5H_5N)	116 (C_9H_8)
	27 (CN)	93 (C_6H_7N)	17 (NH_3)
	29 (CH_2NH)	69 (C_4H_7N)	293 ($C_{14}H_{23}N_5O_2$)
	57 (C_2H_3NO)	71 (C_4H_9N)	
	28 (CO)	139 ($C_9H_{17}N$)	
	110 ($C_5H_6N_2O_2$)	119 (C_8H_9N)	
	142 ($C_6H_{10}N_2O_2$)	176 ($C_{11}H_{16}N_2$)	
	250 ($C_{12}H_{18}N_4O_2$)	148 ($C_9H_{12}N_2$)	
	139 ($C_6H_9N_3O$)	57 (C_2H_3NO)	
	193 ($C_{10}H_{15}N_3O$)	230 ($C_{15}N_{22}N_2$)	
	41 (C_2H_3N)	257 ($C_{16}H_{23}N_3$)	
	276 ($C_{14}H_{20}N_4O_2$)	289 ($C_{14}H_{19}N_5O_2$)	
	303 ($C_{15}H_{21}N_5O_2$)	293 ($C_{14}H_{23}N_5O_2$)	
	206 ($C_9H_{10}N_4O_2$)	2 (H_2)	
	208 ($C_9H_{12}N_4O_2$)	305 ($C_{15}H_{23}N_5O_2$)	
	194 ($C_8H_{10}N_4O_2$)	236 ($C_{11}H_{16}N_4O_2$)	
	32 (CH_3OH)	319 ($C_{16}H_{25}N_5O_2$)	

A

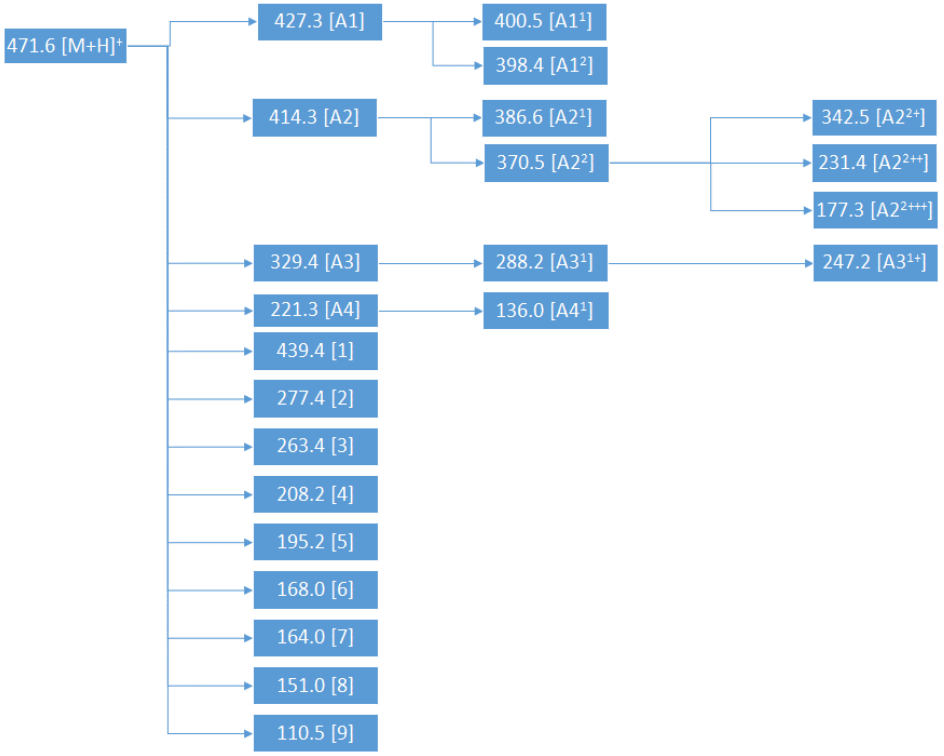
471.6 [M+H]+
427.3 [A1]
400.5 [A1¹]
398.4 [A1²]
414.3 [A2]
386.6 [A2¹]
370.5 [A2²]
342.5 [A2²⁺]
231.4 [A2²⁺⁺]
177.3 [A2²⁺⁺⁺]
329.4 [A3]
288.2 [A3¹]
247.2 [A3¹⁺]
221.3 [A4]
136.0 [A4¹]
439.4 [1]
277.4 [2]
263.4 [3]
208.2 [4]
195.2 [5]
168.0 [6]
164.0 [7]
151.0 [8]
110.5 [9]

B

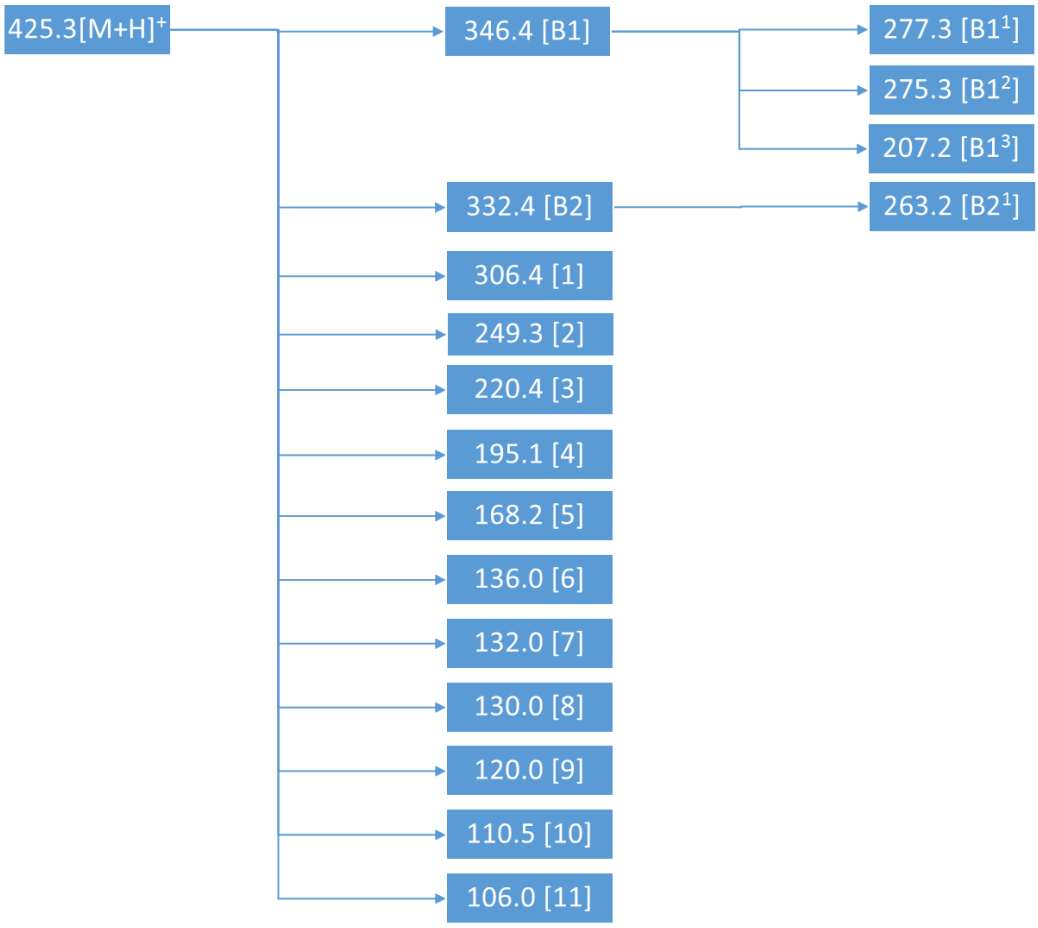
425.3[M+H]+
346.4 [B1]
277.3 [B1^1]
275.3 [B1^2]
207.2 [B1^3]
332.4 [B2]
263.2 [B2^1]
306.4 [1]
249.3 [2]
220.4 [3]
195.1 [4]
168.2 [5]
136.0 [6]
132.0 [7]
130.0 [8]
120.0 [9]
110.5 [10]
106.0 [11]

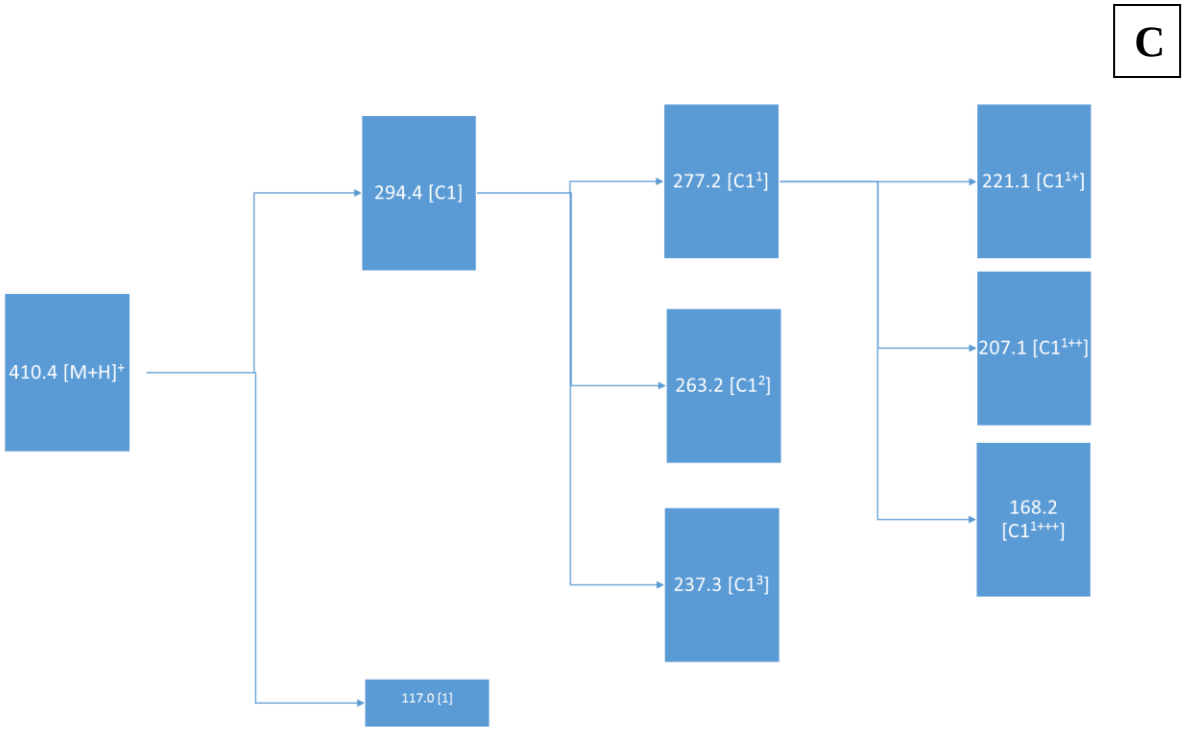

Figure A.2 Summary of MS/MS and MS^3 analysis for C_8-6-C_8 (A), C_8-6-N (B), and C_8-6-I (C).

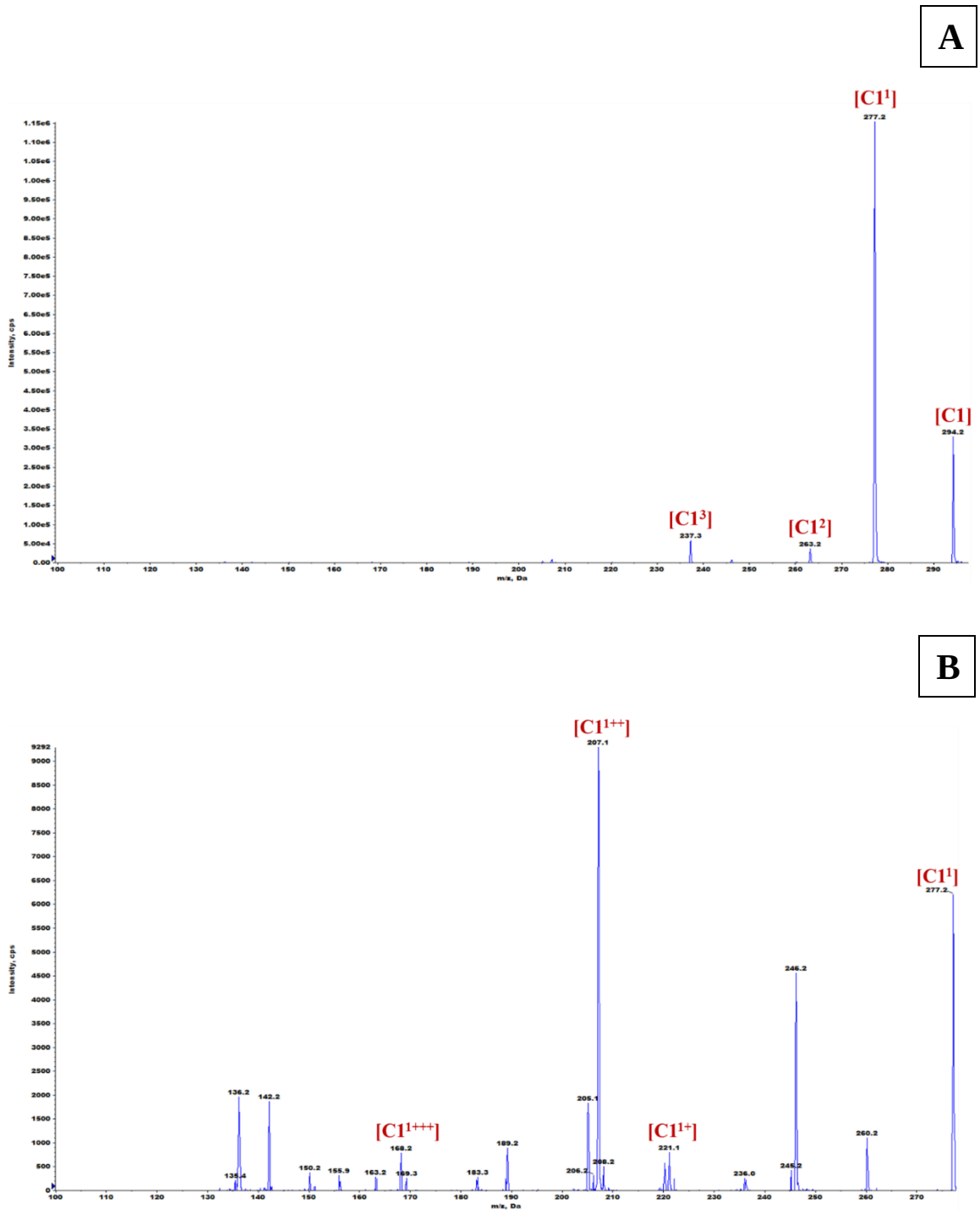

Figure A.3 MS^3 spectra for C1 (A) and C1^1 (B).

Appendix B

Table B.1 HPLC-high-resolution and tandem mass spectrometric data for C_8-6-I and C_8-6-N metabolites detected in human, mouse, and rat liver microsomes (HLM, MLM, and RLM).

Metabolite Designation	Metabolic Reaction	Retention Time (min)	Molecular Formular	Exact Mass (*m/z*)	Mass Error(ppm)	Parent Compound	Matrices
M1	De-alkylation	11.23	$C_{14}H_{24}N_5O_2$	294.1924	0.000	C_8-6-I	HLM, MLM, RLM
M2	Hydroxylation	11.64	$C_{23}H_{32}N_5O_3$	426.2499	6.8035	C_8-6-I	HLM, MLM, RLM
M3	De-alkylation	11.25	$C_{14}H_{24}N_5O_2$	294.1924	0.0000	C_8-6-N	HLM, MLM, RLM
M4	Hydroxylation	11.53	$C_{23}H_{33}N_6O_3$	441.2608	6.1188	C_8-6-N	HLM, MLM, RLM

Appendix C

A

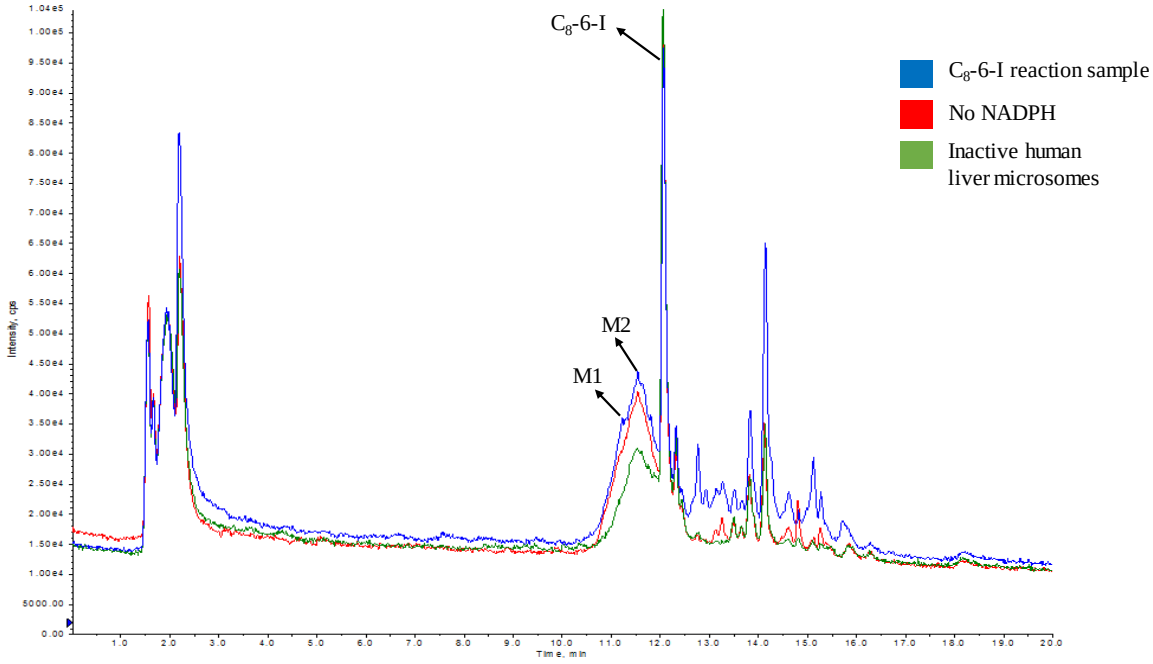
C8-6-I
M2
M1
C8-6-I reaction sample
No NADPH
Inactive human liver microsomes
Intensity, cps
Time, min

B

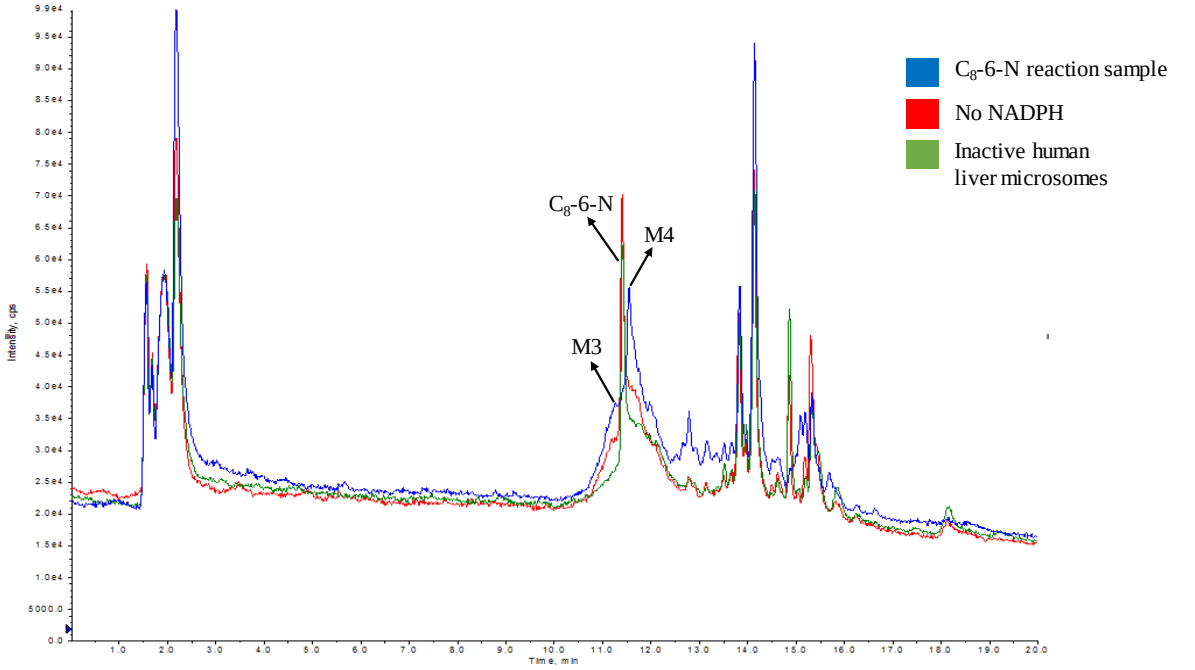
C8-6-N reaction sample
No NADPH
Inactive human liver microsomes
C8-6-N
M4
M3
Intensity, cps
Time, min

C

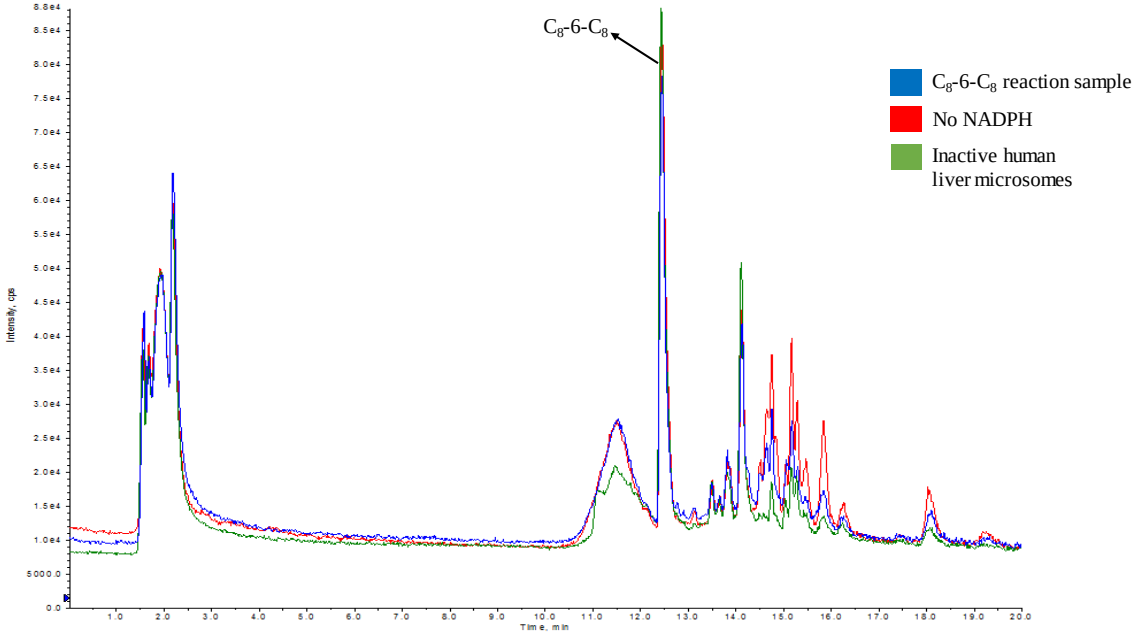
C8-6-C8 reaction sample
No NADPH
Inactive human liver microsomes
C8-6-C8
Intensity, cps
Time, min

D

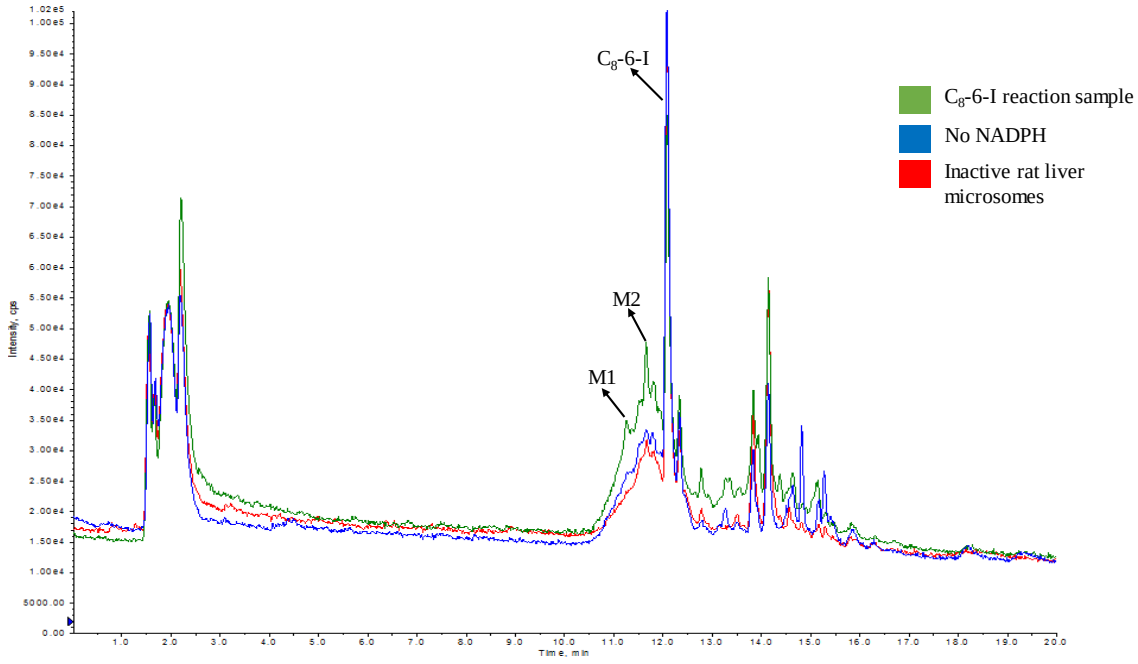
C8-6-I
M2
M1
C8-6-I reaction sample
No NADPH
Inactive rat liver microsomes
Intensity, cps
Time, min

E

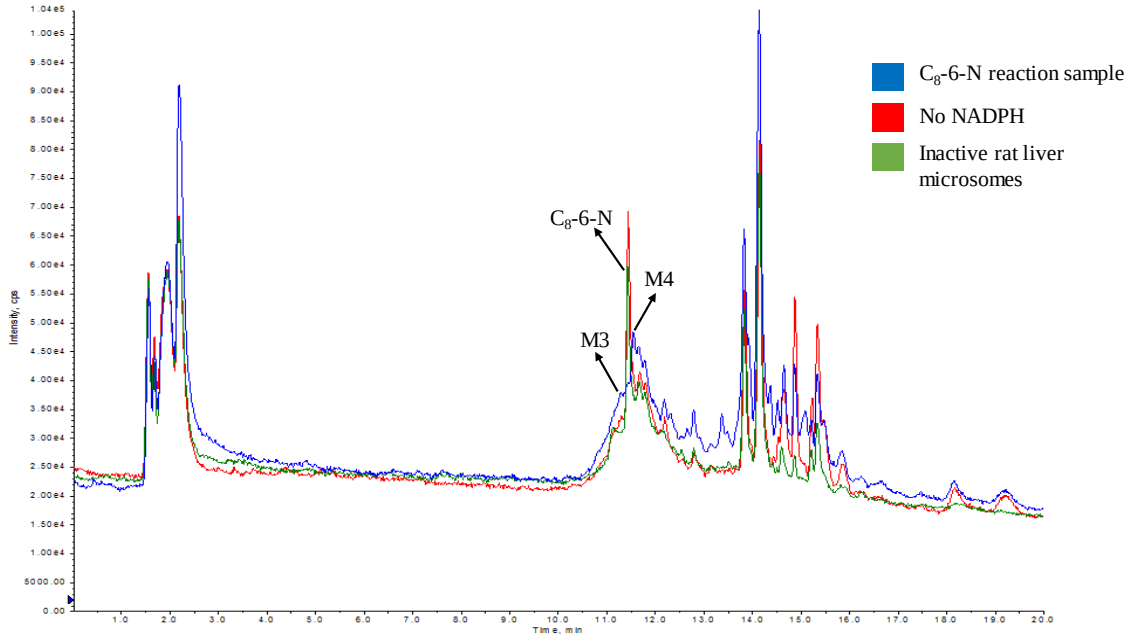
C8-6-N
M4
M3
C8-6-N reaction sample
No NADPH
Inactive rat liver microsomes
Intensity, cps
Time, min

F

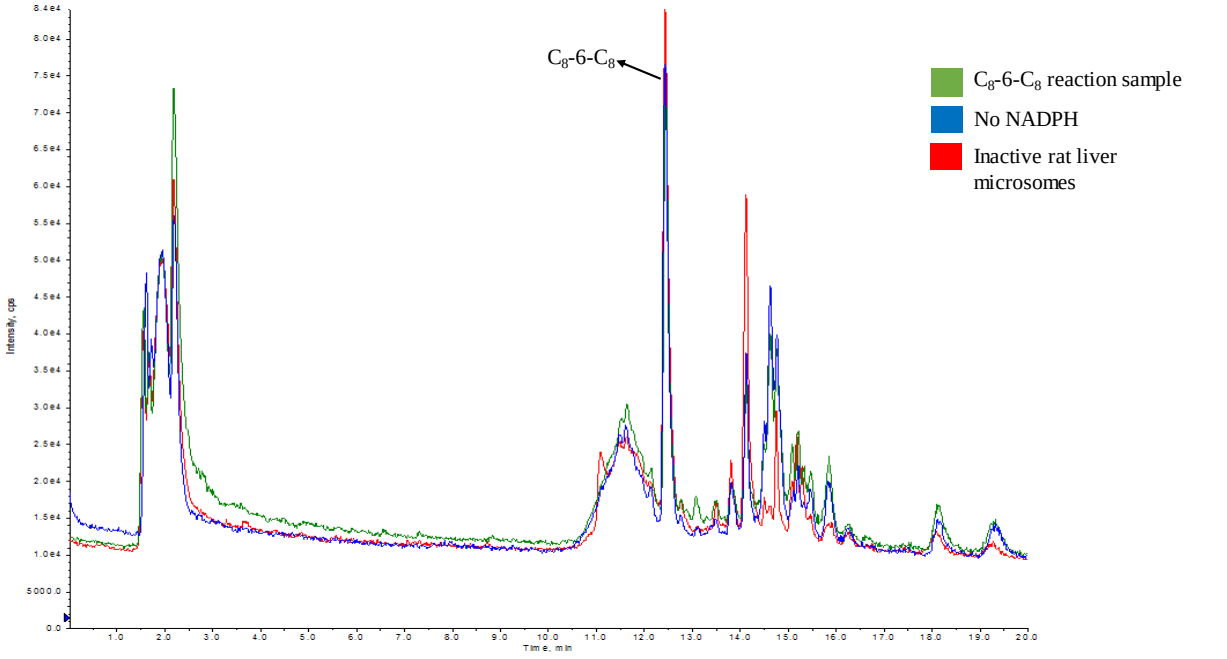

Figure C.1 Total ion chromatogram of LC-MS analysis of samples from *in vitro* human liver microsomal metabolism of C_8-6-I (A), C_8-6-N (B), C_8-6-C_8 (C), and *in vitro* rat liver microsomal metabolism of C_8-6-I (D), C_8-6-N (E), C_8-6-C_8 (F).